DIPLOMARBEIT

# Extraction methods for the MedAustron Synchrotron

ausgeführt am Atominstitut E141
der Technischen Universität Wien

unter der Anleitung von
Privatdoz. Dipl.-Ing. Dr.techn. Michael Benedikt

durch

Gregor Feldbauer
0426070
Am Pfarrerfeld 29, A-4840 Vöcklabruck

Wien, am 11.05.2011

# Abstract

Synchrotron-based cancer treatment facilities use resonant extraction mechanisms in order to extract light hadrons (protons, carbon ions) with a kinetic energy of a few hundred MeV per nucleon over a few seconds.

This thesis makes a comparative study of extraction methods in the context of the MedAustron facility, which is currently in its final design stage. The work focuses mainly on the chosen base-line extraction mechanism - the betatron-core driven, third-order resonance extraction scheme - but also includes the first feasibility studies of RF-Knockout extraction, Stochastic RF-Noise extraction and extraction via a quadrupole-induced tune-shift, using MedAustron parameters.

Furthermore, long term precision requirements on the power converter stability of the magnets in the synchrotron and the high energy beam transfer lines have been defined to ensure the clinically required long term beam energy, size and position stability.

Potential problems with low-energy protons concerning the precision requirements and with the capacity of the betatron-core are flagged.

# Contents

# 1 Introduction

This diploma thesis has been carried out at the European Organization for Nuclear Research (CERN) in Geneva, Switzerland within the framework of the MedAustron project. MedAustron is a particle accelerator based cancer therapy treatment and research center that is currently in its final design stage and will be built in Wiener Neustadt, Austria.

Basically, a particle accelerator is a machine that produces, accelerates and stores a beam of fast moving, charged particles. Strong electromagnetic fields are employed to accelerate the particles and to keep them on track in the accelerators. This can be achieved by various different set ups and methods, however, the emphasis of this thesis lies on the synchrotron, a ring-shaped accelerator type. In the MedAustron project a synchrotron will be used to deliver light ions (e.g. protons or carbon ions) beams mainly for cancer therapy treatment.

Ionizing radiation is employed in cancer treatment for many years now, in particular, X-rays and electrons are commonly used. However, light ions have the advantage that their Linear Energy Transfer (LET) function has a peak at the end of their trajectory. This maximum is called Bragg-peak. After this peak there is quasi no dose. Thus, the energy deposition can be localized more accurately in the tumor volume. Consequently, the surrounding healthy tissue is less disturbed, which is especially important for deep seated tumors and also allows to irradiate tumors close to critical organs.

The accelerator parameters are defined by the needs of the cancer treatment on properties such as beam energy, intensity, beam homogeneity or time structure of the delivered beam. For example to be able to irradiate any part of a human body a penetration depth of roughly 30 cm is required. To achieve this, particles with an energy of a few hundred MeV (Mega Electron Volts)[1] per nucleon are necessary. Assuming a synchrotron that uses only normal conducting magnets a ring circumference of about 100 m is required to produce such energies[2]. Light ions with such energies are flying with velocities between $\approx 30\%$ and $\approx 85\%$ of the speed of light and thus circulate a few million times around the synchrotron in one second.

Active scanning will be used at MedAustron to irradiate tumors. Hence, the homogeneity of the extracted beam over the irradiation time is of special importance, as the whole tumor

[1] 1 eV $\approx 1.6 \cdot 10^{-19}$ *Joule*, this is the kinetic energy gain of a particle with unit charge, e.g. an electron, when it traverses a voltage drop of 1 V

[2] This is a rather small, low energy machine compared to high energy machines such as the Large Hadron Collider (LHC) at CERN with a circumference of 27 km and energies up to 7 TeV.

should be irradiated with a defined dose. To achieve this, two of the most crucial components in the beam delivery process are:

- The extraction process that is used to extract the particles from the synchrotron, after they have been accelerated to the desired energy, into the High Energy Beam Transfer line (HEBT), which then transports the beam to the irradiation room's focal point.
- The stability of the power converter supplying the synchrotron and HEBT magnets.

These are the two main topics covered in this thesis.

A slow resonant extraction is employed to obtain a low intensity beam at the focal point over a time span of a few seconds, which corresponds to several million turns in the ring. This spill length is required to allow for a precisely controlled scanning and monitoring of the beam over the target area.

The nominal extraction method at MedAustron is the betatron core driven, third-order resonance extraction, which is a form of inductive acceleration driven, resonant extraction. Within the framework of this thesis this nominal extraction mechanism has been studied and simulated in detail. Furthermore, several alternative driving mechanism have been analyzed, simulated and compared to the nominal case: RF-knockout extraction, Longitudinal stochastic RF-noise extraction and Quadrupole extraction.

The requirements on the long time precision for the power converters supplying the synchrotron and HEBT magnets have been derived to fulfill the required accuracy in beam energy, size and position.

# 2 MedAustron

In this chapter the MedAustron project is described briefly, followed by an introduction to the MedAustron accelerator complex.

## 2.1 The MedAustron project

MedAustron is a cancer therapy treatment center that is currently in its final design stage [1] and will be built in Wiener Neustadt, Austria. The first treatment of a patient is planned to take place in 2015. Beside the therapeutical facilities MedAustron will also host facilities for clinical and non-clinical research. Medical radiation physics, radiation biology and experimental physics are foreseen as the main research fields [2] [3].

The accelerator design is based on the PIMMS study [4] and the development is done in collaboration with CERN [5], CNAO [6] for the technical systems and the layout of the medical facility and with PSI [7] for the proton gantry development.

The MedAustron accelerator complex is based on a synchrotron. For patient irradiation, the accelerator delivers particles to the irradiation rooms with a nominal energy range of 60 to 250 MeV for protons ($p$) and 120 to 400 MeV per nucleon for carbon ions ($C^{6+}$). For non-clinical research protons up to an energy of 800 MeV are available. Furthermore, the use of other light ion species like nitrogen is envisioned. Figure 2.1 shows the accelerator complex with the four irradiation rooms. The first irradiation room is dedicated to research and is equipped with a horizontal beam line. Protons, above the medical energy range, can only be delivered to this room. The following three rooms are the treatment rooms. The second irradiation room (numbering starts with the research room) hosts a horizontal and a 90° vertical beam line, whereas the third has only a horizontal one. The fourth irradiation room is equipped with a proton gantry. The layout allows to add an additional fifth irradiation room containing an ion gantry as an optional future extension to the treatment center.

The tumor treatment is done by 3D-active scanning of the beam over the whole volume of the tumor. Each tumor is divided into iso-energy depth-layers and each layer into single spots. The different layers are irradiated by changing the extraction energy of the beam from the synchrotron from cycle to cycle. The transverse beam position is altered by changing the

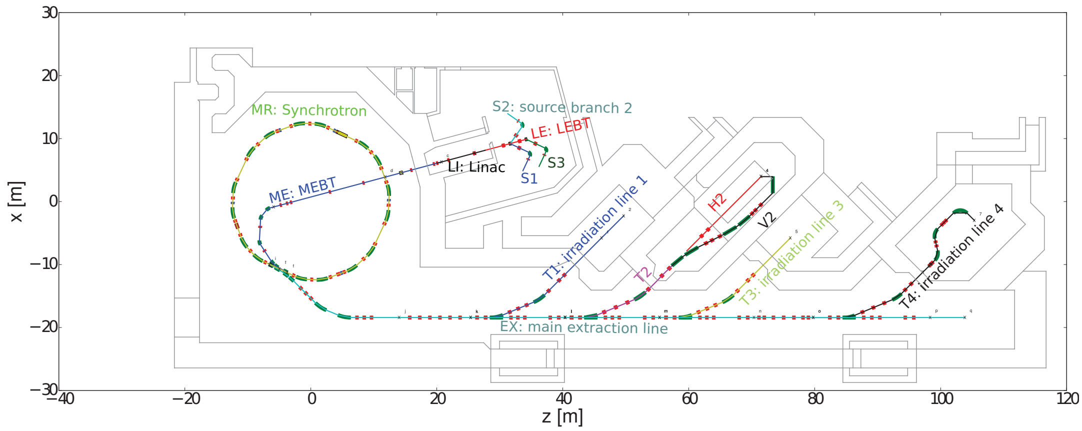


Figure 2.1: Overview layout of the MedAustron accelerator complex including radiation shielding walls

deflecting magnetic field of the scanning magnets. The beam is not turned off while moving between two spots. To ensure the safety of the patients, the beam can be turned off in less than 300 µs by the chopper system [8].

## 2.2 The MedAustron accelerator complex

In figure 2.1 the layout of the MedAustron accelerator complex is shown. The design is based on the PIMMS study [9].

The beam generation starts in the injector hall at one of three independent ion sources. These sources are electron cyclotron resonance (ECR) sources, which can be tuned to produce any of the required particle species. In the first stage $H_3^+$ for protons and $^{12}C^{4+}$ for carbon ions are available (identical charge-to-mass ratio, $q/m = 1/3$). These particles are accelerated by the LINAC (LINear ACcelerator) up to the synchrotron injection energy of 7 MeV/nucleon. At its end a stripping foil is used to strip $H_3^+$ and $^{12}C^{4+}$ ions into three protons and $^{12}C^{6+}$, respectively. More information on the sources, LEBT (Low Energy Beam Transfer line) and Linac can be found in [10].

The beam is transported from the end of the LINAC to the synchrotron injection point by the Medium Energy Beam Transfer line (MEBT) [11]. In order to increase the number of accumulated particles inside the ring a horizontal multi-turn injection (MTI) [12] is performed.

The circumference of the synchrotron is 77.65 m and the lattice type is a split FODO with a super-periodicity of 2 and a mirror symmetry within each super-period. In figure 2.2 the optics of the synchrotron is shown. The lattice has a $\gamma_{transition} = 1.97$, which is well above the relativistic $\gamma$ factor of a 400 MeV/u carbon ion, but limits the maximal proton energy to about 900 MeV, if transition should not be crossed. To have some clearance to this limit, 800 MeV is the chosen top energy for protons, whereas the magnetic fields theoretically allow for about 1.2 GeV protons.

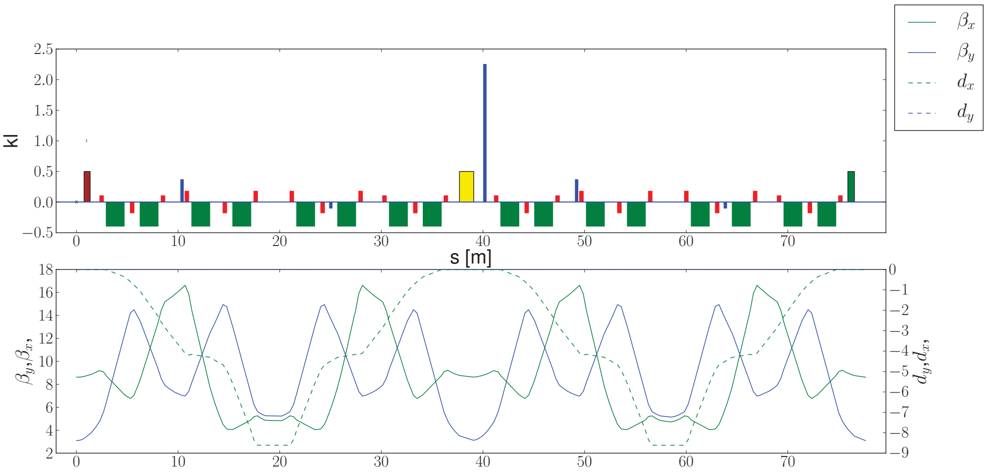


Figure 2.2: Optics of the MedAustron synchrotron

The accelerator consists of 16 dipoles each with a bending radius of 4.231 m. Furthermore the ring hosts 24 quadrupole magnets equally divided into three magnet families (two focusing MQF families 1 & 2, one de-focusing MQD family). Four lattice sextupoles (in two families, focusing and de-focusing) are placed in dispersive areas to allow to control the chromaticity. Thus, these sextupoles are often referred to as chromaticity sextupoles or lattice sextupoles. In addition one single resonant sextupole (MXR) is placed in a zero dispersion region, which allows to change its setting without an impact on the chromaticity[1]. In order to dominate the extraction, the resonant sextupole is significantly stronger than the others. Furthermore, the synchrotron is equipped with corrector magnets, beam diagnostic devices and special elements for injection and extraction such as septa and the betatron core magnet. A single RF-system with harmonic number $h = 1$ is used for acceleration.

The maximum number of particles that can be stored in the machine is $2.3 \cdot 10^{10}$ protons or $1.15 \cdot 10^{9}$ carbon ions. In both planes the normalized emittance ($1\sigma$) is $0.52\,\pi$ mm mrad for protons and $0.75\,\pi$ mm mrad for carbon ions. At injection the machine is set to the following tunes: horizontally $Q_H = 1.739$ and vertically $Q_V = 1.779$. After the acceleration and the preparation for extraction the beam is extracted by employing a third-order resonance extraction at $Q_H = 1.666$ and $Q_V = 1.789$. As the extraction process is a main topic of this thesis, it will be discussed in detail throughout this document.

[1] This is only true in a perfect model. The real situation is briefly discussed in section 4.2.2.

A selection of important synchrotron parameters can be found in the appendix A.2. Further information are available in the MedAustron Accelerator Complex design report [11] and the MedAustron accelerator parameter list [13].

After a particle has been extracted from the synchrotron, it enters the high energy beam transfer line (HEBT). The HEBT consists of a common extraction beam line (EX) and four separated beam lines (T1-4) delivering the beam from the EX line into one of the irradiation rooms. The layout can be seen in figure 2.1. Four magnetic extraction septa are used to direct the beam away from the synchrotron. Next in the HEBT there are a dispersion suppressor with integrated chopper, the phase stepper to change the beam size and 1:1 extension modules. In the following the beam can be deflected from the EX into a T line via the switching dipole magnets according to the targeted beam line. Quadrupole magnets are placed around the switching magnets to match the beam to the following transfer line. In this thesis only two of the possible HEBT beam lines will be used: the EX-T1-line which transports the top energy protons with 800 MeV and the EX-T2-V2-line which allows vertical irradiation by hosting vertical bends. As an example the optics of the EX-T2-V2-line is shown in figure 2.3

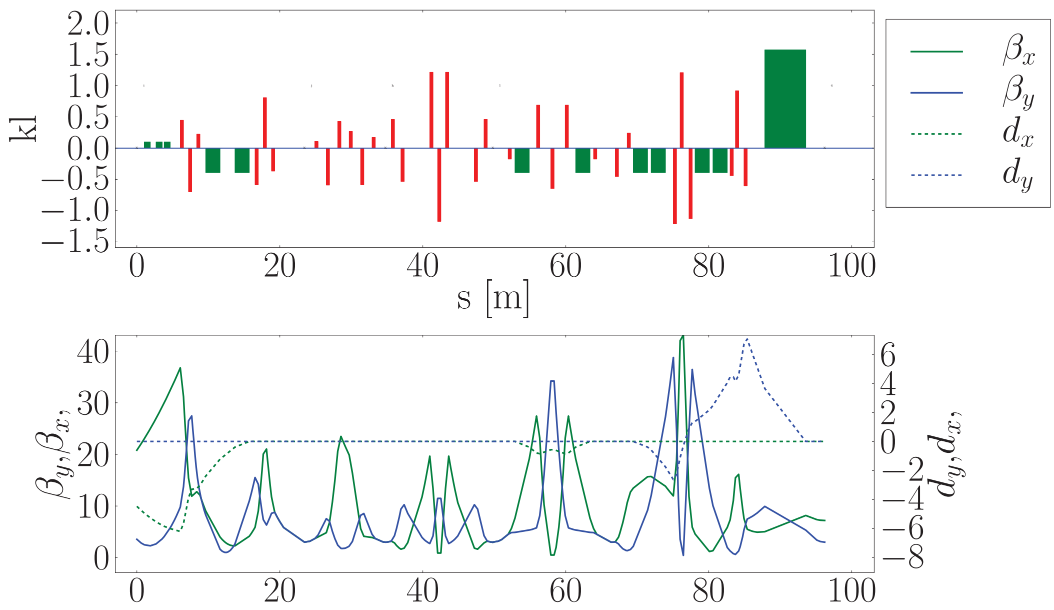


Figure 2.3: Optics of the EX-T2-V2 beam lines in the MedAustron HEBT

All beam lines entering the irradiation rooms are equipped with scanning magnets to scan the beam over a tumor or a target. Just in front of the patient a 'nozzle' is placed for a final beam quality verification and final beam adjustments. A selection of important HEBT parameters can be found in the appendix A.3 and further information is available in the MedAustron Accelerator Complex design report [11] and the MedAustron accelerator parameter list [13].

# 3 Selected topics of Accelerator Physics

This chapter starts with an introduction to selected basic concepts of accelerator physics. In the following, the necessary background on particle stability and 3rd order resonant extraction processes is given, which is required to understand the work described later in this thesis. As the biggest part of this diploma thesis deals with a synchrotron, the introduction will focus on that accelerator type.

## 3.1 Particle motion

Electromagnetic fields are used to inject charged particles into a synchrotron and to store, accelerate and finally extract them at a higher energy. While the particles are circulating at speed $v$, these fields cause forces to act on them according to the Lorentz force for electromagnetic fields $E$ and $B$.

$$\vec{F}_{Lorentz} = q\,(\vec{E} + \vec{v} \times \vec{B}) \tag{3.1}$$

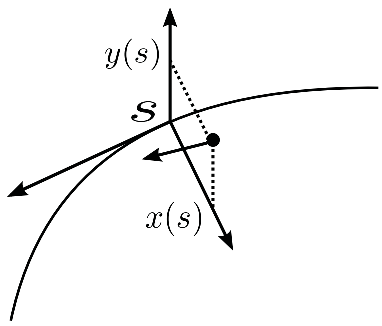


Figure 3.1: The accelerator coordinate system

An accelerator lattice consists of a sequence of elements such as magnets, beam diagnostic devices, septa, kickers, etc. placed along a reference orbit, which is defined as the trajectory of the reference particle, which has the design momentum $p_0$, through idealized elements. The nominal momentum is defined via the force equilibrium between the magnetic force from the bending magnets (assuming a synchrotron) and the force due to the radial acceleration. The periodicity of a ring defines the equilibrium orbit of the reference particle unambiguously and obligates it to be closed. A local curvilinear right handed coordinate system ($x$, $y$, $s$) is defined by the tripod which accompanies the reference orbit (see figure 3.1). The local $s$-axis is the tangent of the reference orbit, whereas the two other axes, $x$ and $y$, are perpendicular to the reference orbit. The axis in the bending plane (this is usually and especially for the MedAustron synchrotron the horizontal plane) of the dipoles is named $x$ and the axis perpendicular to $x$ and $s$ is called $y$. One advantage of this coordinate system choice is that most dipole effects are eliminated from the description of the particle motion, only dispersive, edge and weak focusing effects have to be considered explicitly.

A useful tool to describe the particle motion is the 6-dimensional (6D) phase space, which contains in addition to the already mentioned spatial dimensions $x$, $y$ and $s$, the derivatives $x' = dx/ds$, $y' = dy/ds$ and the relative momentum distance $\Delta p/p$ with respect to the design momentum. A phase space plot gives a Poincaré section along the reference orbit at a certain position $s$. At any time a particle and its motion is given by a point in the phase space spanned by those six coordinates. This point is described by a vector $(x, x', y, y', s, \Delta p/p)$. An important property of the phase space is formulated in the Liouville theorem, which states that the area or volume covered in phase space by a trajectory is an invariant of the motion as long as only conservative forces act on the particle.

### 3.1.1 Electric and magnetic rigidity

For the examination of the effects of electrostatic and magnetic elements on the transverse motion of the particles it is convenient to define the electric ($E\rho$) and the magnetic ($B\rho$) rigidity, which are both beam properties. In order to keep a particle with the velocity $v$ and the charge $q$ on a design trajectory defined by the local radius of curvature $\rho_0$, the centripetal force, which is the Lorentz force here, has to balance out the force due to the radial acceleration of the particle according to its mass $m$ and velocity:

$$F_{acceleration} = \frac{m\, v_0^2}{\rho_0} = -F_{centripetal} = -q\,(E_0 + v_0\, B_0) \tag{3.2}$$

For magnetic elements ($E$ = 0) formula (3.2) can be rearranged by using the momentum $p = m \cdot v$ to write:

$$|B_0 \rho_0| = \frac{p}{q} \tag{3.3}$$

For electrostatic elements ($B$ = 0) equation (3.2) can be rewritten with the relativistic $\gamma$ and $\beta$ factors and the kinetic energy $E_{kin}$ as:

$$|E_0 \rho_0| = \frac{mc^2}{q}\left(1 - \frac{1}{\gamma^2}\right) \tag{3.4}$$

Using $mc^2 = E_{kin}/(\gamma - 1)$ and applying some algebraic manipulations the following expression is found:

$$|E_0 \rho_0| = \frac{E_{kin}}{q}\,\frac{1+\gamma}{\gamma} \tag{3.5}$$

The magnetic rigidity defines the central orbit in a magnetic bend and the electric rigidity in an electrostatic bend respectively. The bending angle $\alpha$ of such electrostatic or magnetic elements with the length $l$ is given by:

$$\begin{aligned}\alpha_{electric} &= \frac{l}{\rho} = \frac{E\,l}{E\,\rho}\\ \alpha_{magnetic} &= \frac{l}{\rho} = \frac{B\,l}{B\,\rho}\end{aligned} \tag{3.6}$$

To simplify calculations the "thin lens approximation" is commonly used. In this approximation the elements are considered to have zero length and thus only affect the direction of a particle's motion, but not the particle's transverse position. This change of the direction is called a kick. The residual lengths of the elements are replaced by field-free drift spaces. In order to improve the quality of the approximation, an element can also be split up into several zero length modules with only a certain fraction of the element's strength and drift spaces in between. In such a thin lens approximation the kick $\Delta x'$ of an electrostatic or magnetic element can be approximated by a bending angle $\alpha$. It is only in the subsequent drift space that the kick changes the position of the particle .

### 3.1.2 Normalized element strengths

A magnetic field close to an axis can always be written in the form of a Taylor expansion, which is given for the horizontal plane as:

$$B_y(x, y=0) = B_0 + \left(\frac{dB_y}{dx}\right)_0 x + \frac{1}{2!}\left(\frac{d^2B_y}{dx^2}\right)_0 x^2 + \ldots \tag{3.7}$$

where the constant term gives a dipole field component, the linear term a quadrupole field, the quadratic a sextupole one and so on. Commonly magnets are characterized by the coefficients in the Taylor expansion. For example a sextupole can be characterized by its sextupole gradient $g_2 = d^2B_y/dx^2$. To avoid momentum dependencies in the characterization of magnetic elements, the coefficients are usually normalized with respect to the magnetic rigidity. For a sextupole this yields the normalized sextupole gradient $k_2$:

$$k_2 = \frac{1}{|B\rho|}\frac{d^2B_y}{dx^2} \tag{3.8}$$

In the same way the normalized quadrupole gradient is defined as:

$$k_1 = \frac{1}{|B\rho|}\frac{dB_y}{dx} \tag{3.9}$$

### 3.1.3 Hill's equation, Twiss functions and the phase space

The properties of real particles deviate from the ideal ones of the on-momentum reference particle. Particles with only slightly deviating spatial properties oscillate around the orbit of the reference one. This motion is referred to as betatron oscillations. Furthermore, due to dispersion, particles with different momenta follow different equilibrium orbits, called off-momentum closed orbits. Of course, an off-axis and off-momentum particle is subject to a combination of the two effects and thus carries out betatron oscillations around its off-momentum closed orbit. In a linear lattice (only dipoles and quadrupoles, no higher order elements), the two transverse planes are uncoupled and the particles motion in each one can be described separately by Hill's equation [14], which is a second order linear differential equation with periodic coefficients $k(s)$ (representing the periodic magnet strengths in a circular accelerator). Assuming continuous focusing by the quadrupoles and that the bending magnets are only in the horizontal plane, Hill's equations can be written as:

$$x'' - (k - \frac{1}{\rho^2})\, x = \frac{1}{\rho} \frac{\Delta p}{p_0} \tag{3.10}$$

$$y'' + k\, y = 0 \tag{3.11}$$

Hill's equation has got a periodic solution which can be written in terms of parametrized trigonometric functions. For on-momentum particles ($\Delta p / p = 0$) the solution reads (off-momentum particles are discussed in section 3.1.4):

$$x(s) = \sqrt{\beta(s)\, \varepsilon}\, \cos\left(\mu(s) + \mu_0\right) \tag{3.12}$$

$$\mu(s) = \int \frac{ds}{\beta(s)} \tag{3.13}$$

where $\beta(s)$ and $\mu(s)$ are lattice properties and are referred to as the betatron amplitude function and the phase advance, respectively. $\varepsilon$ is a particle property called the emittance. From the beta function two additional commonly used functions $\alpha$ and $\gamma$ are derived. These three functions are known as the *Courant - Snyder parameters* [15] or the *Twiss functions*[1]:

$$\alpha(s) = -\frac{1}{2} \frac{d\beta}{ds} \tag{3.14}$$

$$\gamma(s) = \frac{1 + \alpha^2}{\beta} \tag{3.15}$$

The solutions of Hill's equation defines an ellipse on which the particle is found:

$$\varepsilon = \gamma(s)\, x^2(s) + 2\, \alpha(s)\, x'(s) + \beta(s)\, x'^2(s) \tag{3.16}$$

[1] Although these functions are often referred to as Twiss functions, Twiss himself claims that they did not originate with him [16].

The shape and orientation of the ellipse are given by the Twiss functions (see left part of figure 3.2) and thus depend on the position $s$. However, the area is proportional to $\varepsilon$ and thus independent of the location. The emittance depends on the energy of the beam and shrinks with increasing energy. This effect is called adiabatic damping. However, the emittance can also be normalized to obtain a quantity invariant to a change in energy. The normalized emittance $\varepsilon_n$ is defined via the relativistic parameters $\gamma_{rel}$ and $\beta_{rel}$:

$$\varepsilon_n = \beta_{rel}\,\gamma_{rel}\,\varepsilon \tag{3.17}$$

For many applications it is also useful to normalize the phase space such that the ellipse is transformed into a circle (see right part of figure 3.2). However, the transformation must be set up to only scale $x$ and must not mix $x$ with $x'$, as the effect of a magnet on a particle depends solely on the particle's transverse position $x$ and not on its transverse momentum. For $x'$ this restriction is not necessary.

$$\begin{aligned} X &= \frac{x}{\sqrt{\beta\varepsilon}} \\ X' &= x'\sqrt{\frac{\beta}{\varepsilon}} + x\frac{\alpha}{\sqrt{\beta\varepsilon}} \end{aligned} \tag{3.18}$$

The term $\sqrt{\beta\varepsilon}$ gives the beam size.

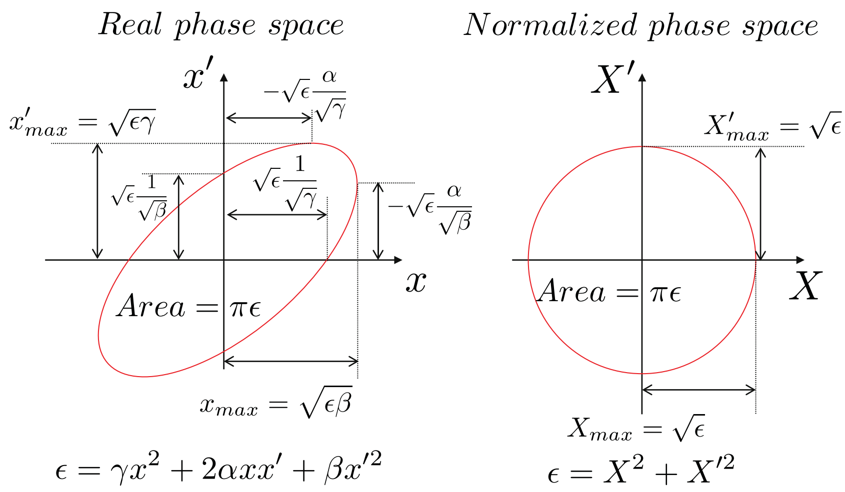


Figure 3.2: Trajectory of one particle in real and in normalized phase space

Like any linear differential equation, Hill's equation can also be represented by a matrix. This matrix is referred to as transfer matrix, because it allows the phase space coordinates ($x$, $x'$) to be transported from one position $s_1$ to another one $s_2$:

$$\begin{pmatrix} x_2 \\ x'_2 \end{pmatrix} = \begin{pmatrix} \sqrt{\frac{\beta_2}{\beta_1}}(\cos\Delta\mu + \alpha_1 \sin\Delta\mu) & \sqrt{\beta_1\beta_2}\sin\Delta\mu \\ \frac{\alpha_1-\alpha_2}{\sqrt{\beta_1\beta_2}}\cos\Delta\mu - \frac{1+\alpha_1\alpha_2}{\sqrt{\beta_1\beta_2}}\sin\Delta\mu & \sqrt{\frac{\beta_1}{\beta_2}}(\cos\Delta\mu - \alpha_2\sin\Delta\mu) \end{pmatrix} \begin{pmatrix} x_1 \\ x'_1 \end{pmatrix} \tag{3.19}$$

The transfer matrix can simply be calculated from the Twiss functions. However, the Twiss functions might be unknown. Then a matrix for each element in the accelerator lattice has to be computed according to that element's properties. In the next step the matrices of succeeding elements have to be multiplied to obtain an overall transfer matrix. From the transfer matrix for a whole revolution around the ring, a one turn map, the Twiss functions can be calculated by searching for the Eigenvalues. It must be kept in mind, that the assumption of a linear machine still applies to the considered accelerator[2].

These matrices provide a very efficient way to track particles with a single matrix multiplication between non-linear elements (e.g. sextupole magnets), which need to be handled separately as single elements. These non-linear elements are often represented by their thin lens models (see section 3.1.1).

The phase advance over a whole turn, meaning a complete revolution around a circular accelerator, is proportional to a quantity called the tune:

$$Q = \frac{\mu_{1\ Turn}}{2\pi} = \frac{1}{2\pi} \oint \frac{ds}{\beta(s)} \tag{3.20}$$

The tune gives the number of oscillations of a particle in phase space during one turn. The tune $Q$ can also be calculated from the transfer matrix for a whole turn by computing the eigenvalues of the matrix $\lambda = \exp(\pm iQ)$.

As long as coupling is neglected, all the properties like the tune and the Twiss functions can be defined and calculated separately for the two planes. So far the calculations have been shown for the $x$ plane. However, the situation is analogous in the y plane except that there is no bending under the assumptions made above.

In the longitudinal plane particles move around the accelerator according to their momentum. As the particles always have slightly different momenta, some particles move ahead while others fall behind. Thus, after some time the particles would be spread out over the whole circumference. Beside pure acceleration, RF cavities also have the capability to capture particles in longitudinal bunches by creating a potential that forces the particles to oscillate around the design momentum. Like in the transverse case a tune can be defined in the longitudinal plane, which is referred to as the synchrotron tune. The effects of the magnets on the particles depend on the momenta. Therefore, momentum deviations in a beam cause a coupling of the transverse and the longitudinal plane and cause effects such as dispersion and chromaticity.

[2]In a good approximation many elements in an accelerator such as dipole and quadrupole magnets can be seen as linear elements.

### 3.1.4 Dispersion

Dispersion describes the dependency of a particle's orbit on its energy. Energy deviations are considered in Hill's equation (3.10) by an inhomogeneity term. Solving the full Hill's equation gives a new orbit $x(s) = x_0(s) + \Delta x(s)$, which is the homogeneous solution $x_0$ plus a deviation depending on the energy offset. The proportionality factor between position shift $\Delta x$ and energy offset is called dispersion $D$.

$$\Delta x(s) = D(s)\,\frac{\Delta p}{p} \tag{3.21}$$

Analogously the derivative of the dispersion is defined as:

$$\Delta x'(s) = D'(s)\,\frac{\Delta p}{p} \tag{3.22}$$

The dependency of the bending properties of a dipole magnet on the particle momentum can already be seen in the magnetic rigidity (see equation (3.3)). With increasing momentum, stronger magnetic fields are necessary to achieve the same bending radius. Hence, the more energetic a particle is, the more resistant to bending, it is.

A non-zero dispersion leads to an increased beam size and causes a correlation of the particle's momentum and its transverse position. This can be desirable at certain points for measurement, correction or selection purposes or, as explained later, to apply the Hardt condition (see section 3.3.3) at extraction. However, at other positions zero dispersion is favorable e.g. in RF cavities or at particle collider interaction points.

The transfer matrix formalism can be extended to include these dispersive effects [17]. In equation (3.23) the transformation between the points 1 and 2 in one plane is given:

$$\begin{pmatrix} x_2 \\ x_2' \\ \frac{\Delta p}{p} \end{pmatrix} = \begin{bmatrix} m_{11} & m_{12} & m_{13} \\ m_{21} & m_{22} & m_{23} \\ 0 & 0 & 1 \end{bmatrix} \begin{pmatrix} x_1 \\ x_1' \\ \frac{\Delta p}{p} \end{pmatrix} \tag{3.23}$$

The terms connecting $x$ and $x'$ are the same as given earlier in equation (3.19) for the transfer matrix without dispersion. The new terms, introduced by dispersion and describing the coupling between the longitudinal and the transverse plane, have the following form:

$$\begin{aligned} m_{13} &= D_2 - m_{11}\,D_1 - m_{12}\,D_1' \\ m_{23} &= D_2' - m_{21}\,D_1 - m_{22}\,D_1' \end{aligned} \tag{3.24}$$

### 3.1.5 Chromaticity

The effect of focusing or de-focusing elements, such as quadrupole magnets, on a particle depends on its momentum. As the focusing properties affect the tune, a change in momentum alters the tune. The difference in tune $\Delta Q$ of an off-momentum and an on-momentum particle is referred to as chromaticity $Q'$:

$$\Delta Q = Q' \frac{\Delta p}{p} \tag{3.25}$$

If the RF system is turned on and a particle is captured, its momentum oscillates around the design momentum. Hence, its tune is also shifted periodically, which can cause stability problems (see section on resonances 3.2).

The chromaticity due to quadrupole effects can be calculated from lattice properties as shown below:

$$Q'_{quad} = -\frac{1}{4\pi} \oint k(s)\, \beta(s)\, ds \tag{3.26}$$

where $k$ denotes the normalized quadrupole gradient (3.9). In a thin lens approximation the integral can be replaced by a sum over all focusing elements in the ring.

Furthermore, a sextupole can also contribute to the chromaticity:

$$Q'_{6-pole} = -\frac{1}{4\pi} \oint k_2(s)\, \beta(s)\, D(s)\, ds \tag{3.27}$$

where $k_2$ gives the normalized sextupole gradient (3.8) and $D$ the dispersion function. Thus, a sextupole only affects the chromaticity in dispersive regions.

### 3.1.6 Transfer lines

In a circular machine the Twiss functions are defined by boundary conditions due to the periodicity of the lattice. However, in a transfer line such a constraint is missing. Hence, the Twiss functions are undefined except where additional information is supplied, e.g. Twiss functions at the exit of a circular machine - entry of transfer line. The Twiss parameters are then simply propagated from the beginning to the end of the transfer line.

If a particle distribution is given at the entrance of the transfer line, a phase space ellipse can be fitted around it, according to the beam shape. This ellipse then defines the Twiss functions. The propagation of this ellipse through the line depends on the transfer line elements and the transfer matrix formalism can be applied. So the lack of periodic conditions mean that the optics in a transfer line are solely defined by the strengths of the transfer line elements and by an initial beam ellipse.

## 3.2 Resonances

In a circular accelerator the particles are bent to follow a design orbit and are focused to perform stable oscillations around it by magnetic fields of dipole and quadrupole magnets. However, any deviation from this perfect guiding field can result in the excitation of resonant transverse particle motion. Such perturbations are inevitable as every accelerator contains multipoles. They can be placed in the machine by design like a sextupole magnet or enter the machine due to errors such as magnet imperfections.

In the following, the case of a single lattice perturbation is considered. If a particle returns after each turn with different phase space coordinates, the effects can level out. However, if the particle's tune is close to a betatron resonance:

$$n\,Q_x + m\,Q_y = p \tag{3.28}$$

where n, m and p are integers, the particle may get resonantly excited. Figure 3.3(a) displays several low order resonances in a tune footprint diagram. In the case of an uncoupled resonance of order $n$, the particle comes back with the same position and angle after $n$ turns, as it can be seen from equation (3.19) with $\mu = 2\pi\, n\, Q$. In this scenario a magnet of order 2n can excite resonant motion and its effects will add up. Hence, the particle's amplitude would increase and finally the particle can get lost. This is illustrated in figure 3.3(b) for a sextupole in an accelerator with a tune at the third integer. If resonances are coupled, energy can be transferred.

Therefore, the control of the tune and resonances is very important for the beam stability. However, the resonances can also be used to make particles unstable on purpose, for example to extract them.

### 3.2.1 Theory of third-order resonance

The third-order resonance can be excited by a sextupole magnet. In a good approximation it is possible to describe the effect of such a sextupole magnet as a perturbation to a linear accelerator lattice. First, a formulation of the magnetic field in the sextupole has to be established. The gap of a magnet is a current free volume. Thus, the field can be obtained as the negative gradient of a scalar potential $\Phi$. Under the assumption that the field only has transverse components, the potential of a magnet with $2\,m$ poles is given by:

$$\Phi = \underbrace{A_m\, Re(x+iy)^m}_{Skewmagnets} + \underbrace{B_m\, Im(x+iy)^m}_{Normalmagnets} \tag{3.29}$$

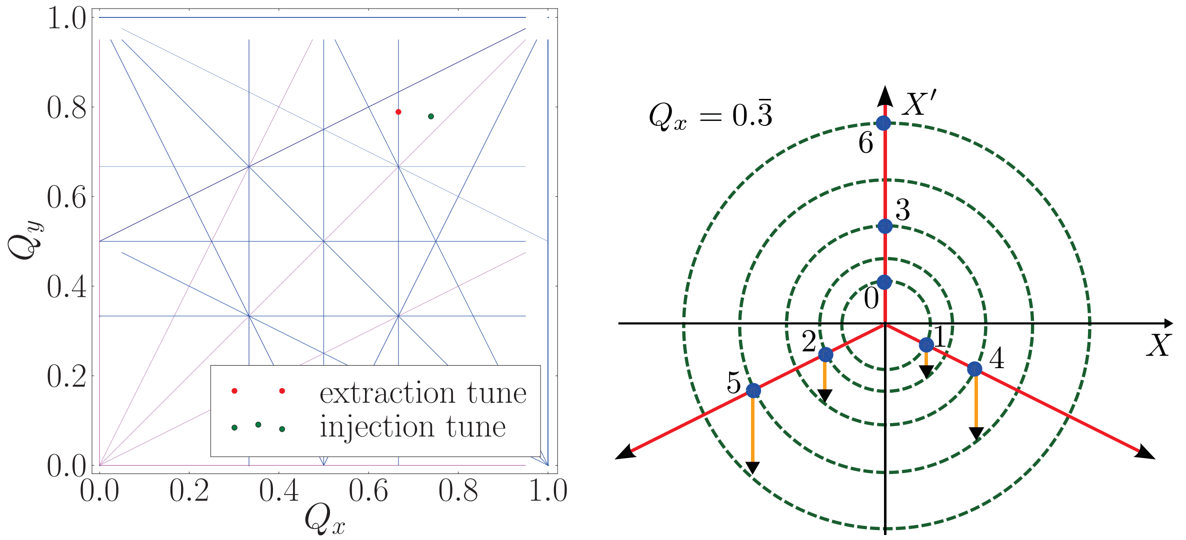


(a) Tune footprint: displays the first, second- and third-order resonance lines and points out the fractional part of the tune at injection and extraction for MedAustron

(b) Position in normalized phase space of (blue dots) and kick by sextupole (see equation (3.33)) (orange arrows) on particle with tune $Q_x = 1/3$ on 6 consecutive turns demonstrating unstable amplitude growth due to sextupole excitation of third-order resonance

Figure 3.3: Subfigure (a) shows a tune footprint and subfigure (b) displays beam dynamics with sextupolar excitation

The transverse field in a normal sextupole magnet ($m = 3$) is found by differentiation of the potential with respect to $x$ and $y$:

$$\vec{B}(x,y) = -\nabla\Phi = \begin{pmatrix} -6\,B_3\,x\,y \\ -3\,B_3(x^2 - y^2) \end{pmatrix} \tag{3.30}$$

An expression for the coefficient $B_3$ is obtained by comparing equation (3.30) with the Taylor expansion of the magnetic field in the horizontal plane (see equation (3.7)). This comparison yields:

$$B_3 = -\frac{1}{6}\left(\frac{d^2B_y}{dx^2}\right)_0 \tag{3.31}$$

Finally, the horizontal and vertical field components in a sextupole are given by:

$$\begin{aligned} B_x &= \left(\frac{d^2B_y}{dx^2}\right)_0 x\,y \\ B_y &= \frac{1}{2}\left(\frac{d^2B_y}{dx^2}\right)_0 (x^2 - y^2) \end{aligned} \tag{3.32}$$

In a thin lens approximation a sextupole only affects the direction $x'$ of a particle's motion (see section 3.1.1):

$$\begin{aligned} \Delta x' &= -\frac{B_y\, l_s}{|B\rho|} = -\frac{1}{2} k_2\, l_s (x^2 - y^2) \\ \Delta y' &= \frac{B_x\, l_s}{|B\rho|} = k_2\, l_s\, x\, y \end{aligned} \tag{3.33}$$

where $B_y$ and $B_x$ are the vertical and horizontal magnetic fields in the sextupole, $l_s$ the length of the magnet, $B\rho$ the particle's magnetic rigidity and $k_2$ is the normalized sextupole gradient (3.8).

In general a sextupole magnet couples the motion in the horizontal and the vertical plane as can be seen in equation (3.33). However, in the following a horizontal extraction is assumed, which means that resonance effects will occur only in $x$. Thus $y$ is much smaller than $x$. The vertical tune will always be kept away from the third-order resonance. Hence, the influence of the vertical motion can be neglected to first order.

Applying the normalization of the phase space described in equation (3.18) yields:

$$\Delta X' = S\, X^2 \tag{3.34}$$

where upper case letters denote normalized quantities like the normalized sextupole strength $S$:

$$S = \frac{1}{2}\, \beta_x^{3/2}\, k_2\, l_s \tag{3.35}$$

To describe the motion in the horizontal $x$ plane under the influence of a sextupole, a simplified Kobayashi Hamiltonian [18] can be used:

$$H = \frac{\varepsilon}{2}(X^2 + X'^2) + \frac{S}{4}(3\, X\, X'^2 - X^3) \tag{3.36}$$

where $\varepsilon = 6\pi\, \delta Q$ is called the modified tune distance with the tune distance $\delta Q = Q_{particle} - Q_{resonance}$ (difference of particle tune and resonant tune). In this approximation terms $O(\varepsilon^2)$ have been neglected.

The Hamiltonian uses three turns as the basic time unit, as the changes during this time are essential for the physics of the third-order resonance extraction. The first term of the Hamiltonian gives the unperturbed motion in the linearized accelerator, where the particle trajectories are circles in normalized phase space. The second term introduces the perturbation due to the sextupole magnet, which distorts the phase space trajectories into a triangular shape. This effect (see figure 3.4(a)) becomes stronger for larger amplitudes, until the excitation becomes too large and the previously closed trajectories open up. Particles on such trajectories become unstable. The trajectories separating the stable and unstable phase space areas are called separatrices, which form the largest stable triangle. From the Hamiltonian the fixed points can be computed from the condition $\partial H/\partial X = 0$ and $\partial H/\partial X' = 0$. As presented in figure 3.4(b), the system has one stable and three unstable fixed points, which give the three intersection points of the separatrices. With the unstable fixed points, the equations for the separatrices can also be derived from the Hamiltonian when $H(X,X') = H(X_f,X'_f)$, where the subscript f denotes one of the unstable fixed points. This yields the condition $H = [(2\varepsilon/3)^2/S^2]$ for the separatrices and their equations:

$$\left(\frac{S}{4}X + \frac{\varepsilon}{6}\right)\left(\sqrt{3}\,X' + X - \frac{4\,\varepsilon}{3\,S}\right)\left(\sqrt{3}\,X' - X + \frac{4\,\varepsilon}{3\,S}\right) = 0 \tag{3.37}$$

From this formula the equation for the three separatrices $A$, $B$ and $C$ follow immediately:

$$\begin{aligned} A: \quad & X = -\frac{2}{3}\frac{\varepsilon}{S} \\ B: \quad & -\frac{\sqrt{3}}{2}X' + \frac{1}{2}X = \frac{2}{3}\frac{\varepsilon}{S} \\ C: \quad & \frac{\sqrt{3}}{2}X' + \frac{1}{2}X = \frac{2}{3}\frac{\varepsilon}{S} \end{aligned} \tag{3.38}$$

From the equations for the separatrices or the unstable fixed points the area of the largest stable triangle (see figure 3.4(b)), also called the acceptance, can be calculated:

$$acceptance = \frac{4}{\sqrt{3}}\frac{\varepsilon^2}{S^2} = \frac{48\pi\sqrt{3}}{S^2}\,(\delta Q)^2\,\pi \tag{3.39}$$

Therefore, the stable area is determined by the ratio $|\varepsilon/S|$. Thus, for an on-resonance particle (i.e. $\varepsilon = 0$) the stable area is zero and the particle can not be stable. In general a particle is stable as long as its single particle emittance $\varepsilon_{particle} = A^2\,\pi$ , which is defined by its normalized amplitude[3] $A = \sqrt{X^2 + X'^2}$, is smaller than the acceptance. This gives the stability condition for particles:

$$\varepsilon_{stable} = A^2_{stable}\,\pi \leq \frac{48\pi\sqrt{3}}{S^2}\,(\delta Q)^2\,\pi \tag{3.40}$$

One should bear in mind that so far momentum dependent effects have not been taken into account. But, the simple Kobayashi Hamiltonian used above can be expanded such that it also describes the motion of off-momentum particles or the effects of closed orbit distortions. This is shown, in detail, in the PIMMS study [4], for example. Here only a few differences between on- and off-momentum particles are discussed briefly. In general, off-momentum particles oscillate around off-momentum equilibrium orbits that are not identical with the on-momentum one (see section 3.1). The difference between these equilibrium orbits is given by the dispersion functions. Hence, in dispersive parts of the accelerator in phase space the

[3] If the sextupole is ramped adiabatically, the amplitude A is equal in normalized phase space before and after the sextupole is activated

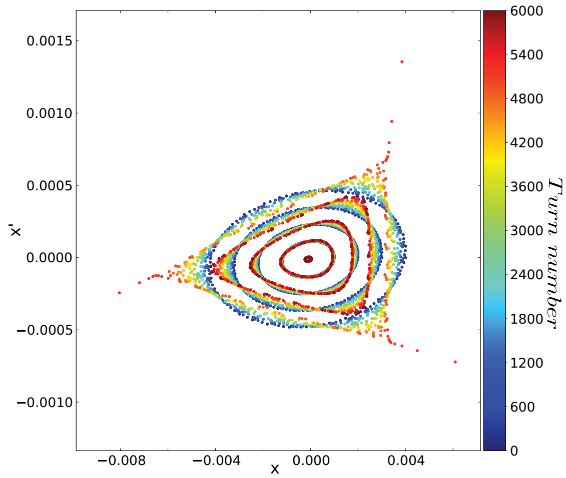


(a) Phase space map at the position of the resonant sextupole depicting the influence of the sextupole on the phase space trajectories of particles with different amplitudes, the color code gives the turn number and the sextupole is ramped for the first 2000 turns

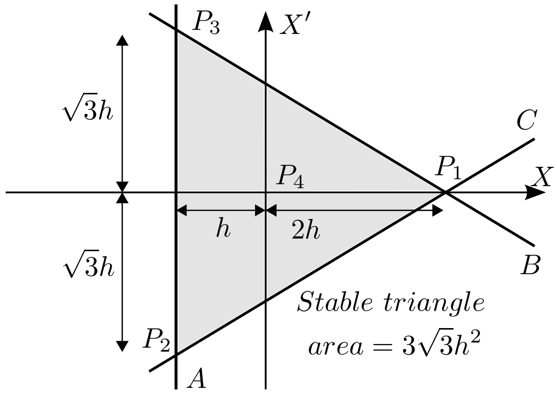


(b) Schematic drawing of the separatrices formed by the resonant sextupole

Figure 3.4: Subfigures (a) and (b) display phase space maps with sextupolar contributions

trajectories (e.g. the stable triangle) of off-momentum particles are shifted with respect to the on-momentum ones. Furthermore, in accelerators with finite chromaticity off-momentum particles have a different tune. Thus, the modified tune distance $\varepsilon$ is different according to the momentum and the size of the stable triangle in phase space as well.

So far only the situation at the sextupole[4], visualized in phase space maps, has been considered. However, it is also important to know the phase space maps at other positions around the accelerator. This transport is performed by applying the transfer matrix $M_{\Delta\mu}$[5] defined by the phase advance $\Delta\mu$ from the sextupole to a position s in the machine.

$$M_{\Delta\mu} = \begin{pmatrix} \cos(\Delta\mu) & \sin(\Delta\mu) \\ -\sin(\Delta\mu) & \cos(\Delta\mu) \end{pmatrix} \tag{3.41}$$

Only the orientation of the stable triangle changes, the size stays constant. In the same way the equation of the separatrices can be transformed. This yields a general form for a separatrix at any position $s$:

$$\left(X - D_n(s)\frac{\Delta p}{p}\right)\cos(\alpha_0 - \Delta\mu) + \left(X' - D_n'(s)\frac{\Delta p}{p}\right)\sin(\alpha_0 - \Delta\mu) = \frac{4\pi}{S}\delta Q \tag{3.42}$$

[4]The actual machine can also consists of several sextupole, however, for the physics behind the resonance excitation a single virtual sextupole (see section 3.3.2) representing all others is enough.

[5]In normalized coordinates the transfer matrix defined in equation (3.19) reduces to a simple phase space rotation matrix.

where the off-momentum effects are included via the normalized dispersion functions $D_n$ & $D'_n$ and $\alpha_0$ denotes the orientation of the separatrix at the sextupole, measured as an angle between the $x$-axis and the normal vector of the separatrix.

## 3.3 Extraction

After the beam has been accelerated in a circular machine, the particles have to be extracted in a way that fulfills the requirements on the extracted beam properties like spatial particle distribution, intensity, energy distribution, extraction time et cetera.

The extraction is performed by directing the beam into the extraction channel of a septum[6]. This septum (or a series of septa) deflects the beam into a transfer line. There are different ways to move the beam into the extraction channel:

- Fast extraction: A kicker magnet[7] is employed to deflect the entire beam into the septum in one turn.
- Non-resonant multi-turn extraction: An orbit bump[8] is used to deflect the whole beam onto the septum, but only a part immediately enters the septum. The tune is used to rotate the beam such that the rest of the beam enters the septum channel within the next turns. Also the bump can be varied to steer the extraction. This is a high loss process, because many particles hit the septum. Thus, a thin septum is crucial.
- Resonant multi-turn extraction: Non-linear fields are used to create stable islands in the phase space. By adjusting the tune, the particles are driven into the islands and captured there. By changing the field strength the islands can be separated in phase space. As in the previous case a bump is used to deflect the beam across the septum and the phase space rotation due to the tune is utilized to extract the islands in a few turns. The advantage of this technique is that it exhibits almost no particle losses.
- Slow resonant extraction: The three techniques mentioned so far extract the beam within a small number of turns. However, for irradiation in medical application a quasi-continuous flux of extracted particles is needed for much longer times, typically in the range of seconds, which corresponds to millions of turns. Slow resonant extraction schemes can offer such extraction times by using non-linear fields to excite a resonance and then by slowly driving the beam into the resonance. This method will be discussed in detail on the following pages.

[6] A septum is a magnetic or electrostatic device with a thin separation between zero field and high field regions.
[7] A kicker magnet is a pulsed magnet with very fast rise times, typical between 100 ns and a few μs
[8] An orbit bump is an arrangement of at least two dipole deflecting magnets with the aim to distort the closed orbit on purpose in one part of the machine without affecting the central orbit outside the bump.

### 3.3.1 Intuitive description of third-order resonance extraction

A third-order resonance slow extraction has been chosen for the hadron therapy at MedAustron. This is a slow resonant extraction method that employs a third-order resonance of the tune. This means the tune is an integer multiply of 1/3, e.g. the tune value of 5/3 has been chosen for MedAustron. This resonance can be excited by a sextupole magnet. A particle that fulfills the resonance condition becomes unstable. Thus, the amplitude of the unstable particle grows, until it reaches a septum, which is positioned to the outside of the beam pipe. Finally, the septum deflects the particle into a transfer line.

During injection and acceleration the machine is carefully tuned away from the third-order resonance[9] to allow for stable particle motion. Only for extraction the tune is moved towards the resonance and instability. This can be achieved by different means. The particle tune depends on three components: the lattice itself, the momentum of particles and their amplitude[10]. A change in any of the components can be used to drive particles into the resonance.

- Lattice: Quadrupole magnets are used to change the lattice tune.
- Momentum: Acceleration is utilized to alter the particles' momenta and thus their tunes via the chromaticity. This method is referred to as acceleration driven extraction. The necessary change in momentum can be achieved by different means like inductive acceleration via a betatron core (see section 4.2.1), application of RF-noise on the beam (see section 4.4.1) or empty bucket acceleration[11].
- Amplitude: The beam is transversely blown up to alter the tune via the amplitude. A common method is RF-knockout, where transverse excitation of the particles is employed to blow up the beam. For more details see section 4.3.1.
- Further alternative: The techniques mentioned so far are only the most commonly used ones. However, one can think of other possibilities to influence the tune such as changing the chromaticity, altering the strength of a sextupole or employing an octupole magnet.

To obtain the intended extraction times, the particles in the ”waiting” beam have to be brought continuously into resonance over that time. This is achieved by creating a ”waiting” beam with a certain spread in the property that is changed to reach the resonance (e.g. momentum or amplitude) and by positioning the resonance line accordingly. Moreover, the strength of the element that drives the extraction has to be chosen in accordance with the targeted extraction time.

[9] Actually, it has to be watched out also for other resonances especially the lower order ones like the integer and half integer resonance. The particles have to be kept in safe distance to these resonances to avoid unwanted beam loss

[10] The amplitude only has an influence in the presence of non linear elements in the accelerator such as a sextupole magnet.

[11] This method is not subject of this thesis, but further information can be found in [19].

A simple way to visualize stability, resonance and extraction is to employ Steinbach diagrams, which show the particles and resonance in amplitude - momentum / tune space. Figure 3.5 shows a typical Steinbach diagram, where the beam is positioned in a stable region. The width of the unstable zone at a given emittance can be calculated from the stability condition (3.40) and is called stopband.

## 3.3.2 Virtual sextupole

So far only one sextupole has been considered. However, a real accelerator normally consists of several sextupole magnets. The overall effect of these sextupoles on a resonance can be described by the 'driving term' $\kappa$ [20]. The driving term for the third-order resonance is written as:

$$\kappa = -\frac{1}{12\sqrt{\pi C}} \sum_n S_n \exp(3i\, \mu_{x,n}) \tag{3.43}$$

The sum of the sextupoles in the driving term can be replaced by a single virtual sextupole with the virtual sextupole strength

$$S_{virt}^2 = \left(\sum_n S_n \sin(3\,\mu_{x,n})\right)^2 + \left(\sum_n S_n \cos(3\,\mu_{x,n})\right)^2 \tag{3.44}$$

and the phase advance of the virtual sextupole

$$\mu_{x,virt} = \frac{1}{3} \arctan\left(\frac{\sum_n S_n \sin(3\,\mu_{x,n})}{\sum_n S_n \cos(3\,\mu_{x,n})}\right) \tag{3.45}$$

which determines where the virtual sextupole is placed in the machine. The description with this virtual sextupole is equivalent to the single sextupoles regarding the excitation of the resonance.

## 3.3.3 Hardt condition

Particles with different momenta, which are close to resonance but still stable, can be found on stable triangles of different size in phase space due to tune shifts via the chromaticity. Additionally, in dispersive regions of the accelerator the triangles are shifted according to their momenta due to dispersion. In general, as soon as these particles become unstable, they will also follow different separatrices. Therefore, they will arrive at the electrostatic extraction septum at different angles. This leads to higher particle losses at the septum and unfavorable spill characteristics.

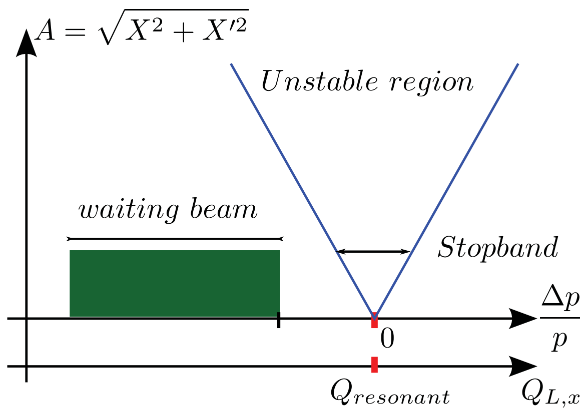


Figure 3.5: Steinbach diagram displaying typical "waiting" beam

The situation can be improved by trying to superimpose the extraction separatrices at the electrostatic extraction septum. Analytically, this can be achieved by removing the momentum dependency in the equation of the separatrices (3.42). In the following it is assumed that the tune distance is determined by the chromatic tune shift due to the momentum difference between the particles. The Hardt condition [21] gives an equation for the superposition of the separatrices:

$$D_n \cos(\alpha - \Delta\mu) + D'_n \sin(\alpha - \Delta\mu) = -\frac{4\pi}{S} Q' \tag{3.46}$$

where $(D_n, D'_n)$ is the normalized dispersion vector at the electrostatic septum, $\alpha$ the orientation of the separatrix at the resonant sextupole, $\Delta\mu$ the phase advance from the resonant sextupole to the electrostatic extraction septum and $S$ the normalized sextupole strength. These values are often determined by other constraints, hence the chromaticity $Q'$ is used to fulfill the Hardt condition. Furthermore, the equation shows that the an efficient lattice for the Hardt condition has a normalized dispersion vector that is orthogonal to the extraction separatrix at the electrostatic extraction septum. A special case is, if the chromaticity is zero, because then the Hardt condition is fulfilled for zero dispersion at the location of interest.

It has to be pointed out that the Hardt condition can not be fulfilled at one time for all three branches of separatrices. The Hardt condition for one superimposed branch of separatrices is illustrated in figure 3.6.

### 3.3.4 Spiral step and spiral kick

After a particle becomes unstable, its amplitude starts to increase, because the particle is in third-order resonance and the kicks from the resonant sextupole add up every turn. While the

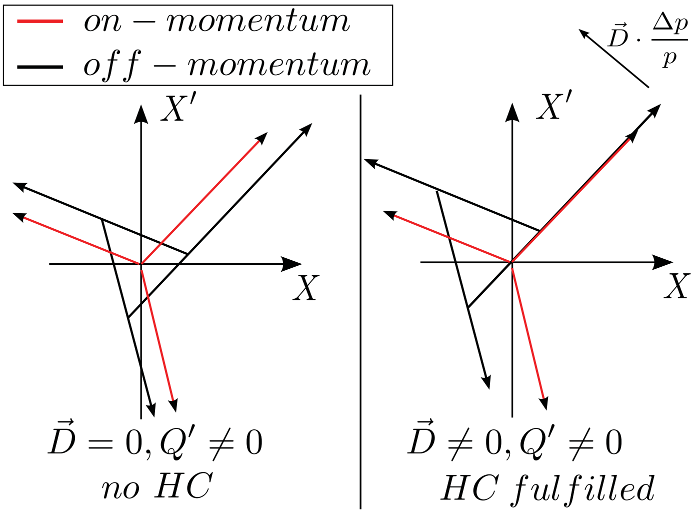


Figure 3.6: Schematic drawing of separatrices to illustrate the Hardt condition (HC), on the left without dispersion the separatrices are not superimposed, on the right with dispersion and an according chromaticity one branch of the separatrices is superimposed

particle moves outwards along the separatrices, it jumps from one separatrix to the next every turn, because its fractional tune is 1/3. After three turns the particle will be back at the same separatrix, only at a larger amplitude. These increases in amplitude during three turns split up into its $x$ and $x'$ contributions, are called the spiral step $\Delta x$ and the spiral kick $\Delta x'$. These two quantities at the sextupole can be obtained by calculating the Hamiltonian equations of motion from the Kobayashi Hamiltonian (3.36):

$$\Delta X = \frac{\partial H}{\partial X'} = \varepsilon\, X' + \frac{3}{2}\, S\, X\, X \tag{3.47}$$

$$\Delta X' = -\frac{\partial H}{\partial X} = -\varepsilon\, X + \frac{3}{4}\, S\, (X^2 - X'^2) \tag{3.48}$$

with the modified tune distance $\varepsilon = 6\pi\, \Delta Q$.

So far only the spiral step and kick at the sextupole have been considered. However, for the extraction the motion of the particles have to be evaluated everywhere along the accelerator for aperture considerations and especially at the electrostatic extraction septum to obtain the properties of the extracted beam. Hence, in the following the electrostatic extraction septum is chosen as the position of interest. Starting from the equations for the spiral step (3.47) and kick (3.48) at the sextupole an equation valid along the machine is derived. As these equations describe the motion of a particle on the separatrices, the equations for a single separatrix (see equation (3.38)) can be inserted. All separatrices are equal, thus the one with the easiest form is chosen, separatrix $A$ with $X = -(2\varepsilon)/(3S)$. For the spiral step and kick at the sextupole, this yields:

$$\begin{aligned} \Delta X &= 0 \\ \Delta X' &= \frac{\varepsilon^2}{S} - \frac{3}{4}\, S\, X'^{\,2} \end{aligned} \tag{3.49}$$

These equations can be transported to any position along the accelerator by applying a transfer matrix (see equation (3.41)) in normalized coordinates with the phase advance $\Delta\mu$ between the sextupole (MXR) and the element of interest, e.g. the septum (ESE).

$$\begin{pmatrix} \Delta X \\ \Delta X' \end{pmatrix}_{ESE} = \begin{bmatrix} \cos(\Delta\mu) & \sin(\Delta\mu) \\ -\sin(\Delta\mu) & \cos(\Delta\mu) \end{bmatrix} \begin{pmatrix} \Delta X \\ \Delta X' \end{pmatrix}_{MXR} \tag{3.50}$$

The transport of the separatrices from the MXR to the ESE is schematically demonstrated in figure 3.7.

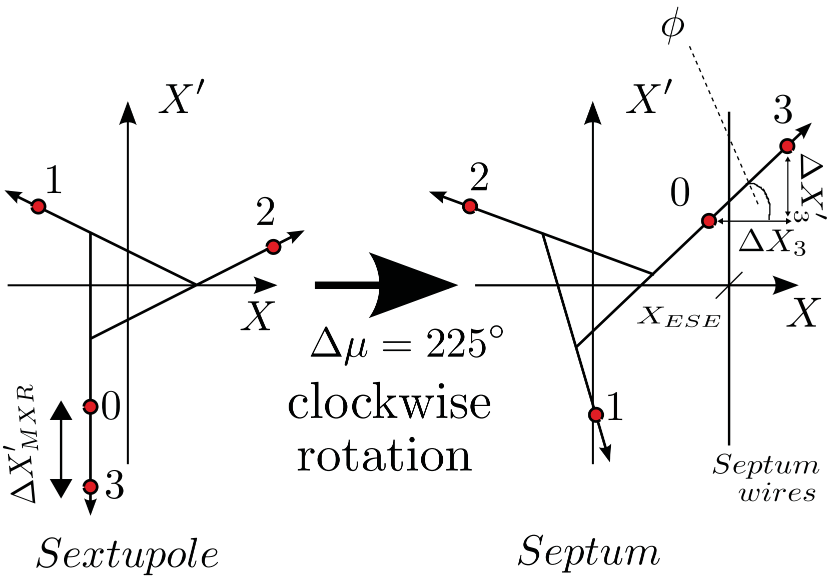


Figure 3.7: Schematic drawing of the transport of the separatrices from the resonant sextupole to the electrostatic extraction septum

Inserting equations (3.49) into (3.50) and computing the matrix-vector product gives an equation for the spiral step at the septum (ESE):

$$\Delta X_{ESE} = sin(\Delta\mu)\, \Delta X'_{MXR} = \left( \frac{\varepsilon^2}{S} - \frac{3}{4}\, S\, (X'_{MXR})^2 \right) \sin(\Delta\mu) \tag{3.51}$$

To get rid of the $X'$ coordinate at the sextupole, it can be expressed by the amplitude $A$ and the distance $h$ of the separatrix to the $y$-axis (see figure 3.4(b)):

$$\Delta X_{ESE} = \left( \frac{\varepsilon^2}{S} - \frac{3}{4}\, S\, (A^2 - h^2) \right) \sin(\Delta\mu) \tag{3.52}$$

Inserting $A^2 = X^2 + X'^2$ and $h = -(2\varepsilon)/(3S)$ yields:

$$\Delta X_{ESE} = \left( \frac{4\,\varepsilon^2}{3\,S} - \frac{3}{4}\,S\,\left((X_{ESE})^2 + (X'_{ESE})^2\right) \right)\,\sin(\Delta\mu) \tag{3.53}$$

With some trigonometric function gymnastics the $\sin(\Delta\mu)$ - term can be rewritten in terms of the angle between the separatrix at the septum and the $x$-axis[12]. In this form the spiral step is just given as the projection of a general change in amplitude onto the $x$-axis:

$$\Delta X_{ESE} = \left( \frac{3}{4}\,S\,\left((X_{ESE})^2 + (X'_{ESE})^2\right) - \frac{4\,\varepsilon^2}{3\,S} \right)\,\cos(\phi) \tag{3.54}$$

A slightly different notation is also common. In equation (3.51) the amplitude can alternatively be expressed in terms of the septum position and the angle $\phi$ between separatrix and $x$-axis as $A_{ESE} = X_{ESE}/\cos(\phi)$. This gives:

$$\Delta X_{ESE} = \left( \frac{3}{4}\,S\,\left(\frac{X_{ESE}}{\cos(\phi)}\right)^2 - \frac{4\,\varepsilon^2}{3\,S} \right)\,\cos(\phi) \tag{3.55}$$

The spiral kick can be obtained by projecting the onto the $x'$ axis, which is equivalent to replacing the cos-term with a sin-term.

For on-resonance particles ($\varepsilon = 0$) equation (3.55) further simplifies to:

$$\Delta X_{ESE} = \frac{3}{4}\,S\,\frac{X_{ESE}^2}{\cos(\phi)} \tag{3.56}$$

So far dispersion has not been considered. However, in a real machine there will be dispersion. In dispersive regions off-momentum particles will be shifted according to the dispersion vector. Hence, the stable triangles and separatrices are moved in phase space accordingly. Therefore, it is convenient to introduce a new coordinate system which has its origin on the off-momentum closed orbit. Coordinates given in the new frame will be denoted with the subscript 'off'. The transformation between the normally used coordinate system and the new one is given by the dispersion vector and the momentum deviation:

$$X_{off} = X - D_n\,\frac{\Delta p}{p} \tag{3.57}$$

$$X'_{off} = X' - D'_n\,\frac{\Delta p}{p} \tag{3.58}$$

where the coordinates and dispersion are normalized.

[12] $\sin(\Delta\mu) = \cos(\frac{\pi}{2} - \Delta\mu) = -\cos(\frac{3\pi}{2} - \Delta\mu) = -\cos(\phi)$

Via a sextupole, dispersion can also affect the chromaticity and thus the tune of off-momentum particles. However, in the following it is assumed, that the sextupole, which excites the resonance, is placed in a dispersion free region. Therefore, the modified tune distance is not affected by the dispersion.

Further it is assumed that the septum is placed in a dispersive region. Thus, the spiral step at the septum has to be reconsidered. The derivation of the spiral step given above can be regarded to as done in the new off-momentum coordinate system. Thus, equation (3.54) has to be transformed into the normal coordinate system with its origin on the on-momentum closed orbit. As the transformation is a simple translation, lengths and angles remain constant and only absolute coordinates are changing. Applying the transformation rules in equations (3.57) and (3.58) to equation (3.54) yields:

$$\Delta X_{ESE} = \left( \frac{3}{4} S \left( \left( X_{ESE} - D_{n,ESE} \frac{\Delta p}{p} \right)^2 + \left( X'_{ESE} - D'_{n,ESE} \frac{\Delta p}{p} \right)^2 \right) - \frac{4\,\varepsilon^2}{3\,S} \right) \cos(\phi) \quad (3.59)$$

In the following the terms spiral step or kick refer to the last step a particle does, during which it jumps into the septum. These two values are crucial to any later application of the extracted particles, as they strongly influence the shape and size of the extracted beam.

Therefore, the spiral step has to be optimized according to the requirements on the extracted beam. The spiral step depends on the following components. (The following considerations concentrate on the maximum possible spiral step, which is encountered by particles that have almost hit the septum, three turns before they jump into it.)

- The normalized sextupole strength $S$: This value is constant for all particles and usually constant during the extraction[13]. Nevertheless, the value of S can be chosen in accordance to the capabilities of the sextupole.
- The phase space position $X$, $X'$ or the amplitude $A$ of the particle: This dependency explains the increase of the steps while a particle moves along a separatrix. For the final spiral step into the septum the position in $X$ is more or less fixed by the position of the septum itself. However, the position of the septum is alterable to some degree, so here adjustment for fine tuning is possible, but still equal for all particles. The position in $X'$ is varying over some distance for different particles, depending on the separatrix they are following e.g. due to the momentum spread. But the better the Hardt condition is fulfilled the narrower the band in $X'$ will be. Moreover, there are further constraints on the separatrices like the phase advance from the sextupole to the septum.

[13] Normally the main sextupole responsible for exciting of the third-order resonance will be ramped adiabatically before the extraction starts. However, extraction could also be achieved by changing a sextupole strength, but this method is not considered to be suitable as enormous sextupole strength would be necessary to extract low amplitude particles.

- For off-momentum particles the spiral step/kick depends on the dispersion at the septum. The dispersion shifts the stable triangle of an off-momentum particle, hence the distance between the triangle and the septum is changed. Therefore, depending on the dispersion vector the particle moves further/less on the separatrix compared to an on-momentum particle. The longer a particle moves on the separatrix, the more the spiral step increases.
- The modified tune distance $\varepsilon$: This value consists of the different tune contributions and decreases the spiral step the further the particle tune is away from the resonant tune. Which contribution is of interest depends on the extraction mechanism. The lattice part, representing the effects from the quadrupole fields, is constant for all particles as long as the quadrupole settings are maintained at constant values. The amplitude one changes while a particle moves along the separatrices. This amplitude dependent tune shift, which is a second order effect, bends the separatrices. Furthermore, for RF Knockout an amplitude increase is used to make the particle unstable. However, for the final spiral step into the septum the amplitude part is similar for all particles, because the last position is similar as explained above. Finally, the chromatic one is not constant, but depends on the momentum of the particle. The more off-momentum a particle with non-zero betatron amplitude, the smaller the spiral step it encounters.

### 3.3.5 Shape of extracted beam

An important property of the extracted beam is its shape, as the shape has to fit later applications and following elements such as transfer lines.

Before the extraction process starts, the beam can be approximated by Gaussian profiles in both planes, horizontal and vertical. In the following it is assumed that the resonant extraction affects only the motion in the horizontal $x$ plane, because the vertical tune is kept away from the third integer resonance. Hence, the shape in the vertical plane remains Gaussian in the extracted beam. However, in the horizontal plane the motion of the particles is strongly affected by the resonant extraction. The unstable particles are slowly moving along the separatrices as it is described in equations (3.47) and (3.48) until they reach a septum. This means the size of the extracted beam segment is only determined by the spiral step and kick of the single particles and how well the Hardt condition is applied. In phase space the extracted distribution is limited in $x$ by the position of the septum and the maximum possible spiral step (see section 3.3.4). As particles jump from different distances to the foil (of course smaller than the next spiral step) into the septum and particles with different momenta experience different spiral steps, the whole distance between the septum foil and the maximum spiral step is filled (not homogeneously) with particles. This is illustrated schematically in figure 3.8(a) and with simulation results in figure 3.8(b). The distribution in $x'$ is given by the spiral kicks and the Hardt condition or how well the separatrices for different momenta are superimposed. However, even in case of a perfectly fulfilled Hardt condition there will always be some, however small compared to $x$, spread in $x'$ as the separatrices belong to different amplitudes and hence the amplitude dependent detuning from the sextupoles bends the separatrices differently. Combining these limits the extracted beam will have a rectangular or more trapezoidal shape in phase space. This special shape is called ”bar of charge”.

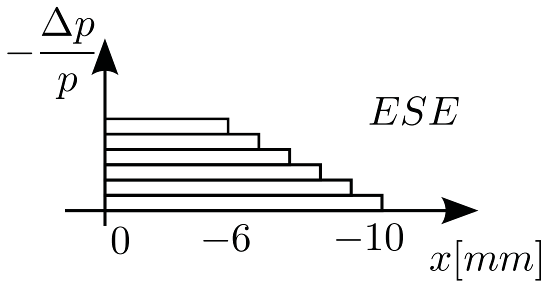


(a) Schematic drawing of a ”bar of charge”

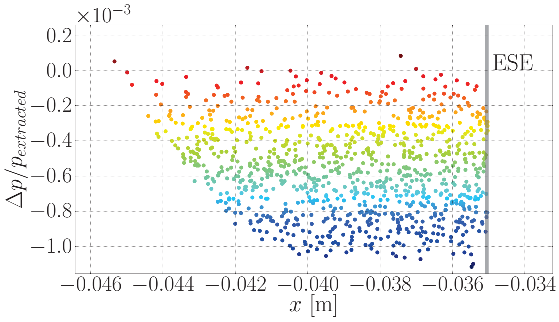


(b) Plot from tracking studies showing the ”bar of charge”

Figure 3.8: Subfigures (a) and (b) display the ”bar of charge” at the electrostatic extraction septum

The ”bar of charge” can not be described by normal beam optics. However, it is possible to fit an ellipse in phase space around the bar. Although, this ellipse is not giving the real shape of the beam, it allows the use of the normal beam optics formalism with Twiss functions. The shape of the ”bar of charge” itself can be influenced via the dispersion function as the particles in the bar are separated to some extent by their momentum .

The special shape of the ”bar of charge” introduces an additional handle for beam size control. In a Gaussian shaped beam, as it still exists in the vertical plane of this extraction example, the beam size can only be controlled by focusing and defocusing and is bound to the Twiss functions. However, due to the asymmetry of the bar of charge in $x$ and $x'$ a rotation of the bar changes the beam size, as only the projection onto $x$ decides the beam size. When passing beam line elements such a rotation happens according to the phase advance. Hence, by controlling the phase advance also the beam size can be changed in the limits (assuming a zero-dispersion region) given by the maximum spiral step and the extent in $x'$. However, if the dispersion is not zero, the dispersion also affects and can be used to influence the beam size by shifting the bars of charge according to their momenta. Additionally, it is still possible to alter the focusing properties of the lattice to affect the beam size. Thus, the ”bar of charge” allows a high flexibility in the beam size, which is of special interest for medical applications.

# 4 Simulation and Optimization of the Extraction

This chapter discusses the work done on the extraction from the MedAustron synchrotron. First, the simulation tools that have been employed are introduced. Next the nominal extraction method i.e. the betatron core driven extraction is examined. Finally, alternatives to the betatron core method like RF-knockout or RF-noise are discussed.

## 4.1 Tracking

### 4.1.1 Tools used for tracking studies and simulations

#### WinAgile

WinAgile (Alternating Gradient Interactive Lattice Design) [22] is a simulation program by Philip J. Bryant for designing accelerator lattices for the MS Windows platform. The program also runs under Linux in an API-emulator like ”Wine”. Philip J. Bryant describes the program in [22] as following:

*“AGILE is a program that works in the IBM-PC, MS-Windows environment and is dedicated to the interactive design of alternating-gradient lattices for synchrotrons and transfer lines. . . . It contains original algorithms for coupling, scattering and eddy currents, and some slightly unusual algorithms for off-axis orbits and space charge. There are also additional features such as engineering design aids, calculators for relativistic and synchrotron radiation parameters, expert routines for optimizing slow extraction, fitting and matching, and the internal storage of constants for over 1000 stable and quasi-stable charged particles. . . . It is particularly suited to practical problems in small and medium-sized rings and transfer lines.”*

WinAgile has been used in the framework of this thesis because of the availability of advanced tools specific for simulating the third-order extraction allowing to make fast optimizations.

### TrackIt!

A central task of this thesis was the further development, enhancement and testing of the particle tracking code TrackIt! [23], which has been programmed in Python [24]. The code structure is designed flexible enough to e.g. allow to choose from different extraction schemes such as betatron core driven extraction or RF-knockout. The tracking-code is part of a code-framework which allows e.g. an easy interface to the MAD-X [25] simulation code or an efficient way to create various different kinds of particle distributions and to visualize/ analyze them.

In order to speed up the computations, a condensed lattice formalism is used, where consecutive elements are lumped together into one transfer matrix. To account for the non-linear effects of and the coupling between the transverse planes due to sextupole magnets, the latter are treated explicitly in a thin lens approximation (see equations (3.33)). To increase the accuracy of the approximation each sextupole is split up into two slices, each representing one half of the sextupoles strength. The two slices are positioned at the two ends of the magnet with a drift section in-between. This way the chromaticity due to the sextupoles is handled.

Furthermore, the code allows to change element parameters as a function of time (turn number) via a generic ramp function. This feature is required to simulate extraction schemes with variable element parameters and to adiabatically turn on the resonant sextupole. The latter is of crucial importance for the emittance conservation and will be discussed in section 4.1.2.

As the linear transfer matrices do not account for the lattice chromaticity, a ”fake” chromaticity rotation element is used. This element employs a one turn phase space rotation that adjusts the phase advance in the machine according to the tune change due to chromaticity and momentum deviation of a particle. This approximation accounts for the chromaticity of the quadrupoles only at a single location in the lattice, whereas in real accelerator the magnets are placed along the ring and thus also their contributions to the chromaticity.

The code allows to add a number of ”special elements” like kicks from e.g. a tune kicker, acceleration by a betatron core, aperture limitations et cetera :

- All special elements that act on one of the phase space coordinates of a particle like a betatron core or a transverse kicker magnets, can be implemented via the simple ”shift-module”. This module allows to influence each coordinate separately. The kicks applied by this shift element can be constant or ramped according to a given function or a provided array.
- The final aperture element stops the tracking for a particle that hits a limitation. Furthermore, the position and the time stamp (turn number) is saved. However, for the other particles the tracking goes on. This element can also be used to determine when a particle has entered an extraction channel.

- Additional tune shifts or chromaticity can be introduced via the phase space rotation element. This element can also be combined with a ramp function e.g. to simulate the extraction via a continuous tune shift.

### 4.1.2 Testing TrackIt!

#### Resonant sextupole

To test TrackIt! the influence of a strong sextupole on a particle was examined. In the presence of a sextupole the phase space ellipse of a particle close to the third-order resonance is distorted into a triangle. If the sextupole is not ramped adiabatically, the particle could be assigned to a wrong triangle (see figure 4.1). A particle on a wrong triangle would not reflect the reality and lead to an emittance growth. However, using the ramp function of TrackIt! it is possible to adiabatically turn on the sextupole and thus fulfill the conservation of the emittance.

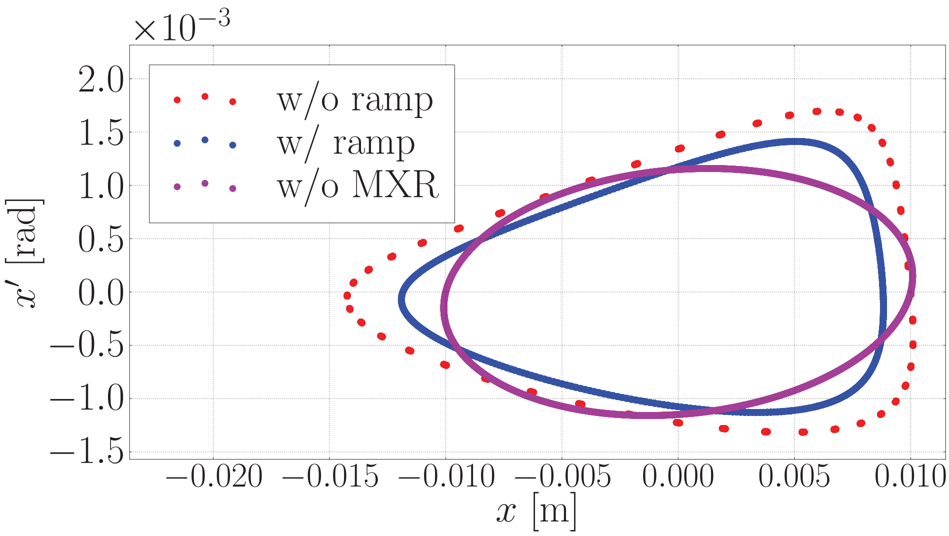


Figure 4.1: Phase space map (x-x') at the resonant sextupole (MXR) displaying the trajectories of three particles with identical initial coordinates but tracked in different set ups: a) the MXR is turned on from the very beginning, b) the MXR is ramped over 2000 turns, c) the MXR is turned off

#### Particle tune

To further test TrackIt!, the code was used to demonstrate different influences on the particle tune. The tune of a particle $Q_T$ consists of two contributions:

- The lattice tune, which is determined by the focusing and de-focusing characteristics of the lattice elements.
- Chromatic tune shift: a momentum deviation shifts the tune due to the chromaticity (see section 3.1.5).
- Furthermore, if there are non-linear elements in the ring such as sextupoles, the particle tune is also sensitive to the amplitude of the betatron oscillations of the particle.

These different contributions can be seen in tracking studies shown in figures (4.2(a)) to (4.2(d)). Particles were tracked for $10^5$ turns in the MedAustron extraction lattice with a horizontal lattice tune of $Q_x = 1.676$ instead of the nominal horizontal extraction tune of $Q_x = 1.666$ in order to avoid the unstable zone created by the resonant sextupole.

Figure 4.2(a) shows the Fast Fourier Transform (FFT) of five particles with the same small momentum deviation from the nominal momentum of $\Delta p/p = -1 \cdot 10^{-6}$ but different amplitudes. The particles were tracked in a lattice without sextupoles to suppress non-linear effects and hence the amplitude dependent contribution to the tune. All five particles exhibited the lattice tune, so the momentum and amplitude dependent parts were zero or too small to have an impact.

The next figure 4.2(b) depicts the FFT of five particles with the same very small amplitude $A = 2.5 \cdot 10^{-7}$ but different momenta. The tracking was done in a lattice which includes sextupoles, however, the particles' amplitudes were chosen sufficiently small to have no impact. The momentum dependence of the particle tune can be seen immediately. From the FFT the chromaticity in this case calculates to be about $Q'_x \approx -4.4$, which is quite close to the value of $Q'_x \approx -4.36$ obtained from WinAgile.

In the following figure 4.2(c) the FFT is plotted for five particles with the same small momentum deviation from the nominal momentum of $\Delta p/p = -1 \cdot 10^{-6}$ but different amplitudes. For better visibility figure 4.3 presents a zoom into figure 4.2(c). In contrast to figure 4.2(a), in this case the sextupoles were included in the underlying tracking job. Hence, the particle tune was shifted by the amplitude dependence due to the non- linearities in the lattice. A fit to the data points in an amplitude - tune diagram shows approximately a quadratic behavior of the tune shift with a fit function of $\Delta Q_x \approx -262.15 \cdot A^{2.18}$.

Finally, figure 4.2(d) shows the FFT of four particles with the same momentum deviation of $\Delta p/p = -2 \cdot 10^{-3}$ but different amplitudes. The de-tuning with increasing amplitude is visible, however the amplitude effect is not as strong as in figure 4.3. Therefore, a simple sum of the different contributing terms to obtain the particle tune is only an approximation.

Figure 4.4 also demonstrates the amplitude dependent de-tuning. This figure presents the phase space map of four on-momentum particles with different initial amplitudes, which were tracked for 5000 turns. As the lattice tune is slightly above the third-order resonance, the two

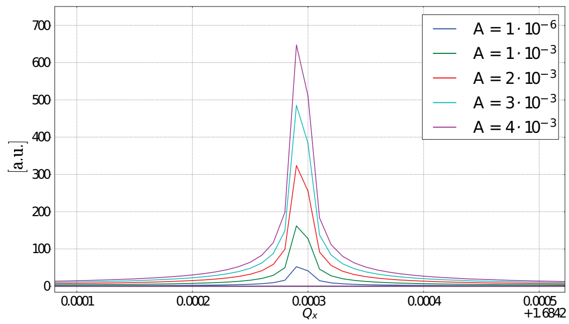


(a) FFT of five particles very close to the nominal momentum ($\Delta p/p = -1 \cdot 10^{-6}$) but different amplitudes A, tracked in a linear ring (no sextupoles)

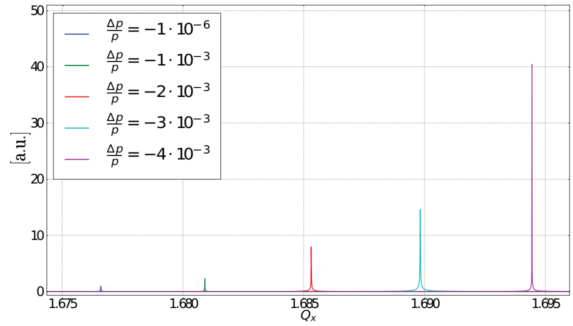


(b) FFT of five particles with almost zero amplitude $A = 10^{-6}$ but different momenta

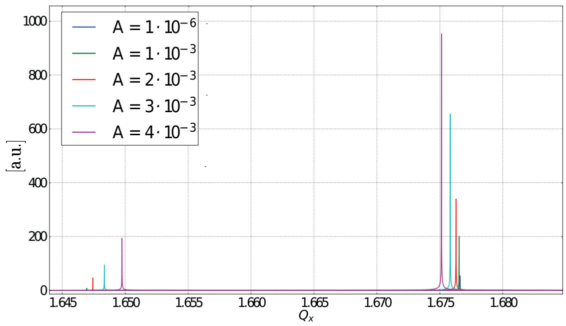


(c) FFT for five particles very close to the nominal momentum ($\Delta p/p = -1 \cdot 10^{-6}$) but different amplitudes A, tracked in a lattice including sextupoles

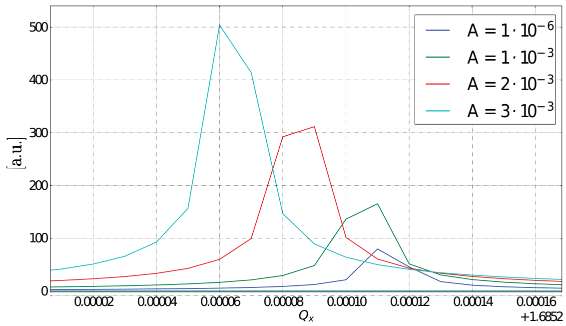


(d) FFT of four particles with the same momenta $\Delta p/p = -2 \cdot 10^{-3}$ but different amplitudes A with $Q' = -4.4$

Figure 4.2: Subfigures (a), (b), (c) and (d) show the horizontal tune $Q_x$ obtained from Fast Fourier Transforms (FFTs) of tracking jobs with $10^5$ turns

particles with smaller amplitudes remain stable. However, the two particles with higher amplitudes become unstable and their amplitudes further increase. As no aperture limitations are included in the tracking job, the amplitudes increase until the amplitude dependent de-tuning drives the particles out of third-order resonance and into the second order resonance. This leads to decreasing amplitudes. However, with decreasing amplitude the tune also approaches the third-order resonance again and the procedure starts over again.

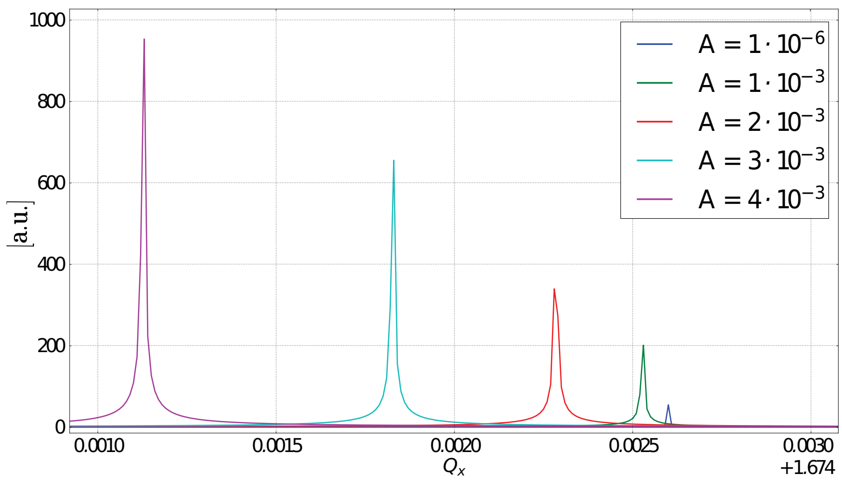


Figure 4.3: Zoom into figure 4.2(c) to point out the amplitude dependency of the particle tune

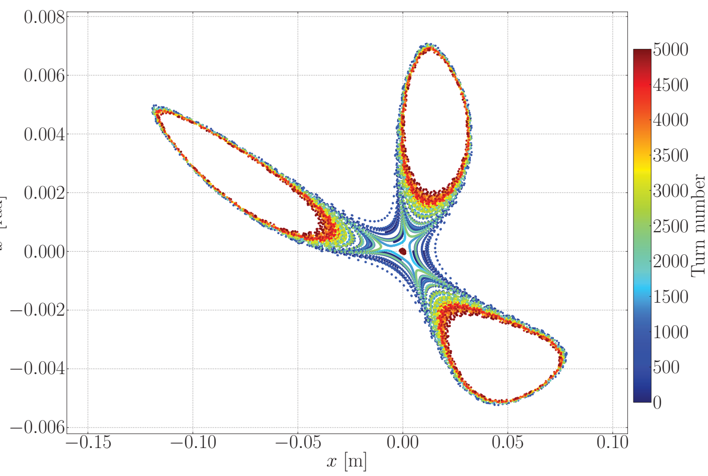


Figure 4.4: Amplitude dependent de-tuning without an aperture limitation. The color indicates the turn number.

## 4.2 Betatron core driven extraction

### 4.2.1 Overview

The betatron core driven extraction is the nominal extraction process for the clinical irradiation at MedAustron. This method is a special form of acceleration driven extraction where induction acceleration is employed to alter the particles' tunes via the chromaticity. As the horizontal chromaticity in the MedAustron lattice is negative, acceleration causes the particle's tune to be reduced. The betatron core set up can be described in analogy to a transformer, where the current windings connected to the power converter are the primary windings and the beam itself is the secondary. The betatron core [26] itself is a closed magnetic circuit which has to be a highly inductive element with a large time constant to reduce the effect of current ripples. Thus, the betatron core is realized as a ferromagnetic ring, which is centered around the beam pipe of the synchrotron (see figure 4.5 for schematic view). By applying a current to the beta-

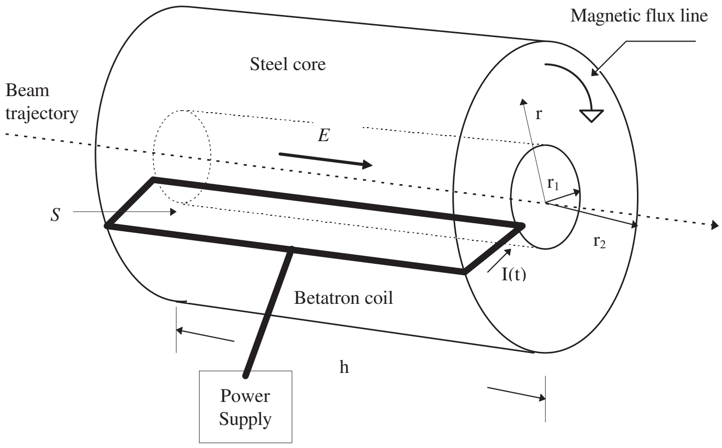


Figure 4.5: Schematic drawing of the betatron core

tron coil the flux inside the circuit is controlled. A time varying current produces a change in the magnetic flux, which itself induces an electric field parallel to longitudinal direction of the accelerator. This electric field affects the energy of the charged particles passing through the betatron core. An increase of the betatron flux $\Delta\Phi$ causes a momentum shift $\Delta p/p$. This can be derived from the Faraday-Neumann-Lenz law:

$$\oint \mathbf{E} \cdot \mathbf{ds} = -\frac{\partial}{\partial t} \int\int \mathbf{B} \cdot \mathbf{dS} = -\frac{d\Phi}{dt} \tag{4.1}$$

where $s$ gives the distance along the orbit. With the mean electric field $\bar{E}$ induced by the betatron core along the orbit of the beam, the average rate of momentum change can be written as:

$$\frac{d\bar{p}}{dt} = q\,e\,\bar{E} \tag{4.2}$$

where $qe$ is the charge of the particles. Combining both equations and inserting the magnetic rigidity (see equation (3.3)) yields the intended relation:

$$\Delta\Phi = C\,B\rho\,\frac{\Delta p}{p} \tag{4.3}$$

where $C$ is the machine circumference and $B\rho$ the magnetic rigidity. As the particles do not see the magnetic field of the betatron core, the magnet can be set to the minus maximum field value before injection. During extraction the betatron core can be ramped to the plus maximum, if the whole flux change is required. This allows to use the betatron core in very efficient way.

Before the extraction process the acceleration of the particles is stopped slightly below the design energy, which is defined by the dipole magnets fields according to the magnetic rigidity. This is done because during the preparation for the extraction the machine is tuned such that a particle with the design energy has the resonant tune. Hence, the resonance is placed at the design energy. Thus, by maintaining the particles at lower energies, the ”waiting” beam is kept stable before extraction. Only the additional acceleration by the betatron core allows the particles to approach the design energy and resonance. Before extraction all particles are off-momentum, thus the whole beam follows dispersive orbits. As the momentum is lower than the design momentum, the orbits are shifted to the inner side of the beam pipe according to the dispersion in the MedAustron synchrotron. This makes it easy to keep the beam away form the extraction septa, which are placed to outer side of the beam pipe. The radial position of the electrostatic extraction septum wires is 35 mm to the outside of the ring[1]. However, one should bear in mind that some sections of the ring are dispersion free as the regions where the resonant sextupole or the RF cavity are placed.

The whole extraction process can be visualized in a schematic way in Steinbach diagrams. To start the extraction process the resonant sextupole is turned on (see figure 4.6(a)), to create an unstable zone around the resonance line at $Q_x = 5/3$ (see figure 4.6(b)). Next the betatron core starts acting and slowly accelerates the particles. This pushes the particles closer to the resonance (see figure 4.6(c)). At first particles with high betatron amplitude arrive at the border to the unstable region. This particles are becoming unstable at energies still below the design energy, typically for MedAustron $\Delta p/p_{unstable,low} = -1.2\cdot 10^{-3}$. To extract low amplitude particles the betatron core has to push further. These particles are getting unstable closer to the design energy (see figure 4.6(d)). When a particle becomes unstable, it starts moving outwards along the separatrices, until its amplitude is large enough to enter the electrostatic extraction septum. During this time the betatron core still acts on the particle and further accelerates the particle. Hence, some particles will be extracted above the design energy. The orbit that corresponds to the design energy is suited in the center of the beam pipe. This gives the particles the full aperture to move outwards on the separatrices. The position of resonance

[1]The reasoning for the choice of this radial position can be found in the PIMMS study [9].

in momentum space is actually given by the tune settings. If the tune is incorrect, the betatron core will have to push longer/shorter and move the beam further/less into the resonance.

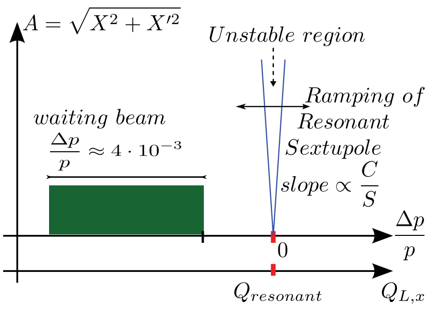


(a) "Waiting" beam at flat top, resonant sextupole is ramping

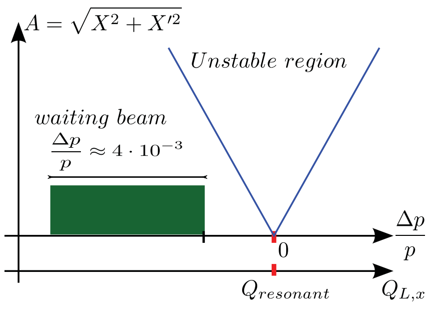


(b) "Waiting" beam at flat top, resonant sextupole has already been ramped

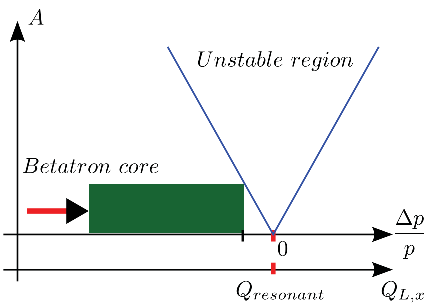


(c) Betatron core accelerates beam towards unstable region

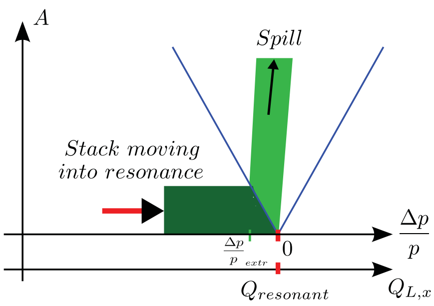


(d) Extraction of spill with momentum spread $\frac{\Delta p}{p}_{extr}$

Figure 4.6: Subfigures (a), (b), (c) and (d) show the betatron core driven extraction in a schematic way, the $x$-axes are the momentum deviation $\Delta p/p$ and the horizontal lattice tune $Q_{L,x}$, on the $y$-axes the normalized particle amplitude is given

Due to the chromaticity there is a one to one correspondence between the betatron amplitude of a particle and the momentum at which it becomes unstable. Hence, the particle density distribution in amplitude $dN/dA$ in the "waiting" beam is handed over into a particle density distribution in momentum space in the extracted beam. As the amplitudes are not distributed homogeneously (see equation (4.14)), an asymmetric beam is created. The dispersion in the extraction line can be used to make to beam symmetric again.

The betatron core is capable of performing extraction times between $1 - 10$ s. To lower times the betatron core is limited by its ramp rate according to the power supply. This is a disadvantage of this extraction method, as lower extraction times are planed to be available for non-clinical research at the MedAustron facility down to 0.1 s. Hence, beside the betatron core different extraction methods have to be foreseen to reach shorter extraction times.

The advantages of betatron core driven extraction are:

- During the extraction the strengths of all lattice elements are kept at constant values. This minimizes the effect of ripple on the extracted beam. Thus, a smooth spill is expected.
- The beam is extracted close to the targeted design energy.
- Some particles become unstable at low amplitudes and on-momentum. These particles are subject to the largest spiral steps, but they are not affected by the chromaticity. This simplifies the adjustment of the spiral step and the Hardt condition.

### 4.2.2 Preparation for extraction

Once finished with acceleration, the machine is filled with a bunched beam, as the RF cavity is still turned on. In order to prepare the machine and the beam for extraction, the following steps are performed:

- RF-phase jump to the unstable fix point. Keeping the beam there for a certain time will create the required energy spread.
- Turn off the RF and wait until a coasting beam[2] is obtained.
- Ramp the resonant sextupole magnet to form the unstable region and to obtain the separatrices. This is done while the beam is still positioned safely away from the resonant tune.
- Start the RF-channeling[3].
- Move the machine tune $Q_L$ closer to the resonance via the quadrupoles.

The list above is only presented to give an idea about the complex preparation process, but details on all the steps will not be covered in this thesis. However, further information can be found in the PIMMS study [4] & [9] or the MedAustron accelerator complex design report [11].

Figure 4.7 shows all the actions during the flat top in the longitudinal phase-space also including the effect of the betatron core.

An important quantity for many of the following considerations is the momentum spread of the beam, which is increased after the acceleration (first bullet point in the list above) to about:

$$\frac{\Delta p}{p}_{\text{"waiting" beam}} \approx 0.4\% \tag{4.4}$$

[2]Coasting beam means that the particles are spread out over the whole circumference of the accelerator, whereas a bunched beam occupies only certain parts.

[3]RF-channeling [27] is a special technique using an empty channeling RF bucket to make the extraction robuster against tune ripple by increasing the velocity of the particles close to the stability limit. Details about this method will not be discussed in the framework of this thesis.

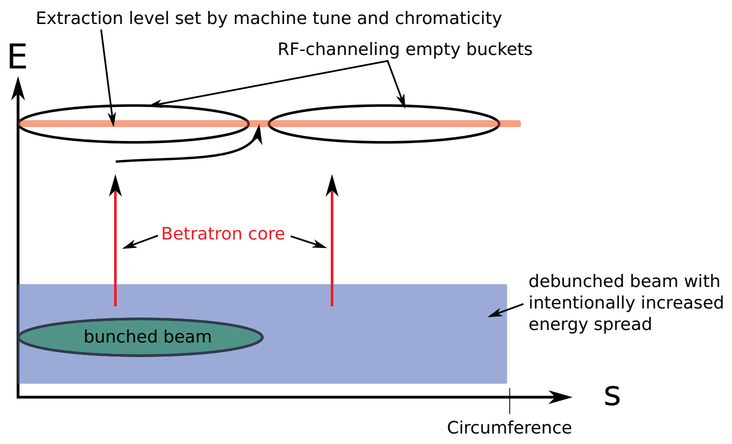


Figure 4.7: Overview of the extraction principle in the longitudinal phasespace. 1) Acceleration has finished, the beam is still bunched (green ellipse) 2) The beam is debunched and the energy spread is intentionally increased. (blue rectangle) 3) The betatron core accelerates the beam (red arrows) 4) The particles are accelerated (black belizier arrow) by the RF-channeling enmpty buckets (black ellipses) 5) The machine tune with the machine chromaticity define the extraction level (red bar), which is different for different betatron amplitudes

for all energies and all particle species. One approach is to make the particle distribution in $\Delta p/p$ as uniform as possible. However, due to loss considerations a Gaussian profile seems to be more favorable (see section 4.2.5). The momentum spread is chosen in order to:

- be larger than the intrinsic energy spread at all extraction energies
- achieve a favorable extraction time according to the medical demands ($1-10$ s) with a reasonable betatron core ramp rate
- fit the beam into the machine aperture as larger momentum deviations lead to larger orbit excursions via dispersion

To obtain an extracted beam featuring the desired spiral step, extracted momentum spread and the Hardt condition, the correct machine settings have to be found. In practice, the machine is tuned to fulfill these conditions using the following sequence (in this order):

- Adjust the strength of the resonant sextupole, to obtain a spiral step of 10 mm for on-momentum particles. Furthermore, the position of the electrostatic extraction septum can be used for fine tuning.
- Adjust the strengths of the other four lattice sextupoles to obtain a chromaticity such that the Hardt condition is fulfilled.
- The emittance in the ring (nominal 7.14 $\pi$ mm mrad for 60 MeV protons) and the values of the previous adjustments determine the extracted momentum spread.

As a resonance condition has to be fulfilled, even small changes can have a strong impact. Thus, several iterations of that process are probably necessary to find the optimal parameters. If the maximum spiral step is not defined by on-momentum particles but by off-momentum ones, the influence of the chromaticity on the spiral step also has to be considered. This makes the adjustment process even more complicated. For example, this is the case, if the lattice tune is not set close to the resonance.

Furthermore, the acceptance (phase space area) of the stable triangles has to be considered with respect to the aperture, especially for particles, which are supposed to be extracted at high off-momenta, as this area (see equation (3.39)) is given by:

$$Acceptance = \frac{48\pi\sqrt{3}}{S^2} \cdot (\Delta Q)^2 \cdot \pi < \pi \cdot A^2_{unstable} \tag{4.5}$$

The acceptance defines the amplitude necessary for a particle to become unstable. The area grows with the distance between the particle tune to the resonant tune, but shrinks with the sextupole strength.

In a real machine, imperfections have to be dealt with and the optics will not be exactly as designed. Thus, some dispersion will leak into the theoretically dispersion free, straight section that hosts the resonant sextupole. Due to the strength of the sextupole, even a small dispersion will influence the chromaticity and consequently the Hardt condition. A solution can be slight variations of the quadrupoles to influence the dispersion. However, the quadrupoles have to be changed in a balanced way such that the tune is not influenced by the adjustments. The following table gives an example for such adjustments of the normalized quadrupole gradients $k'$ of the different quadrupole magnet families. The optimization has been done with WinAgile and the "Fit tunes and Dx" function.

| $\Delta D$ [m] | MQF1 $\Delta k'/k'$ [%] | MQF2 $\Delta k'/k'$ [%] | MQD $\Delta k'/k'$ [%] |
|---|---|---|---|
| $\pm 0.1$ | $\pm 0.71$ | $\mp 0.46$ | $\pm 0.01$ |
| +1 | +6.7 | -4.3 | +0.1 |
| -1 | -7.8 | +5 | -0.2 |

Table 4.1: Necessary changes in quadrupole gradients to obtain a targeted variation of the dispersion

For the $\Delta D = \pm 1$ case starting with zero dispersion the effects on the beta functions and the dispersion functions are shown in figure 4.8.

The control of the dispersion at constant tune, such as it is done in the example above, and on the opposite also the control of the tune at constant dispersion are very important for the future operation of the accelerator, as this is how the machine should be adjusted when it is

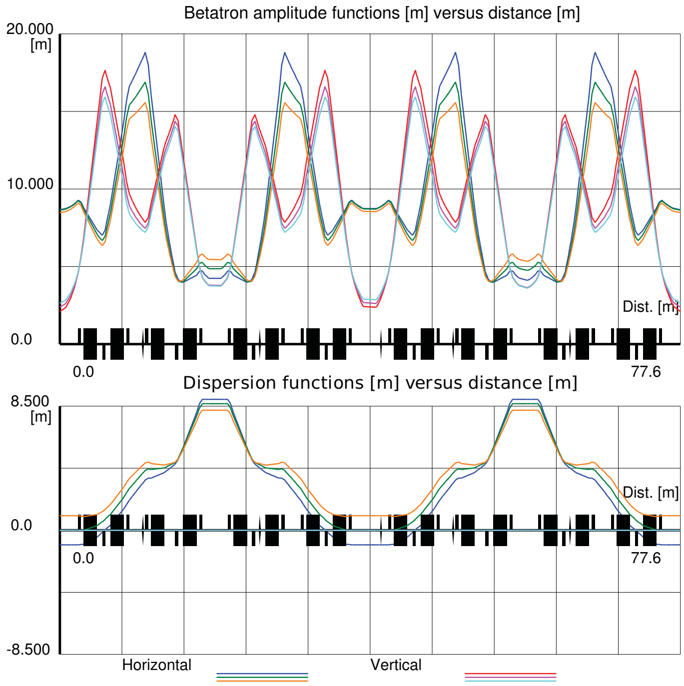


Figure 4.8: Effect of adjustments of $k'$ of quadrupoles to achieve dispersion shifts $\Delta D = \pm 1$ at MXR without tune shift, the green line represents the nominal horizontal dispersion case, yellow $\Delta D = -1$, blue $\Delta D = +1$

being set up for operation. Therefore, this topic - e.g. the linearity of the results and the achievable range of changes, which is determined by the capabilities of the power converters and the magnets - need to be further investigated.

### 4.2.3 Ramping the betatron core magnet

To extract the whole beam, the ”waiting” beam has to be completely moved into the resonance by accelerating the ”waiting” beam via ramping the betatron core. The momentum spread of the ”waiting” beam is set to be about $\Delta p/p_{wait} \approx 0.4\%$. The distance in momentum space between the ”waiting” beam and the resonance is chosen to $\Delta p/p_{gap} \approx 0.13\%$ before extraction, to keep the beam away from the unstable region. Therefore, the total change of the betatron core flux $\Delta\Phi$ during the ramp has to results in a total momentum change of about $\Delta p/p_{beta,total} \approx 0.53\%$. The relation between $\Delta\Phi$ and $\Delta p/p_{beta}$ is given in equation (4.3).

To accelerate the particles, a positive change in the flux of the betatron core is needed. The absolute field value does not matter, only the rate of the change is of interest. As the MedAustron design of the betatron core has not been completed yet, the CNAO design [28] is used in the following. The maximum available flux change is:

$$\Delta\Phi_{max} = 2 \cdot 1.23 \text{ Wb} = 2.46 \text{ Wb} \tag{4.6}$$

From the maximum flux change it is possible to calculate the maximum momentum change $\Delta p/p_{beta}$ for a certain type of particle and energy. The question is whether the flux change is large enough to move the whole beam into resonance. The main issue are the high energy carbon ions with an energy of 400 MeV/u, because they have the largest magnetic rigidity $B\rho$ of all considered cases. Table 4.2 sums up the results for different particles and energies.

| Particle | Energy [MeV/u] | $B\rho$ | $\frac{\Delta p}{p}_{beta}$ [%] |
|---|---|---|---|
| Proton | 60 | 1.137 | 2.7864 |
| Proton | 250 | 2.432 | 1.3027 |
| Proton | 800 | 4.881 | 0.6491 |
| Carbon | 120 | 3.254 | 0.9736 |
| Carbon | 400 | 6.346 | 0.4992 |

Table 4.2: Maximum possible momentum changes due to full betatron core flux change for different particles and energies

As presented in table 4.2, a problem arises for the high energy carbon ions, because the maximum $\Delta p/p_{beta}$ is below the estimated required minimum of 0.53% to extract a whole beam, which exhibits the design parameters. However, as the beam emittance shrinks with increasing energy due to adiabatic damping (see section 3.1.3), the high energy carbon ions exhibit a lower emittance than the protons. The higher the emittance is, the larger the distance of the ”waiting” beam and the resonance has to be, in order to keep particles away from the unstable zone. Therefore, for high energy carbon ions the ”waiting” beam can be moved closer to the resonance before extraction starts. The initial distance can be reduced to about $\Delta p/p_{gap} \approx 0.08\%$ (see equation (4.10)). Thus, the capability of CNAO design betatron core would just be enough. However, there is almost no margin left and if the sum of the energy spread of the ”waiting” beam and the distance to the resonance is larger than about 0.5%, parts of the beam can not be extracted.

The results for the other cases are fine. Especially, for the low energy carbon ions and medical protons the maximum available momentum shift $\Delta p/p_{beta}$ is much higher than 0.53%. That leaves large margins and room for eventual needed or wanted changes in the configuration of the ”waiting” beam or resonance settings like the slope of the unstable zone.

### 4.2.4 Configuration of the resonance

To start the extraction the betatron core has to be activated to accelerate the beam towards the design energy. A particle that has been pushed into the unstable zone, becomes unstable and its amplitude starts increasing steadily. After $N$ turns the particle will just pass "outside" the electrostatic extraction septum. The next two turns the particle will be located on the other separatrices, so it can still gain amplitude, but it is in safe distance to the septum. On the third turn $N+3$ the particle is suited on the first separatrix again and it will have enough amplitude to be inside the septum (see right part of figure 3.7). The propagation of particles in the machine during these three last turns before extraction are illustrated in figure 4.12. The difference in amplitude between the $N$-th and the $N+3$-th turn can be split up into a radial part the spiral step $\Delta x$ and the divergence part the spiral kick $\Delta x'$. At MedAustron the nominal value for the spiral step is 10 mm. An approximation for the spiral step of on-momentum particles can be analytically derived, as it is shown in section 3.3.4:

$$\Delta R = \frac{3}{4} S \frac{1}{cos\phi} X_{ESE}^2 \tag{4.7}$$

where $X_{ESE} = x_{ESE}/\sqrt{\beta_{x,ESE}} = 0.0086[\sqrt{m}]$ is the position of the electrostatic septum in normalized coordinates and $\phi \approx 42.3°$ the angle between the separatrix and the horizontal axis. $\phi$ can be calculated from the separatrix at the resonant sextupole, where it is almost parallel to the vertical axis and the phase advance between resonant sextupole and electrostatic septum of $\Delta\mu_x = 227.75°$. The virtual sextupole strength is $S_{virt} = 36.717$. The calculation followed by a de-normalization gives a spiral step in normal phase space coordinates of about 11.6 mm. From tracking a spiral step of about 10 mm is expected. However, the calculation above neglects non-linear effects in the machine introduced e.g. by the sextupoles. These effects for example bend the separatrices due to amplitude dependent de-tuning. Hence the particles reach the septum at phase space positions deviant to the idealized situation. This can be approximated by an effective angle $\phi_{eff} \approx 26.4°$, obtained from tracking. This leads to an approximated semi-analytic result for the spiral step of about $\Delta x \approx 9.2$ mm

Figure 4.9 displays details in horizontal phase space at the entrance to the electrostatic extraction septum of the slow resonant extraction of two proton lowest extraction energies (60 MeV).

- The yellow trace shows a zero-amplitude particle (precisely: a very small amplitude particle) as it increases in amplitude along the three separatrices.
- The white curve shows a particle with the chosen energy spread of the extracted beam $\Delta p/p = -0.00107$. The amplitude is chosen such that it is the smallest one that is already unstable.

With the growing amplitude, the amplitude dependent tune-shift from the sextupoles increases and thus causes the separatrices to bend. At the electrostatic septum an horizontal extraction separatrix would be ideal. Although the situation will never be perfect, it can be optimized by moving the resonant sextupole in the drift space to change the phase advance between sextupole and septum. Whereas, the separatrix should be locally as horizontal as possible at the ESE position, the angle $\phi$ in phase space between the separatrix and the $x$-axis should be around $\phi \approx 45^\circ$, neglecting the bending due to non linear effects. This constraint is imposed by the other separatrices. An angle larger than $60^\circ$ would mean that the second separatrix crosses the septum before, meaning at lower amplitudes, than the first. This would change the parameters at which the beam is extracted. An angle smaller than $30^\circ$ can lead to a similar problem with the third separatrix at the magnetic extraction septum assuming a phase advance between electrostatic and magnetic septum of $\mu_{ESE-MSE} = 90^\circ$. As the phase advance actually will be smaller also the angle could be smaller. The angle minus the phase advance just have to be larger than $\phi - \mu_{ESE-MSE} > -60^\circ$.

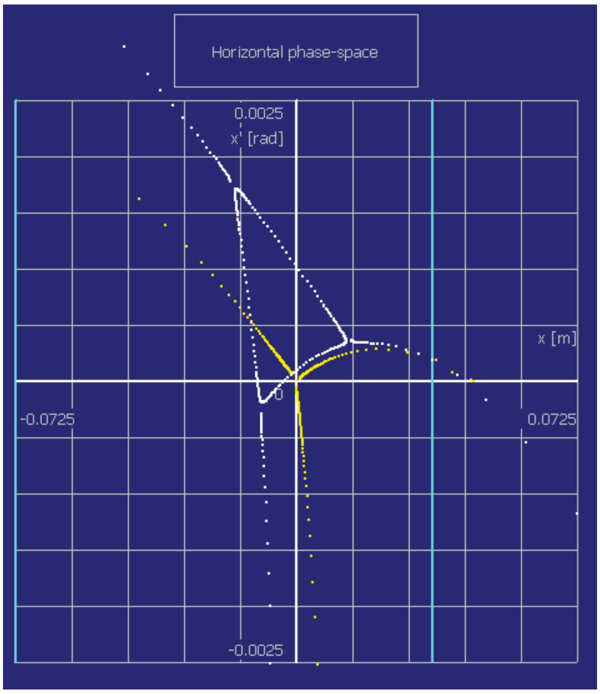


Figure 4.9: Transverse phase space map at electrostatic extraction septum obtained with WinAgile, yellow trace gives on-resonance separatrices, white maximum off-resonance ones according to the emittance

In figure 4.9 unseen between the yellow and white traces there is a continuum of particles with progressively changing stable triangles and separatrices. Both the yellow and white traces (and all the intermediate traces that are not shown) cross the vertical blue line that represents the electrostatic septum foil/wires (at 35 mm to the outside) at the same angular position, showing that the Hardt Condition (see section 3.3.3) has been successfully applied. For the off-resonance particles with a momentum deviation of $\Delta p/p$ = -0.00107 with respect to the on-momentum particles, the amplitude corresponds to an emittance in the ”waiting” beam of 7.11 $\pi$ mm mrad, the closest match that could be obtained to the theoretical value of 7.14 $\pi$ mm mrad (which is 5 times the one sigma emittance and thus the assumed beam size). The spiral step for the on-momentum particles is 10.098 mm. To obtain the beam size of the extracted beam the thickness of the septum wires of 0.1 mm has to be subtracted from the spiral step. Thus, the beam size is effectively identical to the design value of 10 mm.

For off-resonance particles, the spiral step is reduced and in this case the maximum value is 5.38 mm.

At higher energies, the emittance in the ”waiting” beams is smaller due to adiabatic damping and the reduced values lead to reduced momentum spreads in the extracted beam.

The following table lists the coordinates of the limiting particles at the entry to electrostatic extraction septum for the MedAustron lattice. This data has been obtained with the function ’transverse maps’ of WinAgile. The septum width is 0.1 mm. The first information for each particle (’outside septum’) gives the coordinate of a particle that just passes outside the septum wires three turns before it finally reaches the septum. Next, the innermost and outermost possible particle coordinates are given. These extreme particles (on- and off-momentum) define the shape of the extracted beam.

- lowest extraction energies (protons 60 MeV and carbon ions 120 MeV/u)
  - On-resonance particles
    - Outside septum: position $x$: -0.035 [m], angle $x'$: -0.000192 [rad]
    - Position $x$: inner: -0.0351 [m], outer: -0.045098 [m]
      Spiral step = 0.010098 [m]
    - Angle $x'$: inner: -0.000191 [rad], outer: -0.000015 [rad]
  - Off-resonance particles
    - Outside septum: position $x$: -0.035 [m], angle $x'$: -0.000183 [rad]
    - Position $x$: inner: -0.03510 [m], outer: -0.040383 [m]
      Spiral step = 0.005383 [m]
    - Angle $x'$: inner: -0.000182 [rad], outer: -0.000072 [rad]
  - $\Delta p/p$ of resonance: -0.000017
  - $\Delta p/p$ spread wrt resonance: -0.00107
  - Total horiz. emittance: 7.1112 [$\pi$ mm mrad ]
  - Design target emittance: 7.1429 [$\pi$ mm mrad ]
- highest extraction energy protons (250 MeV)
  - On-resonance particles
    - Outside septum: position $x$: -0.035 [m], angle $x'$: -0.000192 [rad]
    - Position $x$: inner: -0.0351 [m], outer: -0.045098 [m]
      Spiral step = 0.010098 [m]
    - Angle $x'$: inner: -0.000191 [rad], outer: -0.000015 [rad]
  - Off-resonance particles
    - Outside septum: position $x$: -0.035 [m], angle $x'$: -0.000204 [rad]

    - Position $x$: inner: -0.0351 [m], outer: -0.042086 [m]
      Spiral step = 0.007086 [m]
    - Angle $x'$: inner: -0.000202 [rad], outer: -0.000062 [rad]
  - $\Delta p/p$ of resonance: -0.000017
  - $\Delta p/p$ spread wrt resonance: -0.00079
  - Total horiz. emittance: 3.3134 [$\pi$ mrad mrad ]
  - Design target emittance: 3.3393 [$\pi$ mm mrad ]

- highest extraction energy carbon ions (400 MeV/u)
  - On-resonance particles
    - Outside septum: position $x$: -0.035 [m], angle $x'$: -0.000192 [rad]
    - Position $x$: inner: -0.0351 [m], outer: -0.045098 [m]
      Spiral step = 0.010098 [m]
    - Angle $x'$: inner: -0.000191 [rad], outer: -0.000015 [rad]
  - Off-resonance particles
    - Outside septum: position $x$: -0.035 [m], angle $x'$: -0.000201 [rad]
    - Position $x$: inner: -0.0351 [m], outer: -0.041796 [m]
      Spiral step = 0.006796 [m]
    - Angle $x'$: inner: -0.000199 [rad], outer: -0.000064 [rad]
  - $\Delta p/p$ of resonance: -0.000017
  - $\Delta p/p$ spread wrt resonance: -0.00084
  - Total horiz. emittance: 3.6686 [$\pi$ mm mrad ]
  - Design target emittance: 3.7222 [$\pi$ mm mrad ]

Since this is a resonance condition, the calculations are extremely sensitive to small changes, which is why the target and design emittances differ slightly.

### 4.2.5 Optimization of Losses during extraction

Figures 4.6(a) to 4.6(d) show the Steinbach diagram for the betatron core driven extraction. Before the extraction the ”waiting” beam is positioned in the stable region with a distance to the resonance in momentum space of about $\Delta p/p_{gap} \approx 0.15\%$. The total momentum spread of the ”waiting” beam is $\Delta p/p_{wait} \approx 0.4\%$. Different values for this momentum spread can be achieved, if needed.

The extraction is started by ramping the betatron core to move the ”waiting” beam into resonance. However, because of the slope of the unstable region, parts of the ”waiting” beam can not be used after the extraction for medical irradiation. High emittance particles become unstable earlier than particles with same momentum but lower amplitudes. Therefore, at the beginning of the extraction there are no low amplitude particles in the extracted beam (see figure 4.10). Whereas, towards the end of the extraction the situation is turning to the opposite and there are no more high amplitude particles in the extracted beam. A stable extracted beam is only obtained when particles of all amplitudes available in the ”waiting” beam becoming unstable at the same time. Thus, this determines the part of the ”waiting” beam, which creates a stable extracted beam. The rest of the ”waiting” beam can not be used for medical treatment as the particle distribution and intensities in the extracted beam are unfavorable. These particles have to be dumped and thus are lost.

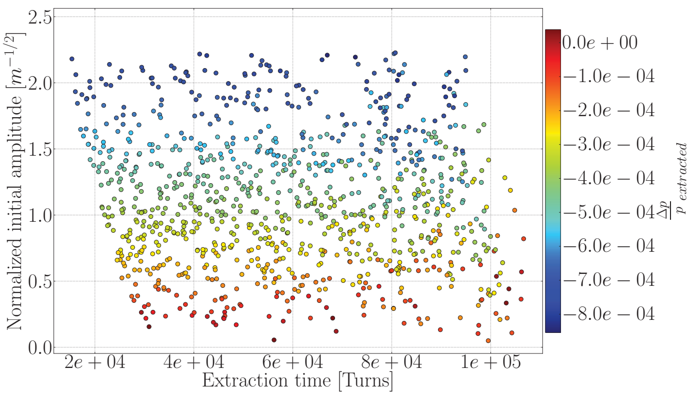


Figure 4.10: Correlation between initial normalized amplitude and extraction time for 400 MeV/u carbon ions, the extracted relative momentum deviation is given as color code

In the following the non-usable parts of the extracted beam are quantified analytically. These parts are referred to losses in this section. The analysis starts from the unstable region and the slopes of its borders, as seen in the Steinbach diagram 4.6(c). The border of the unstable zone is defined by the stability condition (see equation (3.40)) for the particles in the beam:

$$\varepsilon_{stable} = A_{stable}^2\,\pi \leq \frac{48\pi\sqrt{3}}{S^2}\,(\delta Q)^2\,\pi \tag{4.8}$$

For the tune distance $\delta Q$ only contributions of chromatic tune shifts due to momentum deviations are taken into account. Amplitude dependent tune shifts are neglected. This leads to a formula for the border of the unstable zone:

$$A = \sqrt{48\pi\sqrt{3}}\,\left|\frac{Q'}{S}\right|\,\left|\frac{\Delta p}{p}\right| \tag{4.9}$$

Rearranging this formula and using the emittance of the ”waiting” beam to calculate the maximum amplitude of particles in the beam, gives the instantaneous momentum spread of the extracted beam:

$$\left|\frac{\Delta p}{p}\right|_{inst} = A_{max}\sqrt{\frac{1}{48\pi\sqrt{3}}}\,\left|\frac{S}{Q'}\right| \tag{4.10}$$

As all the parameters are more or less fixed by other constraints, the momentum spread can be calculated. The normalized sextupole strength $S$ strongly influences the spiral step. Hence, $S$ is determined by the desired spiral step. For the Med Austron lattice the resonant sextupole strength becomes $S_{MXR} = 29.435$. The virtual sextupole strength which also takes the other sextupoles into account is $S_{virt} = 36.717$.

The chromaticity $Q'_x$ has to be set to fulfill the Hardt condition and has the nominal value for the Med Austron lattice of $Q'_{x,MedAustron} = -4.041$

The maximum amplitude $A_{max}$ is given by the emittance of the "waiting" beam. Low energy protons with 60 MeV have a nominal total geometric emittance of $\varepsilon = 7.143\ \pi$ mm mrad. Hence, the maximum amplitude becomes

$$A_{max} = \sqrt{\varepsilon/\pi} = 2.673\ 10^{-3}[\sqrt{m}] \tag{4.11}$$

Finally, all that put together yield an extracted momentum spread for low energy protons of:

$$\left|\frac{\Delta p}{p}\right|_{inst,p60} = 1.205\ 10^{-3} \tag{4.12}$$

For top energy carbon ions with 400 MeV/u the nominal total geometric emittance decreases to $\varepsilon$ =3.663 $\pi$ mm mrad. The extracted momentum spread is then computed to be:

$$\left|\frac{\Delta p}{p}\right|_{inst,C400} = 8.735\ 10^{-4} \tag{4.13}$$

Starting with the extracted momentum spread, the losses at the beginning and end of the extraction can be investigated. At first this is done for the low energy protons. Only from the time when the first 'zero'[4] amplitude particles are moved into resonance, the extracted beam can be used, because these particles are extracted at zero tune distance and hence get the maximum spiral step. Therefore, they determine the maximum beam size of the extracted beam. Similarly, towards the end of the extraction the beam is not used anymore as soon as there are no more particles with large amplitudes in the "waiting" beam, because the distribution in the extracted beam would be changed. Therefore, the extracted beam can only be seen as stable within this time interval.

If the amplitudes and the energies in the "waiting" beam would both be homogeneously distributed, the losses at the start and the end of extraction could be easily calculated as the ratio of extracted momentum spread and whole momentum spread of the "waiting" beam. This would give about 30.8% loss of beam. Anyway, in reality the distributions are not homogeneous, at least not in the transverse planes. A better approximation for the real situation is to assume Gaussian distributions in phase space for the amplitudes in the "waiting" beam. This

[4]Actually particles with very small amplitude, as theoretically there are no zero amplitude particles

approximation leads to the probability density function (PDF) for the normalized amplitudes A=$\sqrt{(X^2+X'^2)}$ in the "waiting" beam:

$$PDF(A) = \frac{A}{\sigma^2} \exp^{-\frac{A^2}{2\sigma^2}} \tag{4.14}$$

where $\sigma = \sqrt{\varepsilon_{RMS}/\pi}$ is the root of the RMS horizontal emittance. This probability density function is shown in figure 4.11 for 60 MeV protons and 400 MeV/u carbon ions assuming the nominal MedAustron emittances at flat top. In this figure the amplitudes are only normalized with respect to the Twiss functions but not to the emittance, because the emittance is not constant for particles of different energy.

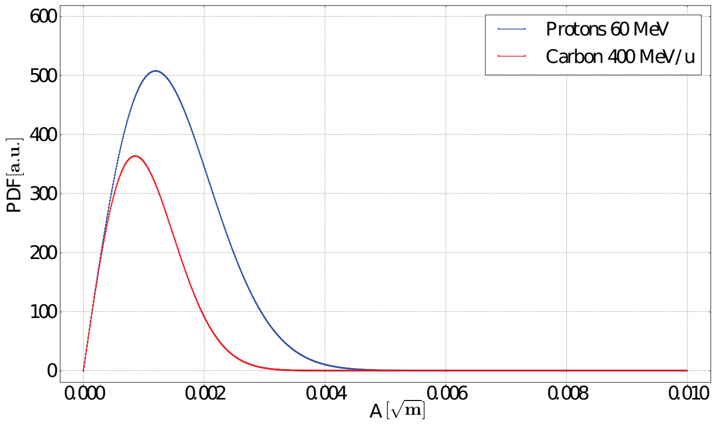


Figure 4.11: Probability density function for the normalized amplitudes in the "waiting" beam for protons 60 MeV and carbon ions 400 MeV/u, amplitudes only normalized with respect to the Twiss functions but not to the emittance

The following loss calculations are done with probability calculus. From the stability condition the border of the unstable zone in momentum-amplitude space is obtained. Then, the "waiting" beam is sectioned in thin vertical stripes. For each strip (in the following 1000 stripes have been used) the probability is computed for a particle to be lost at the beginning or end of the extraction. This is achieved by integration over the probability density function of the amplitudes. As integration boundaries the areas of the "waiting" beam are used that reach the unstable zone, but do not form a useful[5] beam from the medical point of view. By summing up the probabilities that particles are in these 'useless' areas the losses can be calculated. In the case of a non homogeneous distribution in energy, an additional integration over the probability function of the energies has to be done to obtain the losses.

The assumption of Gaussian distributed amplitudes does not change much about the losses. They are calculated to be about 30.1%.

[5]The extracted beam does not have the targeted beam size or particle distribution.

A possibility to improve the situation concerning the losses is to abandon a uniform energy distribution and create a ”waiting” beam which also has a Gaussian energy distribution. In the following a Gaussian distribution with a sigma of $\sigma = 0.0007$ was assumed. This decreases the losses immensely to about 6.4% in total. The disadvantage is that a variable betatron core ramp rate is needed over the whole extraction time to obtain a constant intensity in the extracted beam.

Higher energy particles correspond to smaller emittance due to adiabatic damping and thus to smaller maximum amplitudes. The losses are also smaller, because the extracted momentum spread is lower. Therefore, the ratio of the extracted momentum spread to the whole momentum spread of the ”waiting” beam is lower as well. So in the case of 250 MeV protons the losses at the beginning and the end of extraction assuming Gaussian distributions in phase space are about 20.6% for a uniform energy distribution or 2.9% for a Gaussian one.

For carbon ion beams the situation is very similar to protons. A carbon beam with an energy of 120 MeV/u has the same emittance as a low energy proton beam and thus the losses are equivalent. For a top energy carbon ions beam with 400 MeV/u the emittance is slightly higher than for a 250 MeV proton case and therefore the losses increase a bit to 21.6%, respectively 3.1%.

| Particle | Energy [MeV/u ] | Energy distribution | Losses [% of ”waiting” beam] |
|---|---|---|---|
| Proton | 60 | uniform | 30.1 |
| Proton | 60 | Gaussian | 6.4 |
| Proton | 250 | uniform | 20.6 |
| Proton | 250 | Gaussian | 2.9 |
| Carbon | 400 | uniform | 21.6 |
| Carbon | 400 | Gaussian | 3.1 |

Table 4.3: Losses for different particles, energies and energy distributions

### 4.2.6 Gap at and position of the magnetic septum

In section 4.2.4 the phase space coordinates of the edges of the segments of the separatrix that are just entering the electrostatic extraction septum are listed. Three limiting cases are covered: protons and carbon ions of all energies that are extracted exactly on resonance, off-momentum protons at the highest proton extraction energy and off-momentum carbon ions at the highest carbon ion extraction energy.

Figure 4.12 shows how these segments of separatrix continue through the lattice to the ”thin” magnetic extraction septum after having been deflected by the electrostatic extraction septum. Furthermore, it depicts how these segments relate to the circulating separatrices. The important features are:

- The gap that is opened between the circulating separatrices and the extracted beam segments, because the wall of the magnetic septum has to fit into it.
- The outermost position of the circulating separatrices at the entrance to the "thin" magnetic septum, as this sets the minimum limit for the placement of the magnetic septum.
- The furthest excursion of the segment between the septa, because the motion has to fit into the aperture.

The trajectories that determine the minimum gap are the on-resonance particles in the circulating beam and the off-momentum particles in the extracted beam.

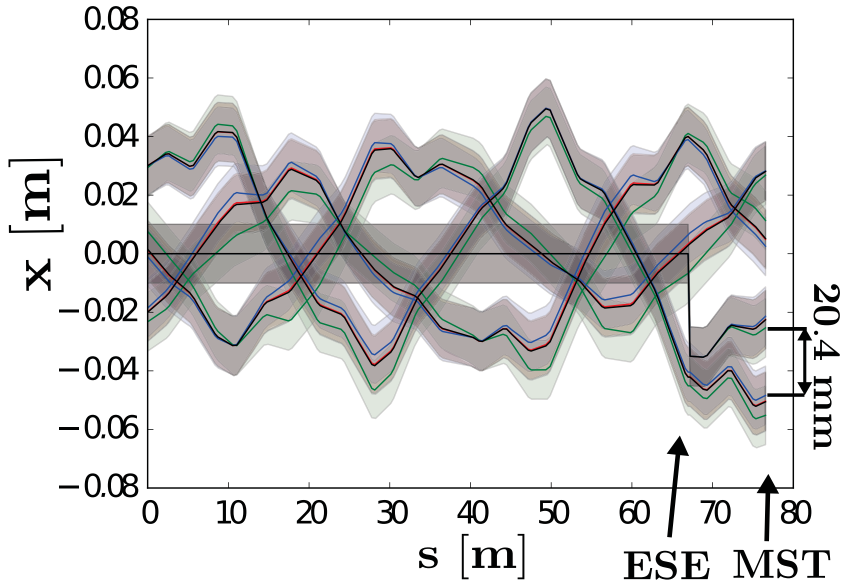


Figure 4.12: Trajectories of the four limiting particles (2 on- & 2 off-momentum) during last three turns before entering the electrostatic extraction septum (ESE) (tracking starts at ESE), particles that enter the ESE receive a kick and continue to the thin magnetic extraction septum (MST), where the gap between extracted and circulating segments is displayed.

The available gap, meaning the space between the circulating and the extracted beam, is crucial as parts of the magnetic septum has to fit into it. If the gap is to small, particles will hit the septum wall and be lost. The gap at the magnetic septum is calculated by applying the transfer matrix from the electrostatic to the magnetic septum $T_{ESE-MSE}$ on extreme particle positions[6] at the electrostatic septum (see the table for the MedAustron lattice in section 4.2.4):

$$\begin{pmatrix} x_{MSE} \\ x'_{MSE} \\ s_{MSE} \\ \frac{\Delta p}{p} \end{pmatrix} = T_{ESE-MSE} \cdot \begin{pmatrix} x_{ESE} \\ x'_{ESE} \\ s_{ESE} \\ \frac{\Delta p}{p} \end{pmatrix} \tag{4.15}$$

The transfer matrix follows from the Twiss functions and the phase advance $\Delta\mu$ to:

$$\mathbf{T_{ESE-MSE}} = \begin{bmatrix} 0.70620590 & 9.52255079 & 0 & 3.18038929 \\ -0.05729855 & 0.64339829 & 0 & 0.63019051 \\ -0.62727594 & -3.95476410 & 1 & 6.99651702 \\ 0 & 0 & 0 & 1 \end{bmatrix} \tag{4.16}$$

The linear description with the matrix is valid, because there is no sextupole placed between the electrostatic and the magnetic extraction septa.

For particles that have been deflected by the electrostatic extraction septum, the septum kick of $-2.5$ mrad has to be considered before applying the transfer matrix. The computation of the simple matrix vector multiplication between the transfer matrix and the particle coordinates at the electrostatic septum yields the following results:

- The largest excursion in $x$ in the circulating beam at the magnetic septum is $x_{Cmax} = -26.5$ mm for on-resonance particles of all types and energies.
- On the other side the smallest excursion at the magnetic septum for particles, which have been inside the electrostatic septum, is given by $x_{Emin} = -46.9$ mm. This value has been found for 60 MeV off-momentum protons, because off-momentum particles with higher energies exhibit larger spiral steps.
- The largest excursion at the magnetic septum has been computed to $x_{Emax} = -55.8$ mm. This value is valid for all particle energies, as all on-resonance particles are subject to the same spiral step.
- Finally, the outermost position of the extracted segment, while it is moving between the septa, is $-56.3$ mm, which has been obtained by tracking on-resonance particles. This value imposes an important requirement on the aperture.

As a result, the gap between circulating and extracted beam at the magnetic septum evaluates to

$$\mathbf{gap_{MSE}} = |x_{Emin} - x_{Cmax}| = 20.4 \text{ mm} \tag{4.17}$$

The numbers above are calculated with a maximum momentum deviation in the extracted beam of $\Delta p/p = -1.07 \cdot 10^{-3}$. This value has been obtained with WinAgile. However, analytic calculations suggest a slightly larger absolute value of $\Delta p/p \approx -1.2 \cdot 10^{-3}$. Such a

[6]The entries for the vertical plane are not given, as the vertical plane is not of interest here and coupling effects are neglected.

change in momentum would alter the trajectories of the off-momentum particles. The effect on $x'$ is negligible, but the limiting off-momentum case at the magnetic septum would be shifted to $x_{Emin} = -046.5$ mm. This would yield a gap of 20 mm.

The gap that is needed at the magnetic septum to place the necessary equipment between the circulating and the extracted beams is 21.4 mm. All contributions to this space requirement are listed in the table 4.2.6. The space requirement for the equipment is larger than the gap by 1 mm. However, the margins between the beam and the vacuum pipe are already included in the requirement. The current design foresees the inner vacuum wall of the septum to be placed at $-48.8$ mm, which results in a clearance to circulating beam of 1.9 mm, which is almost the aimed 2 mm. But, on the inside of the septum only 1 mm clearance to the extracted beam is given with this extraction setup. If the 1 mm is not enough and problems with particle loss occur, it is still possible to increase the kick given by the electrostatic septum. In the current design a kick of 2.5 mrad is assumed, but the septum is capable of applying kicks up to about 5 mrad. However, already a kick of 2.6 mrad would increase the innermost excursion at the magnetic septum by about 1 mm and yield the targeted clearance of 2 mm.

| | | |
|---|---|---|
| Clearance between circulating separatrix and vacuum pipe | [mm] | 2.0 |
| Main vacuum pipe | [mm] | 3.0 |
| Alignment tolerance | [mm] | 1.0 |
| Magnetic shield | [mm] | 0.4 |
| Septum current 'wall' | [mm] | 10.3 |
| Alignment tolerance | [mm] | 1.0 |
| Extraction vacuum pipe | [mm] | 1.7 |
| Clearance between vacuum pipe and extracted beam | [mm] | 2.0 |
| Total | [mm] | 21.4 |

Table 4.4: Space requirements of magnetic septum

The parameters for positioning the entry of the "thin" magnetic septum are summarized in the table 4.2.6.

| | | |
|---|---|---|
| Outermost extent of the circulating separatrices | [mm] | -26.5 |
| 'Gap' between circulating separatrices and extracted segment | [mm] | 20.4 |
| Outermost excursion of the beam at entrance to magnetic septum | [mm] | -55.8 |

Table 4.5: Spatial limitations of the beam at the entrance to the magnetic septum

The positions and angles at the electrostatic and the magnetic septum for the limiting particles (on- & off-momentum 60 MeV protons) are summarized in table 4.6. Two important circumstances have to be made clear:

- Due to the horizontal phase advance between the septa, the angles turn into positive values at the magnetic septum. This means that the particles trajectories point towards the center of the beam pipe and thus towards the wall of the septum. Therefore, to reduce losses, the septum should be positioned with the maximum angle 0.96 mrad of the innermost extracted particles.
- The beta function and the dispersion are increasing from the electrostatic to magnetic septum. Hence, on the first glance one would expect increasing beam sizes while the particles are transported between the septa. However, actually the beam size shrinks. Again this can be explained by taking the phase advance into account. The bar of charge, which is almost horizontal at the electrostatic septum, is rotated according to the horizontal phase advance between the septa of about 70°. Only the projection onto the $x$-axis gives the beam size. So due to the phase advance the beam size shrinks to about a third compared to a horizontal bar of charge.

The evolution of an extracted 60 MeV proton beam between the septa is shown in figure 4.13 by depicting the limiting on- and off-momentum particles.

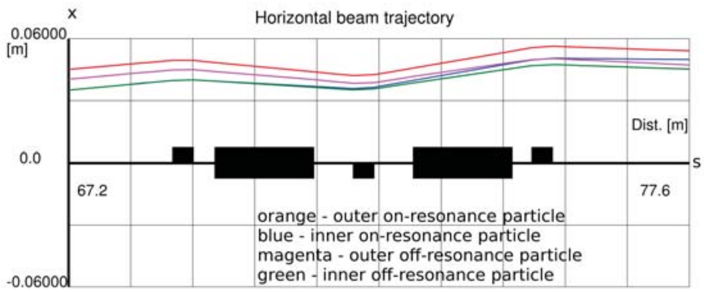


Figure 4.13: Evolution of the limiting on- and off-momentum particles of an extracted 60 MeV proton beam between the septa. Attention: Plot created with WinAgile, which uses a different coordinate system, hence the sign of the $x$-axis has to be reversed to get same results as above.

### 4.2.7 Extracted beam parameters

So far the extracted beam segment has been considered as part of the main ring and treated accordingly. Meaning for example to use the Twiss functions defined by the main ring for calculations. However, once a beam segment is in the extraction channel (entrance to the electrostatic extraction septum), it is not governed by the periodic boundary conditions of the ring anymore. Hence, it is possible to choose new Twiss functions to describe the beam with a new central orbit and corresponding Twiss and dispersion parameters. This new beam must then be brought out of the main ring, into the extraction transfer lines and finally to the beam delivery points.

| | Momentum | | ESE | MSE |
|---|---|---|---|---|
| circulating | on | x [mm] | -35 | **-26.5** |
| outermost | on | x' [mrad] | -0.19 | 1.88 |
| | off | x [mm] | -35 | -23 |
| | off | x' [mrad] | -0.18 | 2.56 |
| extracted | on | x [mm] | -35.1 | -50.4 |
| innermost | on | x' [mrad] | -0.19 | 0.28 |
| | off | x [mm] | -35.1 | **-46.9** |
| | off | x' [mrad] | -0.18 | **0.96** |
| extracted | on | x [mm] | -45.1 | **-55.8** |
| outermost | on | x' [mrad] | -0.02 | 0.97 |
| | off | x [mm] | -40.4 | -49.6 |
| | off | x' [mrad] | -0.07 | 1.34 |

Table 4.6: Positions and angles at the electrostatic (ESE) and the magnetic (MSE) septum for the limiting particles (on- & off-momentum 60 MeV protons). Most important numbers are highlighted.

The circulating beam in the main ring can be approximated by Gaussian distributions in both planes - the horizontal and the vertical. However, the extraction process is only acting on the particle motion in the horizontal plane. This introduces an asymmetry between the distributions in the two planes:

- The vertical plane is not affected by the extraction process as coupling is neglected. At the entry to the extraction line, the beam has still the vertical phase-space characteristics of the ring and thus can be approximated by a Gaussian distribution. Hence, the vertical emittance and Twiss functions of the ring are just handed over to the extraction line. The vertical beam size in the extraction line can only be controlled via the beta function.
- In the horizontal plane, particle distribution in the extracted beam can not be approximated by a Gaussian form anymore. Instead it has got a near rectangular shape and is therefore referred to as ”bar of charge”. Its length is limited by the spiral step and its height by the Hardt condition. Actually, a trapezoidal shape is an even better approximation as particles of different momenta are subject to different spiral steps. The length of this extracted segment is clearly dominating its height. Hence, the extracted beam can be represented as a ”diameter” of an unfilled ellipse in phase space. This ellipse is fitted around the extracted particle distribution to obtain Twiss parameters. The phase advance gives the orientation of the extracted beam in the ellipse. This allows to control the beam size in the extraction line not only via the beta function but also by adjusting the phase advance.

More details on the concepts introduced rather briefly above can be found in the PIMMS study [4] and the MedAustron accelerator design report [11].

#### Dispersion function of the extracted beam

At the entrance to the electrostatic extraction septum the extracted beam segment consists of the ”bars of charge”. These bars for the different momenta are not aligned. This misalignment is due to transverse amplitude distribution in the ring and the extraction method which limits the extracted distribution on the inner side by the septum wires and on the outer side by the spiral steps for the different momenta. The misalignment even grows on the way to the magnetic septum and there the beam shows a stairway shape in a $\Delta p/p$ over amplitude plot. As one wants to have a symmetric beam at the irradiation room’s ISO-center, dispersion is needed. Now this can be done ”inversely” by choosing the dispersion function at the start of the extraction line such that zero dispersion creates an aligned beam. The effect of this dispersion vector on the extracted beam at the septa and the ISO-center is schematically shown in figure 4.14.

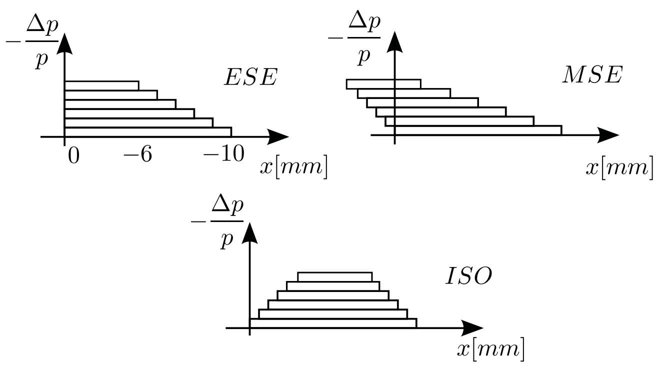


Figure 4.14: Effect of the dispersion vector on the extracted beam in a momentum deviation over position plot at the septa and the ISO-center

For operation this means: If one measures an asymmetric horizontal beam profile in the HEBT e.g. at the ISO-center, one can try to correct this by adjusting of the dispersion function.

Table 4.7 summarizes the calculation of the dispersion and its derivative at the electrostatic septum. The values for higher extraction energies differ slightly, but these differences are not significant and will be ignored as far as the dispersion vector is concerned and the values as calculated in Table 4.7 will be applied universally.

On the way from the electrostatic to the magnetic septum the dispersion grows to the values of $D_x = -4.5445$ and $D'_x = 0.48725$. However, after the dispersion suppressor in the extraction line the dispersion is zero.

| | On-resonance particles $\Delta p/p$=**-0.000017** | | Off-resonance particles $\Delta p/p$=**-0.00107** | |
|---|---|---|---|---|
| | Position [m] | Angle [rad] | Position [m] | Angle [rad] |
| Inner edge of segment | -0.0351 | -0.000191 | -0.0351 | -0.000182 |
| Outer edge of segment | -0.045098 | -0.000015 | -0.040383 | -0.000072 |
| Average radial position/angle | -0.040099 | -0.000103 | -0.0377415 | -0.000127 |
| Shift of average position due to momentum [m] | | | 0.00236 | |
| Shift of average angle due to momentum [rad] | | | -0.000024 | |
| Dispersion $D_x$ = (Radial shift / $\Delta p/p$) [m] | | | $D_x$ = -2.23884 | |
| Derivative of dispersion $D'_x$ = (Angular shift / $\Delta p/p$) [rad] | | | $D'_x$ = 0.02279 | |
| Momentum of central orbit of extracted beam | | | -0.000535 | |
| Momentum spread of extracted beam | | | Δp/p = 0.001053 | |
| Radial position of central orbit of extracted beam [m] | | | x = -0.0392395 | |
| Angle of central orbit of extracted beam [rad] | | | x' = -0.0001265 | |

Table 4.7: Dispersion and central orbit of extracted beam at entry to the electrostatic extraction septum

#### Horizontal Phase advance

As explained above the extracted beam is horizontally described by an ellipse that is fitted around the extracted beam distribution and is chosen to be horizontally aligned at the electrostatic septum. However, at the septum the bar of charge is not in a perfect horizontal position but lies slightly tilted in the ellipse. This tilt is described as an initial phase advance. The value of this phase advance can be calculated from the values of the inner and outer limits of the extracted beam. The complete set of values is given in section 4.2.4. The initial phase advance $\mu_{x,initial}$ is derived with simple geometry:

$$\mu_{x,initial} = \arctan\left(\frac{\Delta x'_{inner,outer}}{\Delta x_{inner,outer}}\right) \tag{4.18}$$

Using the limiting parameters of the extracted beam the initial pase advance calculates to a deviation of $\mu_{x,initial} = -1.0085°$ from a horizontal bar. As the beam moves on to the magnetic extraction septa and then along the transfer lines, the phase advance grows according to the beta function. As the tilt of the ”bar of charge” in the fitted ellipse depends on the phase advance, the bar rotates inside the ellipse.

For tracking and defining parameters such as the phase advance between the electrostatic septum (ESE) and the magnetic septum (MST), one has to be careful in which reference frame this is done. In principle there are two main ways to look at the section between the septa for particles that will be extracted at the MST:

- On the one hand, the section can still be seen as a part of the synchrotron. Thus, the ring lattice and the according TWISS functions have to be used.
- On the other hand, for an extracted beam the ESE can be regarded as the start of the extraction line. In this frame the section is dealt with as a transfer line with the Twiss functions, which are defined by the chosen ellipse and which are presented in the PIMMS study [9]: $\beta_x = 5$ m, $\alpha_x = 0$ and $\varepsilon_x = 5\,\pi$ mm mrad. The Twiss functions and emittances in the $y$-plane are simply taken over from the ring.

Also for normalization the correct set of Twiss parameters, according to the chosen frame, has to be used. In the end the transfer matrices for the section in both frames are identical and thus describe the same physics. Therefore, as expected the same results on questions like beam position are obtained independently of the used frame. Nevertheless, parameters like the phase advance differ from frame to frame. In the normalized ring frame the horizontal phase advance is chosen to be $\Delta\mu_{x,Ring} \approx 51^\circ$. This angle transforms to $\Delta\mu_{x,Transferline} \approx 70^\circ$ in the transfer line frame. This is shown in figure 4.15, where the phase advance angle gives the rotation of the "bar of charge" around its center between two points and also the rotation of the center of the "bar of charge" around the beam line center. In a normal (non-normalized) coordinate system the on-momentum "bar of charge" has got an angle of $-1^\circ$ at the ESE and of $-7.3^\circ$ at the MST.

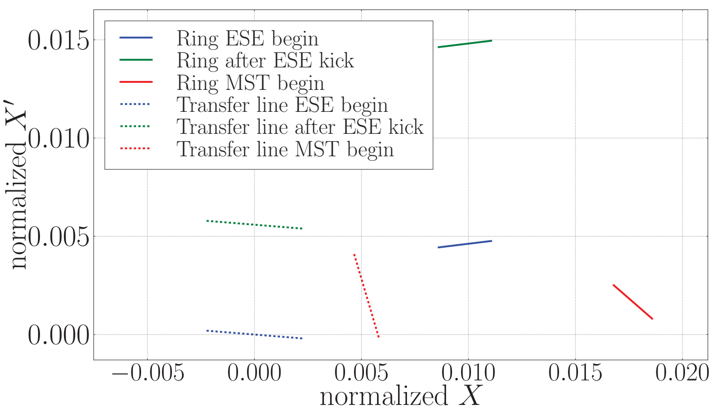


Figure 4.15: On-momentum "bar of charge" at the electrostatic and the "thin" magnetic extraction septum, one time normalized in the ring frame (solid lines), one time in the transfer line frame (dashed lines)

The phase advance of off-momentum particles also depends on the momentum via the chromaticity. Hence, the "bar of charges" for different momenta exhibit slightly different rotations inside the ellipse. Thus, the bars are tilted against each other. Especially, this has to be taken into account in the HEBT, as there are large chromaticities which affect the beam profile at the ISO-center. As an example this effect is presented for the V2 line. The horizontal chromaticity of the V2 line is computed with WinAgile to be $Q_{x,V2} = 46.3$. The momentum spread is assumed to be $\Delta p/p = 1 \cdot 10^{-3}$. Hence, the horizontal phase advance difference is calculated to be:

$$\Delta\mu_x = Q' \frac{\Delta p}{p} \approx 0.05 rad \approx 3^\circ \tag{4.19}$$

This effect influences the particle distribution. Furthermore, if the beam is supposed to be upright at the ISO-center, the different tilts have an impact on the horizontal beam size.

### 4.2.8 Tracking for Betatron core driven extraction

At first the developed tracking code has been used to simulate the betatron core driven extraction to cross check the results with those obtained with WinAgile. In a second step the aim was to obtain a typical particle distribution at the entrance to the extraction line to be used as a standard.

#### Encountered problems with the tracking code and solutions

In the first job, described here, 1000 particles with Gaussian distributions in the transverse planes and a homogeneous one in the longitudinal plane are tracked over 5000 turns. During the first 2000 turns the resonant sextupole is ramped to ensure it is applied adiabatically. Afterwards the sextupole is maintained at constant level. 200 turns after the sextupole is fully turned on, the betatron core is activated to accelerate the particles by $\Delta p/p_{betatroncore} = 5 \cdot 10^{-6}$ per turn. This rather large momentum boost compared to the real situation[7] is chosen to keep computation time short. The particle distribution obtained from this tracking job is presented in figure[8] 4.16(a).

The lower part of the plot 4.16(a) shows the expected bar of charge with expected spiral steps. However, the picture is far from being perfect. Compared to WinAgile the extent of the bar of charge in $x'$ is about a factor two too large. This can be seen in more detail in figure 4.16(b).

This raises the question whether the chromaticity is applied in a correct way, as the Hardt condition does not seem to be fulfilled good enough. Furthermore, all particles should be

[7] Actually, accelerations per turn in the order of $\Delta p/p_{betatroncore} = 5 \cdot 10^{-9}$ are expected in the real machine, as a total momentum shift of $\Delta p/p_{totalshift} \approx 5 \cdot 10^{-3}$ has to be achieved in a few millions of turns depending on the energy and type of particles.

[8] This phase space plot and all following expect mentioned otherwise show the distribution at the electrostatic extraction septum as this is the entrance to the extraction channel.

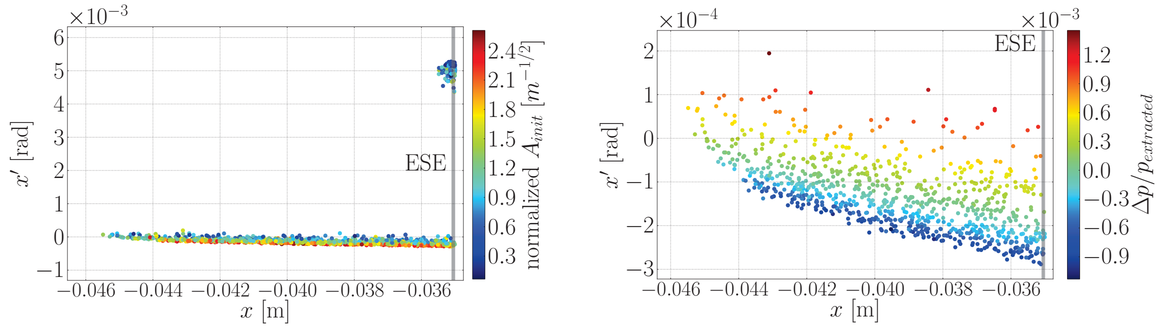


(a) $x$-$x'$-normalized $A_{init}$ (b) $x$-$x'$-$\Delta p/p_{extracted}$

Figure 4.16: Subfigures (a) and (b) show phase space maps at the electrostatic extraction septum for low energy protons.

extracted with negative directions, meaning that their motions are pointing away from the center of the beam pipe and the electrostatic extraction septum wires. Otherwise the losses at the septum would increase. The particles extracted with positive $x'$ values have also got rather high momenta around 0.1% above the design energy, whereas a momentum spread from about on-momentum to $\Delta p/p \approx -1.2 \cdot 10^{-3}$ is expected. Hence, also a problem with the betatron core seems possible. Additionally, in figure 4.16(a) there are particles extracted at very large $x'$ values around $x' \approx 5$ mrad and at high momenta of up to 0.8% above the design momentum. Finally, the initial normalized amplitude is calculated in a wrong way.

The problem with the initial normalized amplitude was easy solve after realizing that the dispersion was not taken into account for the calculation. For the correct computation of the amplitude, the shift due to dispersion has to be subtracted first.

The reason for the particles extracted at very large momentum and $x'$ can be found in figure 4.17(a).

Whereas some particles become unstable and are extracted with more or less expected values, others just stay stable. As the momentum of these stable particles is continuously increased by the betatron core[9], due to the large momentum the particles are shifted via the dispersion until they hit the aperture. This happens at large $x'$ values according to the dispersion vector at the electrostatic extraction septum. Figure 4.17(b) sheds some light on the question why these particles stay stable. This figure shows one single particle which stays stable. The particle starts at some initial coordinates in the lower right of the plot. With increasing number of turns (given as color code) the particle gains momentum due to the accelerating effect of the betatron core and is shifted according to the dispersion. As the particle

[9]In reality the maximum momentum gain is limited by the betatron core capabilities itself. However, in this simulation the betatron core is able to increase the momentum of a particle each turn until the particle hits the aperture or the tracking ends.

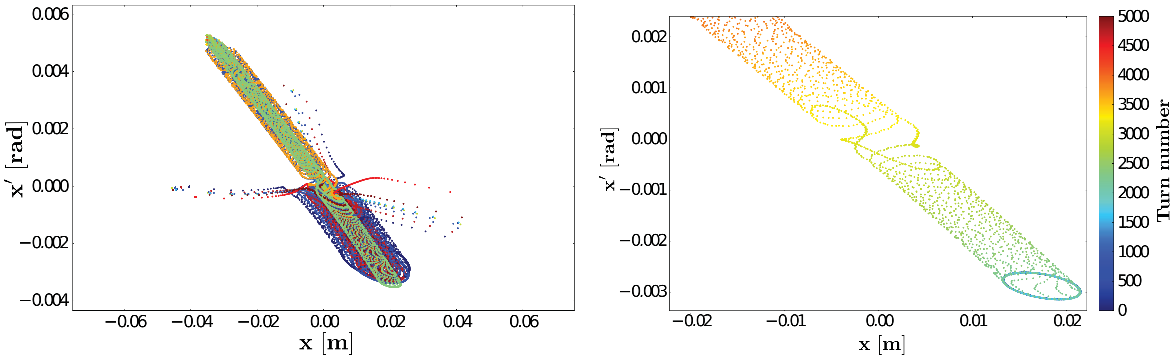


(a) $x$-$x'$-Particle number

(b) $x$-$x'$-Turn number

Figure 4.17: Subfigures (a) and (b) show phase space maps at the electrostatic extraction septum for low energy protons.

comes closer to the center of the beam pipe, which is identical to the origin of plot, its momentum approaches the design one and its tune is shifted towards the resonant one via the chromaticity. Indeed, the motion is changing close to the origin and seems to get unstable. However, the particle returns to a stable motion after a short period of time. Thus, the particle just continues gaining momentum and following the dispersion vector. The reason for this behavior can be found in a Steinbach diagram (for example see figure 4.6(c). The betatron core moves the particle towards the unstable zone. As the particle reaches the border to the unstable region, it becomes unstable. However, after the particle has gotten unstable, it is not extracted instantaneously, but it takes the particle some time to move outwards along the separatrices and to finally reach the extraction septum. During this time the betatron core still acts on the particle and increases its momentum. In the Steinbach diagram this means the particle is moved further along the $x$-axis. If the betatron core is too powerful, the particle is eventually pushed out of the unstable region and returns to stable motion again. As the betatron core strength has been set to unrealistic high values to keep computation time low, this might just be a computational problem. In several following tracking jobs the betatron core strength is decreased and as expected the number of 're-stable' particles shrinks. For a realistic betatron core strength, all particles stay unstable as soon as they have entered the unstable zone. However, the computation time increases as the strength decreases. Therefore in the following a few 're-stable' particles in a full distribution are accepted, as this is only a computational effect and a value of $\Delta p/p_{betatroncore} = 5 \cdot 10^{-8}$ per turn is used to keep simulation time at reasonable values. This measure of decreasing the betatron strength also brings the momentum limits of the extracted particles in the bar of charge closer to the expected theoretical boundaries of $\Delta p/p_{extracted,low} \approx -1.2 \cdot 10^{-3}$ and $\Delta p/p_{extracted,high} \gtrsim 0$. Although all particles become unstable at or below the design momentum, some will be extracted with slightly higher values, because the betatron core still accelerates them in between becoming unstable and being extracted. However, in the tracking jobs the limits of the momentum distribution are still too high and the extent in $x'$ as well. Thus, the Hardt condition is not fulfilled in a satisfactory way. So probably there is still a problem with the integration of the chromaticity.

In the first simulations a fake chromaticity rotation was used to introduce the chromaticity to the system. However, this is not correct, as the chromaticity due to the sextupole is already accounted for by the explicit treatment of the sextupoles. Only the sextupoles placed in dispersive regions contribute to the chromaticity. Hence, the powerful resonant sextupole magnet, which is placed in a dispersion free region, has no influence on the chromaticity. Thus, the chromaticity stays constant during the ramp of the resonant sextupole, at least in this idealized description, but in reality the region will not be completely dispersion free. To come back to the tracking, just leaving the fake chromaticity rotation away also does not bring the correct results. Beside the sextupoles, the quadrupoles in the lattice also influence the chromaticity. But, the transfer matrix formalism does not account for this chromaticity. Therefore, a fake chromaticity rotation dealing with the none sextupole induced chromaticity is needed. From WinAgile the chromaticity in the lattice without the sextupoles is obtained and put into a fake chromaticity rotation [10]. In WinAgile the intrinsic chromaticity of a quadrupole lattice is included by modifying the normalized quadrupole gradients for each momentum.

$$\begin{aligned} Q'_{x,\ w/o\ sextupoles} &= -0.632 \quad (Q'_{x,full} = -4.041) \\ Q'_{y,\ w/o\ sextupoles} &= -1.008 \quad (Q'_{y,full} = -0.195) \end{aligned} \tag{4.20}$$

In brackets the full chromaticity of the lattice with sextupoles is given for comparison.

Figures 4.18(a) and 4.18(b) show a distribution tracked with all improvements described above. It is very similar to WinAgile results with a spiral step of $\Delta x \approx 9.6$ mm and a spiral kick of $x' \approx 0.2$ mrad. All particles are extracted at negative values in $x'$, the Hardt condition is well fulfilled and the normalized initial amplitude is calculated correctly.

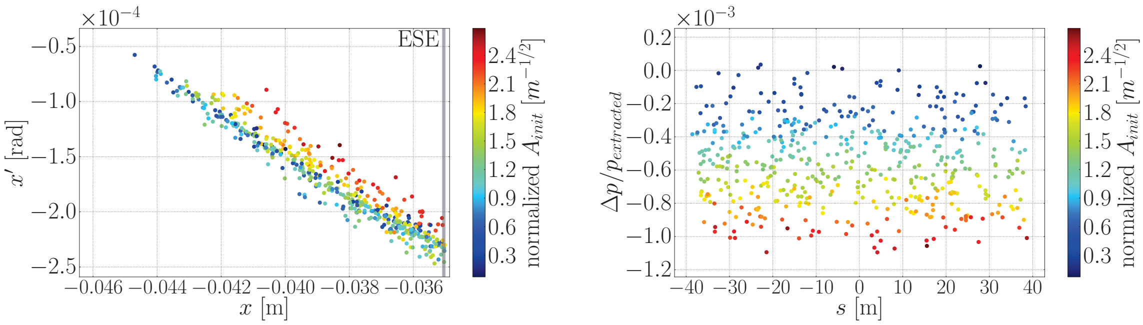


(a) $x$-$x'$-normalized $A_{init}$ (b) $s$-$\Delta p/p$-normalized $A_{init}$

Figure 4.18: Subfigures (a) and (b) show phase space maps at the electrostatic extraction septum for low energy protons.

[10]One should bear in mind that the chromaticity values in WinAgile are calculated via an extrapolation formula from the central orbit tune values. Hence, the given chromaticity figures are only approximations.

### Standard extraction jobs for betatron core driven extraction

With all the improvements described above, it is possible to obtain a distribution that can be used as a standard for studies of the extracted beam. To achieve this goal a distribution of 1000 particles (60 MeV protons) is tracked over 150 000 turns. The particles are created following a Gaussian shape in transverse phase space with a sigma according to a RMS geometric emittance of $\varepsilon = 1.43\ \pi$ mm mrad and truncated at $\sqrt{5}\cdot\sigma$. In longitudinal phase space the particles are placed homogeneously all along the machine with an also homogeneous momentum distribution between $\Delta p/p_{initial,low} = -5.3\cdot 10^{-3}$ and $\Delta p/p_{initial,high} = -1.3\cdot 10^{-3}$. The resonant sextupole is ramped over the first 2000 turns. After a further 200 turns the betatron core starts acting on the particles, applying an acceleration of $\Delta p/p = 5\cdot 10^{-8}$ per turn. Table 4.8 displays the most important beam and lattice parameter used for this standard extraction job.

| **Beam parameter** | | **Lattice parameter** | |
|---|---|---|---|
| Particle | Protons | Accelerator | Synchrotron |
| Energy | 60 MeV | Lattice | MedAustron |
| Number of particles | 1000 | Tracked turns | $1.5\cdot 10^{5}$ |
| Transverse distributions | Gaussian | Horizontal tune | 1.6666 |
| RMS geometric emittance | $1.43\ \pi$ mm mrad | Vertical tune | 1.78916 |
| Truncated | $\sqrt{5}\cdot\sigma$ | $Q'_x$ (Quadrupoles) | -0.632 |
| Total geometric emittance | $7.14\ \pi$ mm mrad | $Q'_y$ (Quadrupoles) | -1.008 |
| Longitudinal distribution | homogeneous | Sextupole ramp | first 2000 turns |
| Momentum distributions | homogeneous | $k_2 l$ | 2.25 |
| Lowest initial momentum | $-5.3\cdot 10^{-3}$ | Betatron core | from turn 2200 |
| Highest initial momentum | $-1.3\cdot 10^{-3}$ | Acceleration | $5\cdot 10^{-8}$ per turn |

Table 4.8: Beam and lattice parameter used in the standard proton extraction job for the betatron core driven extraction

In the following, several figures, depicting interesting features of the extracted particle distribution, are presented and explained:

- Figure 4.19(a) shows the horizontal phase space position for the last three turns before the extraction turn[11] and the extraction turn itself for each particle. The figure clearly demonstrates the spiral step behavior and the application of the Hardt condition.
- Figure 4.19(b) gives the particle distribution at the entry to the electrostatic extraction septum in horizontal phase space and the normalized amplitude as color code. It has

[11] Extraction turn is used here as synonym for the turn when a particle enters the extraction channel of the electrostatic septum.

to be mentioned that this picture has not been taken at one time, but displays the accumulations of all extracted particles over the whole extraction time. Furthermore, the amplitude dependency of the spiral step is clearly illustrated.

- Figure 4.19(c) depicts the particle distribution at the entrance to the electrostatic extraction septum in the vertical phase space. Again this plot presents all extracted particle over the whole extraction time. As the vertical motion is not affected by the resonant extraction the vertical distribution can still be approximated by an ellipse in phase space.
- In figure 4.19(d) the spiral step is plotted versus the extracted relative momentum deviation. Furthermore, the initial normalized amplitude is used as color code. The dependency of the spiral step on momentum and normalized amplitude are immediately visible. The maximum spiral step can only be achieved by on-momentum particles. Moreover, only low amplitude particles can be extracted on-momentum (see Steinbach diagram 4.6(c). The range of spiral steps for one momentum is due to the effect that the spiral step depends on the particle's position in phase space and that the particles 'jump' from different distances to the septum wires into the extraction channel. The more off-momentum a particle is extracted, the smaller is the spiral step, it exhibits. Furthermore, the highest density in the distribution is reach for particles with medium amplitudes, because of the amplitude distribution in the waiting beam (see figure 4.11).
- Figure 4.19(e) presents the extracted relative momentum deviation plotted over the position in $x$ with the normalized amplitude as color code. This figure displays the bar of charges shape as sketched in figure 4.14.
- Figure 4.19(f) shows the extracted relative momentum deviation plotted versus the initial position of a particle along the synchrotron. As expected there is no correlation between the initial position and the extracted momentum. All particles are extracted in a momentum range that is slightly above the theoretical lower instability limit and also above on-momentum which is the theoretical upper instability limit. This shift compared to theory is due to the continuing acceleration between the time a particle becomes unstable and the time it is actually entering the septum.

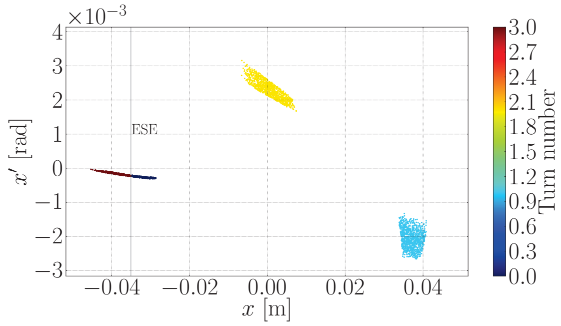


(a) $x$-$x'$-4 last turns

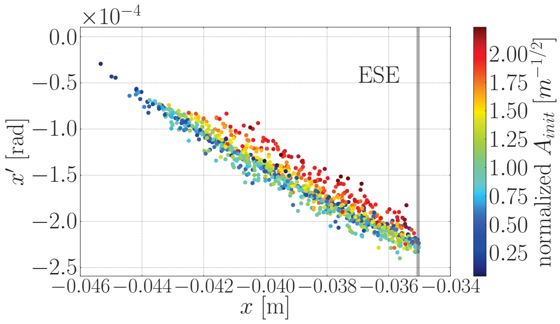


(b) $x$-$x'$-normalized $A_{init}$

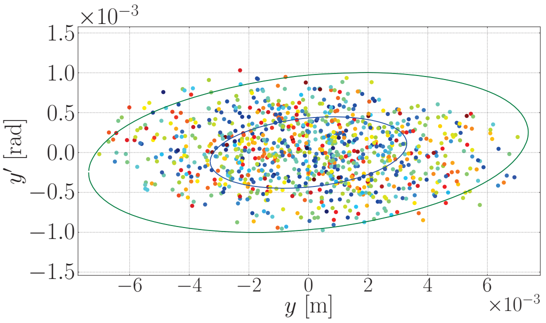


(c) $y$-$y'$

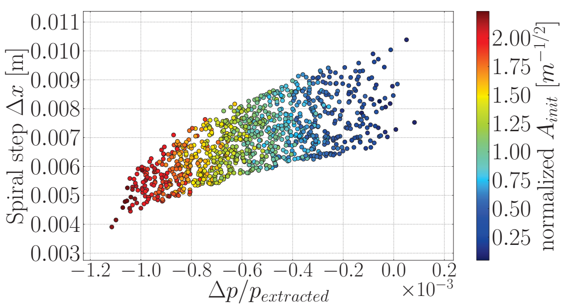


(d) $\Delta p/p_{extr}$-$\Delta x$-normalized $A_{init}$

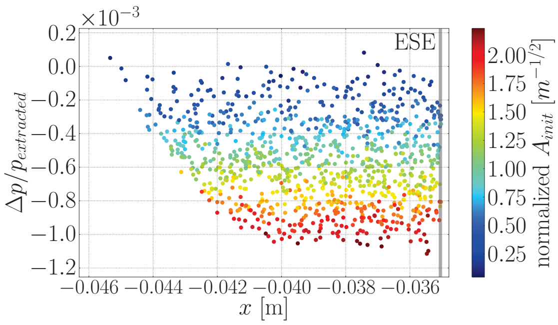


(e) $x$-$\Delta p/p_{extr}$-normalized $A_{init}$

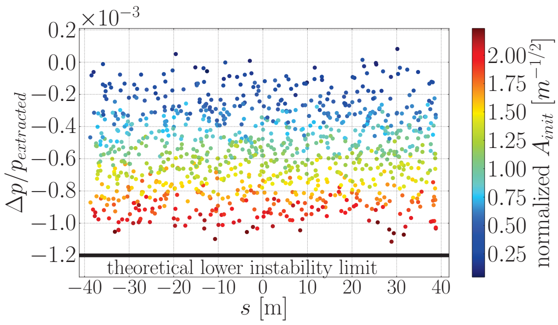


(f) $s$-$\Delta p/p_{extr}$-normalized $A_{init}$

Figure 4.19: Subfigures (a), (b), (c), (d), (e) and (f) show phase space maps at the electrostatic extraction septum for a low energy proton beam.

With the same settings as used in the tracking job above, a beam of top energy carbon ions (400 MeV/u) has been tracked. The results are almost the same as for the low energy protons. As expected the extracted momentum spread is lower for the higher energy particles, because the beam has a smaller RMS geometric emittance of $\varepsilon = 0.73\,\pi$ mm mrad. This yields smaller amplitudes in the beam and finally a smaller extracted momentum spread according to equation (4.10). Figure 4.20 displays the extracted distribution at the entry to the electrostatic extraction septum in horizontal phase space with the extracted relative momentum deviation as color code.

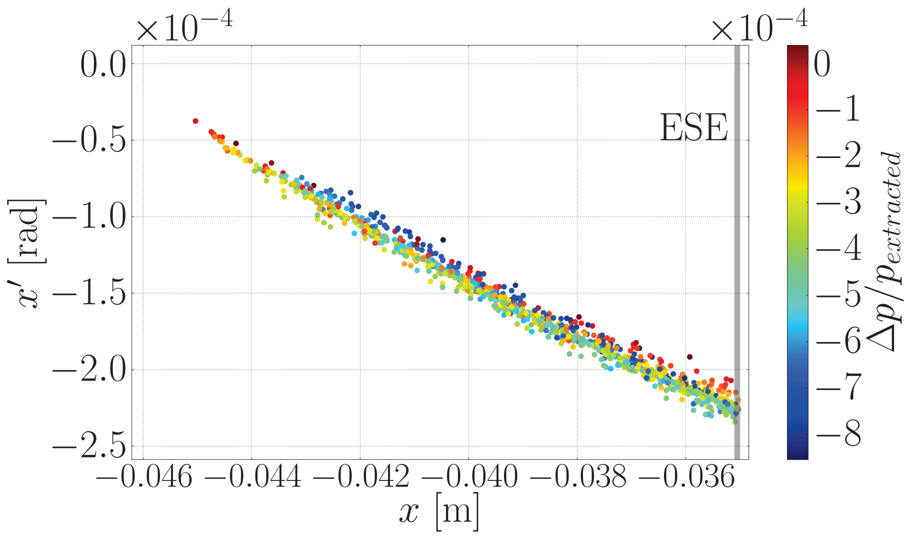


Figure 4.20: Phase space map ($x$-$x'$) at electrostatic extraction septum with the extracted momentum as color code for top energy carbon ions

## 4.3 RF-Knockout

### 4.3.1 Overview

RF-knockout [29] is under investigation to determine whether it is suitable to be used as an alternative extraction mechanism to the nominal betatron core driven extraction at MedAustron. Of special interest is the achievable minimum extraction time, as the betatron core extraction is limited to minimum spill times of 1 s, whereas for non-clinical research, times down to 0.1 s are desired. The RF knockout method is a standard extraction scheme at hadron therapy facilities such as HIMAC (Heavy Ion Medical Accelerator in Chiba) [30] or HIT (Heidelberger Ionenstrahl-Therapiezentrum) [31].

RF-knockout employs amplitude control to move stable particles into the unstable region around the third-order resonance line. Steinbach diagrams 4.21(a) to 4.21(c) are convenient tools to visualize the process. As in the betatron core scheme a resonant sextupole is used to excite the resonance and to create an unstable region. Before the extraction the particles are placed in the stable region below the instability border (see figure 4.21(a)). By increasing their amplitude, the particles can be brought into the unstable area (see figure 4.21(b). This method utilizes the amplitude dependency of the particle tune due to non-linear effects introduced by the sextupole magnets. To obtain the necessary amplitude growth, a transverse RF field is applied to the beam to increase its horizontal emittance. For this purpose an RF field that resonates with the tune or a noise signal can be used. In the betatron core method the particles move along the $x$-axis in the Steinbach diagram, as they gain momentum until they reach the unstable zone. In contrast, with RF knockout the particles maintain their momenta, but move vertically along the $y$-axis, as their amplitude is increased. Therefore, the extracted relative momentum spread $\Delta p/p$ and also the absolute momentum values are determined by the momentum distribution of the whole ”waiting” beam, which stays constant during the extraction process. Hence, the spread and the position of the ”waiting” beam in momentum space have to be carefully set in the preparation for the extraction phase. This preparation (see section 4.2.2) is very similar to the betatron core case, except that the momentum properties have to be chosen differently and RF channeling will not be used.

The momentum spread of the ”waiting” beam has to be set to a lower level compared to betatron core extraction. This is necessary to achieve a similar extracted momentum spread for RF-knockout as in the betatron core scheme. Hence, a momentum spread in the ”waiting” beam of about $\Delta p/p \approx 0.1\%$ should be created. Furthermore, as long as the instability border has got a finite slope, the larger the off-momentum value (meaning further away from the resonance) of the particles, the higher amplitudes have to be achieved to enter the unstable region. If the necessary amplitudes become too large, particles will hit the aperture or enter the extraction septa before they become unstable. Although, stable particles that enter the septum would be extracted, they can not form a useful extracted beam from the applications point of view, which asks for beam sizes of about 10 mm. Such extracted stable particles do not exhibit the typical spiral step behavior, as they still move along stable triangles. Hence, they can only enter the septum very close to the septum’s wires, but they can not jump further into the septum, which is necessary to obtain larger beam sizes. A solution to this problem can be to create an instability border with a rather flat slope. This can be achieved by a chromaticity close to zero or large sextupole strengths. However, the sextupole strength is of course limited by the magnet’s design. Another option is to further decrease the momentum spread in the ”waiting” beam.

To extract particles on the design energy, the ”waiting” beam has to be set at this energy, because the momentum and hence the energy stays constant during RF-knockout extraction. Consequently, to keep particles stable before extraction the resonance has to be positioned away from the design energy. This is achieved by adjusting the lattice tune via changing the

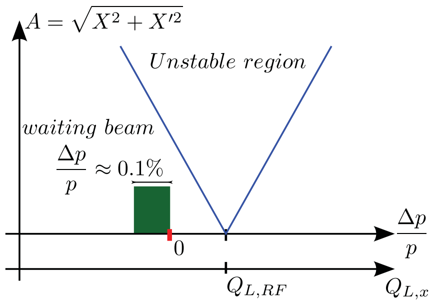


(a) ”Waiting” beam at flat top, resonant sextupole has already been ramped

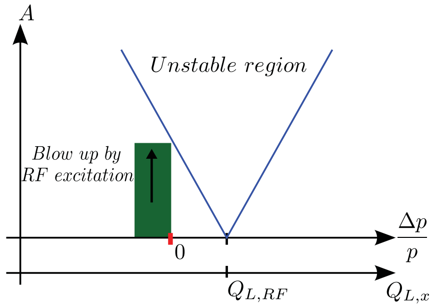


(b) Transverse RF excitation is used to blow up the beam

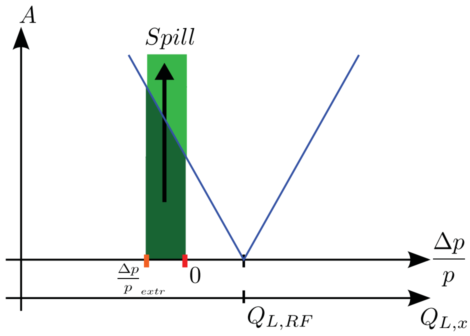


(c) Extraction of spill

Figure 4.21: Subfigures (a), (b) and (c) display the RF-knockout extraction method in a schematic way, the $x$-axes are the momentum deviation $\Delta p/p$ and the horizontal lattice tune $Q_{L,x}$, on the $y$-axes the normalized particle amplitude is given

quadrupole settings. Assuming a finite chromaticity, the necessary tune shift can be approximated analytically by using equation (4.10) for the betatron core extraction:

$$\left|\frac{\Delta p}{p}\right|_{inst} = A_{max}\sqrt{\frac{1}{48\pi\sqrt{3}}}\left|\frac{S}{Q'}\right| \tag{4.21}$$

where $A_{max}$ is the maximum amplitude of the ”waiting” beam before the transverse excitation starts. To maintain the stability of the particles placed on the design energy, the resonance has to be moved away from the ”waiting” beam and the design energy by this calculated instantaneous momentum spread in momentum space. The shift in tune space can be calculated via the chromaticity $Q'$ as $\Delta Q = Q'\,\Delta p/p$. This leads to:

$$\Delta Q = A_{max}\sqrt{\frac{1}{48\pi\sqrt{3}}}\,|S| \tag{4.22}$$

which is independent of the chromaticity.

An intrinsic feature of RF-knockout is that no particles are becoming unstable on-resonance (meaning that the tune distance in equation (3.36) is zero) as in the betatron core scheme. The resonance line $Q_x = 5/3$ has to be kept away from the beam during the whole extraction and of course also before the extraction. This means according to equation (3.54) that the full spiral step defined by the sextupole strength can never be achieved, as there is always a reducing contribution from the tune distance. On the first glance, an increase of the sextupole strengths seems to be an easy solution, however, the tune distance also depends on the sextupole strength. Therefore, a simple solution can not be given and an optimization process is inevitable.

### 4.3.2 Tuning the machine for RF-knockout

As discussed in the previous section 4.3.1 the accelerator settings have to be changed for RF knockout compared to the betatron core extraction. Especially, the tune, the chromaticity and the resonant sextupole strength have to be altered.

Whether an increase of the resonant sextupole magnet strength is possible, depends on the magnet properties itself. In the current design, a significant increase is not possible, however a more powerful sextupole might be necessary to achieve reasonable spiral steps. Hence, a re-design of the sextupole is currently under discussion. This will be discussed in more detail later in this thesis in section 4.3.5.

In the table 4.9 the nominal values (from the betatron core extraction) for the quadrupole ($k_1$) and sextupole ($k_2$) gradients, already prepared for extraction, are given.

| **Quadrupoles** | | **Sextupoles** | |
|---|---|---|---|
| MQD | $k_1 = 0.5134$ | MXR | $k_2 = 8.65$ |
| MQF1 | $k_1 = -0.2959$ | MXD | $k_2 = 1.4125$ |
| MQF2 | $k_1 = -0.5012$ | MXF | $k_2 = -0.3765$ |
| $Q_x = 1.66599$ | | $S_{virt} = 36.7168$ | |
| | | $Q'_x = -4.041$ | |

Table 4.9: Nominal extraction values for quadrupole and sextupole gradients, the virtual sextupole strength, tune and chromaticity values

For the chromaticity, values lower than the nominal are wanted, maybe even close to zero. To control the chromaticity, the chromaticity sextupoles can be used. Also the quadrupole magnets could be employed, however this is more complicated as they have a strong impact on the Twiss functions and the phase advance, whereas the sextupoles can be tuned such that the chromaticity is altered without affecting these lattice properties. The necessary optimization can be done in WinAgile with the function 'Fit chromaticity'. As an example it has been tried to obtain a horizontal chromaticity of $Q_x' = -0.01$ instead of the nominal one of -4.041. With only adjusting the chromaticity sextupoles the gradients have to be set to the following values according to WinAgile: MXF $k_2$ = 0.5555 and MXD $k_2$ = -0.4583. The resonant sextupole is retained at its nominal value, as its strength does not influence the chromaticity. The Twiss functions are also not altered. The virtual sextupole strength computes to $S_{virt} = 36.7174$, which is identical to the nominal one.

From the sextupole strength, the necessary tune shift, to keep the beam stable before the extraction starts, can be calculated from equation (4.22). For the nominal sextupole strength this computation gives a tune shift of $\Delta Q = 0.0061$. To obtain this tune shift the quadrupole settings have to be changed, ideally without influencing the Twiss functions. This optimization can also be done in WinAgile with the function 'Fit tunes / phase advances'.

As an example, an increased resonant sextupole gradient of $k_2 = 20.19$ has been assumed, because an increase seem to be necessary due to spiral step considerations (see section 4.3.5). This change yields a virtual sextupole strength of $S_{virt} = 85.7125$ and a necessary tune shift of $\Delta Q = 0.01417$. This can be achieved for example by changing the gradients of two of the three quadrupole families. Here, MQF2 and MQD have been chosen. The computation with WinAgile gives the following values: MQF2 $k_1 = 0.5081$ and MQD $k_1 = -0.5164$. However, this affects the chromaticity, thus the chromaticity optimization has to be redone. Therefore, it is better to start with the tune and to do the chromaticity afterwards. In the end both ways lead to the same result, which are summarized in the table 4.10. The vertical chromaticity was remained at the nominal value during the optimization process.

| **Quadrupoles** | **Sextupoles** |
|---|---|
| MQD $k_1$ = -0.5164 | MXD $k_2$ =-0.3487 |
| MQF2 $k_1$ = 0.5081 | MXF $k_2$ = 0.5962 |
| $Q_x = 1.68077$ | $S_{virt} = 85.7127$ |
| $\Delta Q_x = 0.01417$ | $Q_x' = -0.01$ |

Table 4.10: Adjusted RF-knockout extraction values for quadrupole and sextupole gradients, the virtual sextupole strength, tune and chromaticity values

The small effects on the horizontal Twiss and Dispersion functions are shown in figure 4.22.

### 4.3.3 Choosing a kicker element

For RF-knockout extraction an element is needed that is able to increase the amplitude of the particles in the "waiting" beam. This can be done by transverse excitation with electrical or

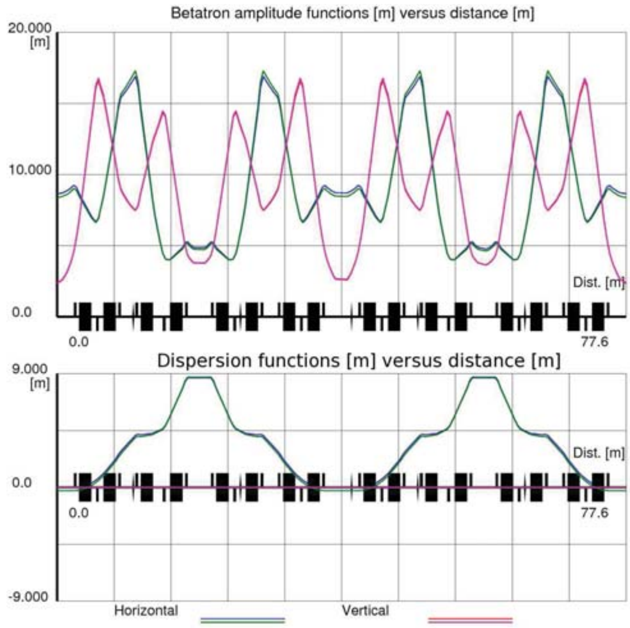


Figure 4.22: Effect of the adjustments of quadrupole and sextupole gradients to obtain targeted values of chromaticity and tune for RF-knockout, the blue line denotes the nominal horizontal case, green the adjusted scenario, pink gives the vertical situation

magnetic fields. The kicks applied on the beam by these fields have to be fluctuating to achieve a continuous amplitude growth. A constant kick would only create a new orbit, unless the tune is set to an integer value. Non constant kicks can be generated from trigonometric functions or by noise generators.

In the MedAustron synchrotron existing elements capable of producing the kicks are the horizontal tune kicker (MTH) and the horizontal Schottky monitor (SHH). The efficiency of the kicks depends on the Twiss beta function. A higher beta value means a stronger effect of a kick on the beam. For a maximum beta value the phase space ellipse lies flat on the $x$-axis, whereas for a minimum beta it stays upright in the horizontal phase space. In the flat case a kick $\Delta x'$ is relatively larger compared to the directions $x'$ of the particles in the beam than in the upright position. Hence, in the flat case the beam is described by a larger ellipse after the kick, in which it can filament. A glimpse at the beta functions at the two elements allows for an easy choice:

$$\begin{aligned} \beta_{MTH} &= 4.906 \\ \beta_{SHH} &= 15.735 \end{aligned} \tag{4.23}$$

Consequently, the horizontal Schottky monitor is the element of choice for RF knockout at MedAustron. A Schottky monitor can be approximated as a parallel-plate capacitor with a plate distance $d$, which is $d_{SHH} = 0.13$ m in the current MedAustron design. The length of the Schottky monitor is currently set to $l_{SHH} = 0.9$ m. The available voltage is limited by the feed cable of the Schottky monitor to about $U_{max} \approx 1000$ V. Consequently, maximum electric fields of $E_{max} = U_{max}/d = 7693$ V/m can be produced.

### 4.3.4 Approximation of kick for RF-knockout

An essential question for RF-knockout extraction is, how large the kick applied by the horizontal Schottky Monitor (SHH)[12] has to be. Especially the maximum necessary kick per turn is of interest, as this determines the maximum electric field, which has to be produced by the Schottky monitor. This electric field is limited by the design of the Schottky monitor, as the field is determined by the available voltage and the geometry of the Schottky monitor to about $E_{max} = 7693$ V/m.

The necessary kick depends on beam properties such as particle type or energy and on the desired extraction time. Table 4.11 gives important beam properties for MedAustron like energy, revolution frequency $f_{rev}$, emittance $\varepsilon_x$ and the electric rigidity $E\rho$.

| Particle | Energy [MeV/u] | $f_{rev}$ [MHz] | $\varepsilon_x$ [$\pi$ *mm mrad*] | E$\rho$ [MV] |
|---|---|---|---|---|
| Proton | 60 | 1.3184 | 7.1429 | 116.4 |
| Carbon | 400 | 2.7588 | 3.6627 | 1359.7 |
| Proton | 800 | 3.2502 | 1.6639 | 1231.8 |

Table 4.11: Properties of low and top energy proton and top energy carbon beams

To approximate the necessary electric fields, two particles in the ”waiting” beam, a zero- and a maximum- amplitude one both with the same momentum, are examined. The maximum amplitude is given by the total geometric emittance $\varepsilon_x$ via $A_{max} = \sqrt{\varepsilon_x/\pi}$. The spill time can be approximated by the time it takes to increase the amplitude of the zero amplitude particle to the maximum one by applying horizontal kicks. It is assumed that particles with the maximum amplitude are very close to the border of the unstable region created by the resonant sextupole. Thus, the time to increase the amplitude from the maximum one in the ”waiting” beam to an unstable amplitude is small compared to the time from zero to maximum amplitude and therefore, neglected in this approximation. Further, as soon as a particle becomes unstable, it will be extracted in typically a few hundred turns. This duration is equivalent to a time of a few microseconds. Hence, the time between instability and extraction is negligible compared to the spill time, which will be larger than 0.1 s. Furthermore, it is assumed that the same extraction settings are used for all particle types and energies. To keep all ”waiting” beams

[12]Kick could also be applied by other elements, but due to the reasoning in section 4.3.3 the horizontal Schottky Monitor is assumed to be the kicker element.

stable, these parameters have to be set according to the beams with the largest emittances, which are the low energy proton beams. This means that all beams have to accomplish the same emittance growth to become unstable.

The horizontal kicks are approximated by white noise to account for the stochastic nature of the RF-knockout process. Each turn a random kick within the limit of a maximum available kick is exerted on the beam. Thus, after one turn a beam with the initial emittance $\varepsilon_0$ is given by $\varepsilon_1 = \langle (x+\Delta x)^2 \rangle / \beta$, where the expectation value has to be taken over all particles in the beam. Because of the linearity of the expectation value this can be rewritten:

$$\varepsilon_1\,\beta = \underbrace{\langle x^2 \rangle}_{\varepsilon_0} + \underbrace{\langle 2x\Delta x \rangle}_{0} + \underbrace{\langle (\Delta x)^2 \rangle}_{\langle \Delta x \rangle > 0} \tag{4.24}$$

The first term on the right side of the equation gives the unperturbed initial emittance $\varepsilon_0$. The second term is equated to be zero, because it is assumed that the unperturbed beam distribution and the white noise are not correlated. However, the third term gives a non zero contribution. After $N$ turns the emittance is calculated to be $\varepsilon_N = \varepsilon_0 + \sum_{turns} \langle (\Delta x)^2 \rangle$. Hence, a quadratic dependency of the emittance growth on the kick strength is expected. This dependency has also been found in tracking studies.

To obtain the emittance growth via tracking, a Gaussian particle distribution has been simulated in the MedAustron lattice. To limit computation time, 50 particles with a homogeneous energy distribution ($\Delta p/p = [0, -1 \cdot 10^{-3}]$) have been tracked over 50 000 turns. To avoid resonance effects due to the emittance growth the sextupole magnets have been turned off. Moreover, all aperture limitations have been removed. The studies have been done for protons with the nominal energy of 60 MeV and for carbon ions with 400 MeV/u.

For large turn numbers the emittance is approximately increasing linearly with the turn number for one kick strength. Figure 4.23 displays this behavior for carbon ions and a maximum kick strength of $\Delta x'_{max} = 10^{-5}$ rad.

The comparison of the emittance growths for different kick strengths shows the expected quadratic behavior. This can be seen in the figure 4.24(a) for protons and in figure 4.24(b) for carbon ions. The figures are given in double logarithmic scale, thus, a linear equation $y = k\,x + d$ describes a polynomial behavior $\bar{y} = \bar{d}\,\bar{x}^k$ of order $k$. As the linear equations of the fits to the data points in the figures 4.24(a) and 4.24(b) have got "$k$" values close to two, the dependency of the emittance growth on the kick strength is indeed quadratic. Because of the rather small number of particles the quality of the fits is limited.

To obtain the necessary kick strength it is assumed that the spill time is given by the time it takes to increase a very small single particle emittance to the nominal beam emittance. From the tracking studies on the emittance growth it can be concluded that kicks per turn about $\Delta x' \approx 10^{-6}$ rad for protons (60 MeV) and $\Delta x' \approx 7.2 \cdot 10^{-7}$ rad for carbon ions (400 MeV/u)

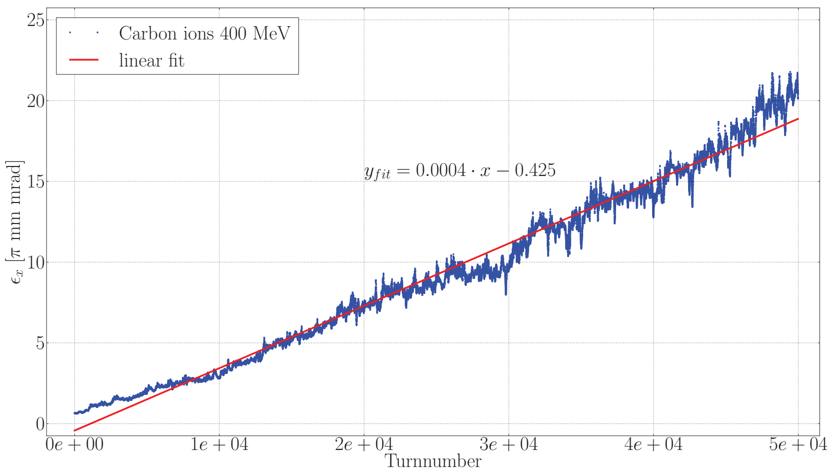


Figure 4.23: Emittance growth of a carbon ion beam (400 MeV/u) over 50,000 turns due to stochastic horizontal kicks with a maximum strength of $\Delta x'_{max} = 10^{-5}$ rad.

are necessary to achieve spill times of $t_{spill} \approx 1$ s. These values are in good accordance with the numbers from other facilities (e.g. from CNAO [32]).

From the maximum kick per turn the necessary electric field in the Schottky monitor can be derived. In a thin lens approximation a kick $\Delta x'$ is approximated by the bending angle $\alpha$ of an electrostatic element. Thus, the electric field can be calculated by rearranging equation (3.6) to:

$$E = \Delta x' \frac{E\rho}{l_{SHH}} \tag{4.25}$$

with the electric rigidity $E\rho$. The necessary voltages ($U = E\ d$) are computed to be $U =$ 141 V for carbon ions (400 MeV/u) and $U = 17$ V for protons (60 MeV) respectively. These numbers are well below the maximum available $U_{max} \approx 1000$ V. Table 4.12 presents the results from the calculations for the necessary electric fields and voltages at the horizontal Schottky monitor.

| Particle | Energy [MeV/u] | $t_{spill}$ [s] | $\Delta x'_{max}$ [rad] | E [V/m] | U [V] |
|---|---|---|---|---|---|
| Proton | 60 | 1 | $10^{-6}$ | 130 | 17 |
| Carbon | 400 | 1 | $7.2 \cdot 10^{-7}$ | 1088 | 141 |

Table 4.12: Results for the calculations of the necessary electric fields and voltages at the horizontal Schottky monitor for 1 s spill times

For research purposes, spill times of down to 0.1 s are foreseen at MedAustron. As the nominal betatron core extraction is not feasible of achieving times shorter than 1 s, alternative

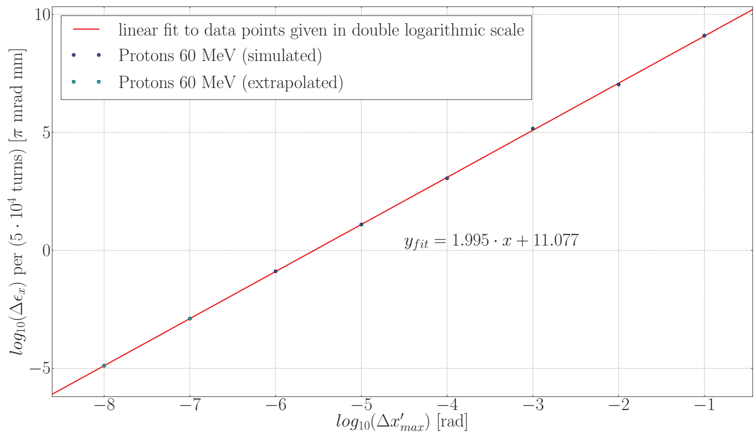


(a) Protons

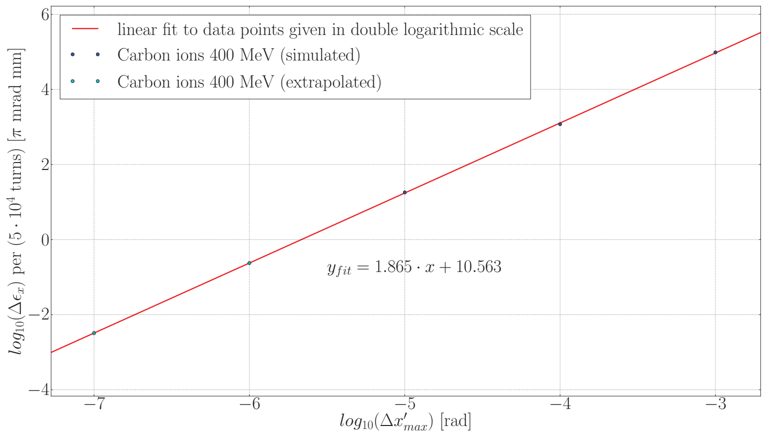


(b) Carbon ions

Figure 4.24: Subfigures (a) and (b) show the emittance growth for proton and carbon beams due to stochastic horizontal kicks of different strengths in double logarithmic scale

extraction schemes like RF-knockout have to be employed. Especially the top energy protons with 800 MeV have to be considered, as they are only used for research. In the following the calculation of the necessary electric fields and voltages at the horizontal Schottky monitor is done on the same assumptions as above. The results are summarized in table 4.13. The necessary voltages are at least a factor 2 below the maximum available voltage, therefore spill times of $t_{spill} = 0.1$ s seem to be feasible with RF-knockout.

Still the numbers calculated above are approximations and some factors have not been accounted for yet:

- The kicks applied to the beam will not be white noise but following a sinusoidal function with a frequency modulation according to the revolution frequency and the tune to effect

| Particle | Energy [MeV/u] | $t_{spill}$ [s] | $\Delta x'_{max}$ [rad] | E [V/m] | U [V] |
|---|---|---|---|---|---|
| Proton | 60 | 0.1 | $4.6 \cdot 10^{-6}$ | 598 | 78 |
| Carbon | 400 | 0.1 | $2.5 \cdot 10^{-6}$ | 3762 | 489 |
| Proton | 800 | 0.1 | $2.6 \cdot 10^{-6}$ | 3543 | 461 |

Table 4.13: Results for the calculations of the necessary electric fields and voltages at the horizontal Schottky monitor for 0.1 s spill times

the whole beam with its finite energy spread in a similar way.

- The electric field is not homogeneous on the full length of the Schottky monitor, thus the effective length is shrinking.
- The aim of the extraction is to obtain a homogeneous extracted beam. However, the beam profile of the "waiting" beam is not homogeneous. Hence, a modulation of the kick amplitude over the extraction time [32] is necessary. The kick amplitude has to be increased over the extraction time by approximately a factor of three. The necessary electric field also has to grow by that factor. However, it should be possible to start with kick values below the ones mentioned above and increase during the extraction to values above the calculated ones. Hence, the achievable kicks in the order of a few μrad should be sufficient.
- In the approximation above it was assumed that the unstable region is situated just above the maximum amplitudes in the "waiting" beam, if this is not the case, the time between the start of the extraction process and the extraction of the first particles would increase. Furthermore, because of the slope of the unstable region, off-momentum particles need to gain more amplitude than on-momentum ones to become unstable, this would increase the spill time. However, for RF-knockout the machine will probably be tuned such that the slope is very flat (see section 4.3.2) and thus conditions should be similar for on- and off-momentum particles.

### 4.3.5 Tracking for RF-knockout

So far it has not been verified whether RF-knockout is working with the MedAustron accelerator at all and if yes whether it is possible to achieve useful extracted beams. Hence, in the first place the feasibility has to be shown and a working set of machine parameters has to be found. In the second step the machine settings have to be optimized to obtain good results for the usual suspects such as e.g. the spiral step.

To be able to do many tracking jobs to check many different settings, the tracking jobs are restricted to a few particles, which mark the borders of the "waiting" beam in amplitude-momentum space. The initial momentum spread is assumed to be smaller than in the betatron core method to obtain similar or smaller extracted momentum spreads and to avoid aperture problems, thus $\Delta p/p_{initial} \lesssim 1 \cdot 10^{-3}$. The emittance is the same as in the betatron core scheme, therefore, the maximum initial amplitudes in the "waiting" beam are about $A_{max} \approx 0.00267[\sqrt{m}]$. For reasons explained in section 4.3.1 the beam is placed at and below the design energy. Thus, in momentum space the particles are placed between $\Delta p/p = -\Delta p/p_{initial}$ and $\Delta p/p = 0$. The kicks from the Schottky monitor (SHH) are assumed to have white noise characteristics. This is simulated by using a fixed amplitude which is weighted with random number in the interval between [-1 and +1]. The SHH is set to start acting 1000 turns after the resonant sextupole magnet has been ramped. Like in the earlier tracking simulations the resonant sextupole is ramped over 2000 turns and the contribution to the chromaticity from the quadrupole magnets is accounted for by a fake chromaticity rotation.

In a first try the chromaticity has been maintained at the constant value of $C_x \approx -4.041$, but the sextupole gradient has been varied starting from nominal value $k_2 l = 2.25$ to almost three times larger values. The necessary tune shift, to keep the beam stable before the SHH starts acting, is calculated with equation (4.22). A few values around this theoretical number are tested to verify the computation and for optimization reasons. The initial momentum spread has been set to $\Delta p/p_{initial} = 0.5 \cdot 10^{-3}$. The results are shown in figures 4.25(a) to 4.25(f). For the on-momentum particles a normalized sextupole strength $S$ around the value 60 seems to be optimal. This would mean that the current sextupole design is not powerful enough, as this value is about twice the current capability. Moreover, the theoretical tune shift $\Delta Q_{th}$ is a good approximation, because lower tune shifts cause particles with high amplitude to get unstable just by ramping the sextupole (denoted by the black points in the plots). Nevertheless, values for the tune shift slightly below the calculated number ($\Delta Q_{th}$ - 1/1000) seem to be better in terms of spiral step. With these numbers a spiral step of about 6 mm can be achieved. This result is not surprising, as the situation is similar to the off-momentum particles in the betatron core case. However, the off-momentum particles in this simulation rarely become unstable and only hit the septum because of their amplitude growth due to the transverse excitation. As a counter measure in the next step the chromaticity is varied and brought closer to zero, to further flatten the slope of the instability border.

The following tracking study is almost identical to the one above, only the chromaticity has been set close to zero. This is achieved by adding a further fake chromaticity rotation to cancel out the existing chromaticity. In the real machine the chromaticity sextupole would need to be changed as demonstrated in section 4.3.2. The results are given in the figures 4.26(a) to 4.26(f). For the on-momentum particles the results are similar to the upper case. However, the difference is found in the off-momentum ones, which also become unstable in this scenario and exhibit similar spiral steps as the on-momentum ones. Again the best results are obtained for normalized sextupole strengths around 60 and tune shifts slightly lower than the analytically computed ones. Spiral steps in the range of 5 to 7 mm have been obtained.

Still the spiral steps are away form the nominal 10 mm. As only few particles have been tracked so far, some improvement can be expected from larger distributions, because this increases the chances to have particles that pass very close to the septum wires before their final spiral step.

The spiral step depends quadratically on the radial position $x_{ESE}$ of the electrostatic extraction septum (see equation (3.55)). Therefore, by placing the septum further away from the center of the beam pipe, a larger spiral step can be achieved. The nominal position of the septum in the MedAustron design is $x_{ESE} = 35$ mm and it is designed to be movable in a range of about $\pm 10$ mm. To increase the spiral step by a factor of 2, the septum has to be moved outwards by a factor of $\sqrt{2}$. This yields a new septum position of $x_{ESE,new} \approx 49.5$ mm. However, this would already need a larger shift than possible with the current design. Furthermore, even if such a shift would be possible, the shift of the septum has to be checked in the whole accelerator whether conflicts are arising for example with the aperture. A main issue is the magnetic extraction septum, which has got a fixed position and a rather thick wall of about 20 mm. In the nominal design the position of the magnetic septum is optimized such that unstable particles, in the turns before they enter the electrostatic septum, will also pass outside the magnetic septum. Only when the particles enter the electrostatic septum, a kick is applied by the septum. This kick transforms into a gap at the magnetic septum between the circulating beam and the extracted one, larger than the magnetic septum wall. However, if just the position of the electrostatic septum is increased, particles will have too large amplitudes to pass the magnetic septum before they enter the electrostatic septum. These particles will hit the wall of the magnetic septum and be lost. A decrease of the beta function around the magnetic septum could shrink the amplitudes of the particles, however, this is probably not possible due to many other constraints in that region.

The tracking simulations demonstrate that bringing the ”waiting” beam closer to the resonance, meaning a decrease of the tune shift, would result in larger spiral steps. However, with such a setup particles with large amplitudes become already unstable during the sextupole ramp and would be lost for later applications of the extracted beam. Nevertheless, if higher losses are acceptable for a certain application, this could help to obtain larger spiral steps.

Another issue is the Hardt condition. Because of the changes of the chromaticity and the sextupole strength in a way that is not fulfilling the Hardt condition, the extent of the extracted beam in $x'$ is increased. Especially, particles extracted with positive $x'$ values are problematic, as their motion points towards the septum wires after they have entered the septum. This would increase losses due to collisions with the septum wires. According to the equation (3.46) it is possible to fulfill the Hardt condition at the electrostatic extraction septum for the zero chromaticity scenario, if this septum is placed in a dispersion-free region. However, such a setup does not seem to to possible with the MedAustron lattice, because it is designed for the non-zero chromaticity case. [23]

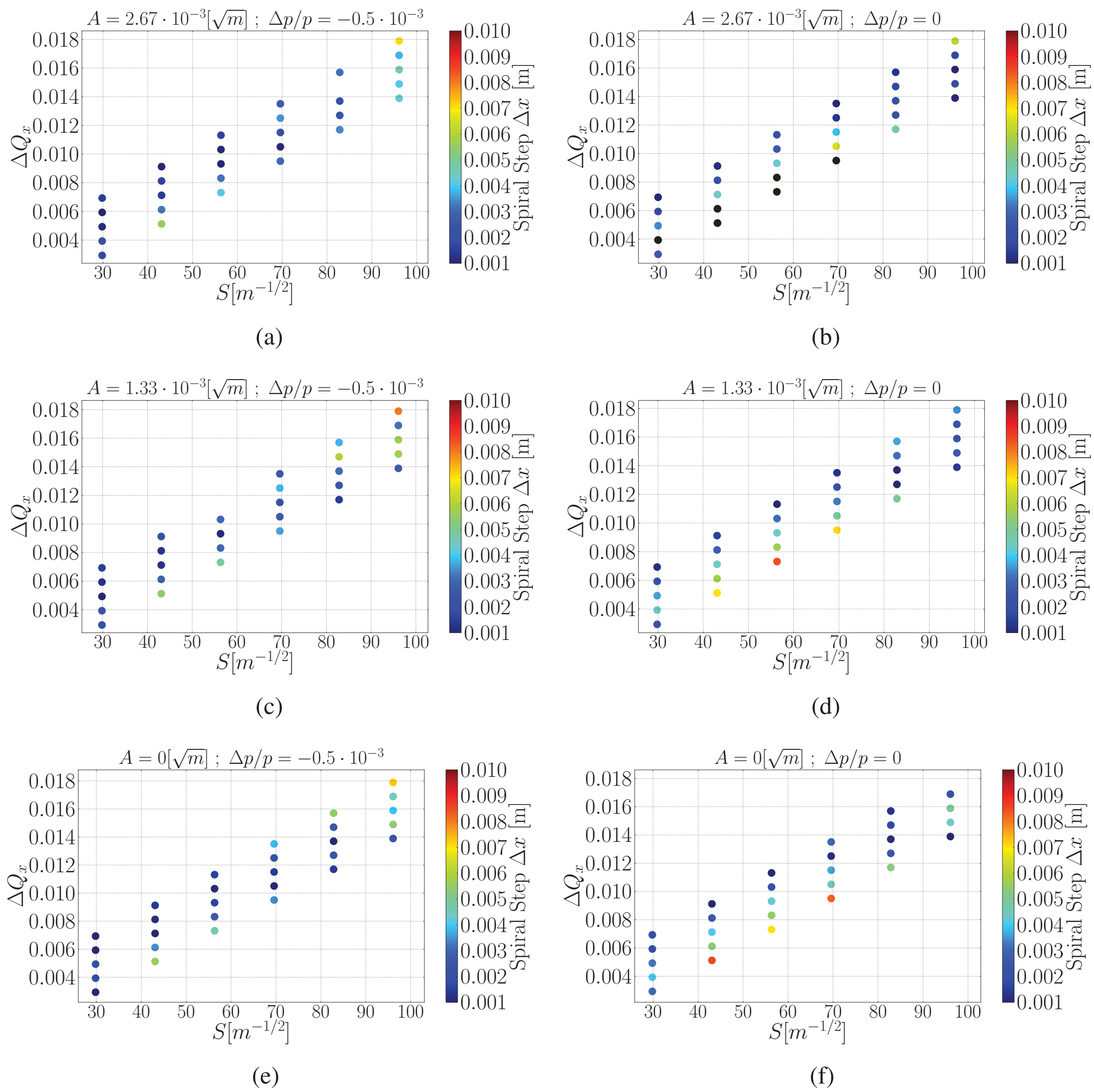


Figure 4.25: Subfigures (a), (b), (c), (d), (e) and (f) show the spiral steps for the nominal chromaticity but different initial conditions such as sextupole strength $S$, tune shift $\Delta Q$, particle amplitude $A$ and momentum deviation of the particle $\Delta p/p$. Black dots indicate particles that become unstable before RF-knockout is started.

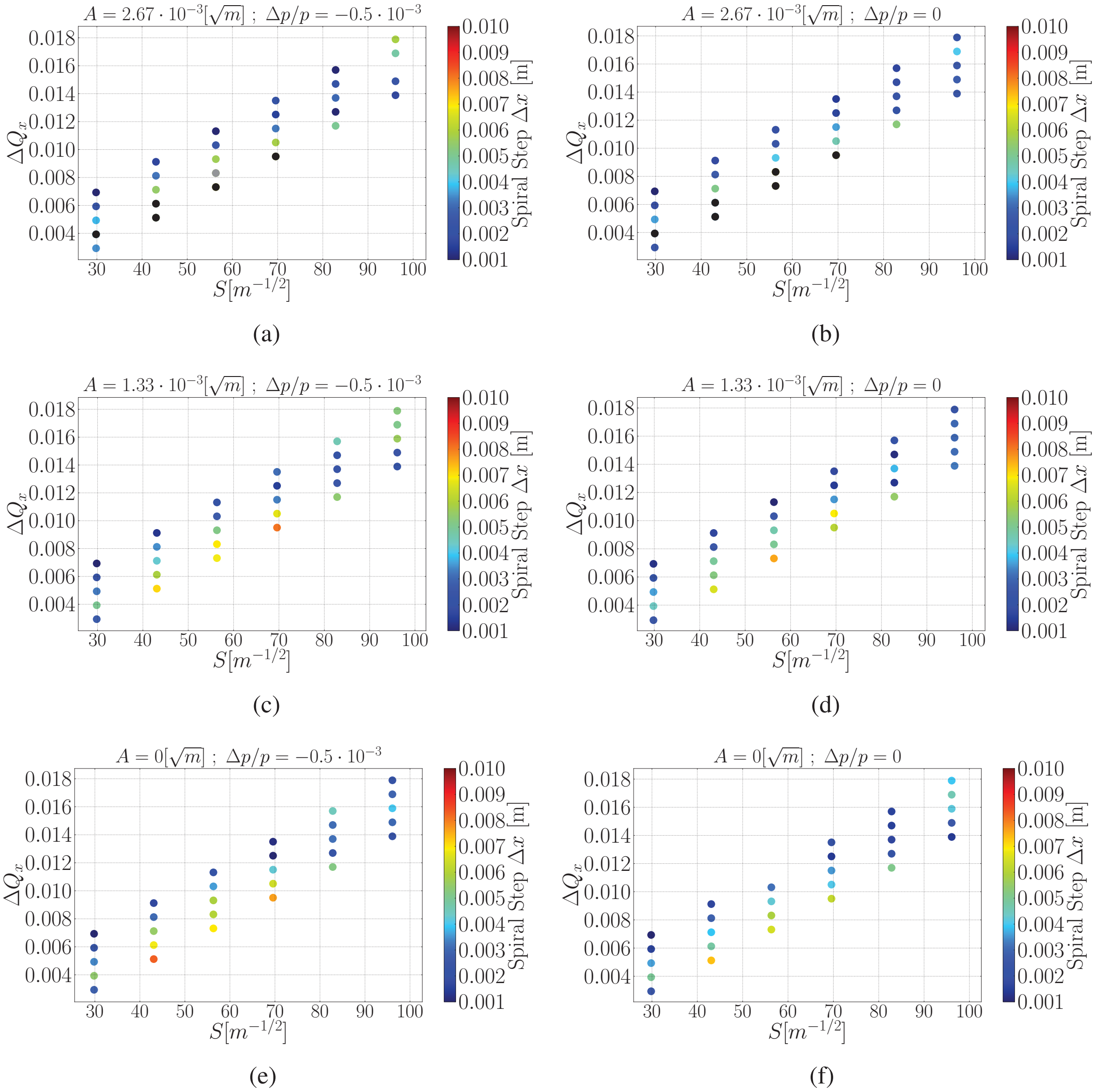


Figure 4.26: Subfigures (a), (b), (c), (d), (e) and (f) show the spiral steps for a chromaticity close to zero and different initial conditions such as sextupole strength $S$, tune shift $\Delta Q$, particle amplitude $A$ and momentum deviation of the particle $\Delta p/p$. Black dots indicate particles that become unstable before RF-knockout is started.

# 4.4 Alternative extraction methods

## 4.4.1 RF-noise extraction

### Overview

The stochastic RF-noise extraction method [33] is an acceleration driven method. To move the particles into resonance, longitudinal RF-noise with a particular frequency bandwidth is applied to act on the momenta of the particles. The frequency spectrum has to match the revolution frequencies of the "waiting" beam to be able to excite all particles. In later simulations the noise will be applied by the RF cavity, which is also a probable implementation for MedAustron, because no additional equipment is needed. Alternatively the noise could be applied by special longitudinal kickers. The noise forces the particles to carry out random walks in longitudinal phase space similar to Brownian motion. The behavior can also be seen as a diffusion process and treated as such. The noise randomly accelerates and decelerates the particles, which leads to a blow up of the momentum distribution. Therefore, the particles are more diffused towards and across the instability border than driven as in the betatron core method. The unstable region is placed at one end of the frequency spectrum. Figure 4.27 illustrates the extraction principal. This extraction method promises a low ripple extraction and similar results as the betatron core one as the machine settings and preparation for the extraction can be the same for both schemes. Moreover, the machine settings can be remained at constant values during the extraction as in the betatron core method. This method has been successfully employed for slow extraction for example at CERN's LEAR (Low Energy Antiproton Ring) and SPS (Super Proton Synchrotron) [34].

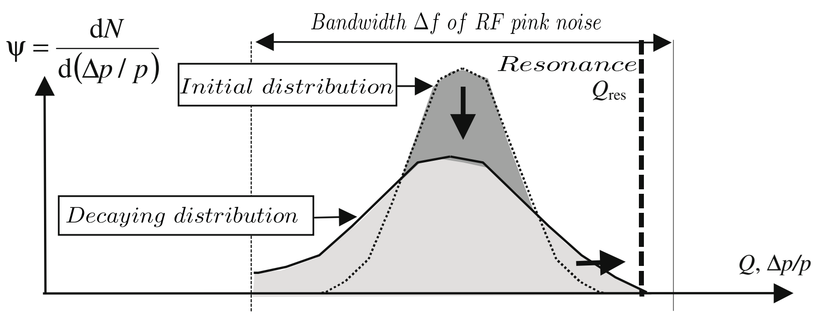


Figure 4.27: Principal of RF-noise extraction with band-limited noise

As the process can be described as diffusion, the particle blow-up in momentum space obeys the diffusion equation (Fick's second law):

$$\frac{\partial \psi}{\partial t} = \frac{\partial}{\partial x}\left(D\,\frac{\partial \psi}{\partial x}\right) \tag{4.26}$$

where $t$ gives the time, $x$ denotes the chosen space (e.g. tune, momentum), $\psi$ is the particle density in the chosen space $\psi = dN/dx$ and $D$ the diffusion constant $D = 1/2\, d(\bar{x^2})/dt$. The diffusion constant can be expressed in momentum space as a function of the RMS noise voltage $V_N$ and the noise frequency spectrum $\Delta f$ [4]:

$$D_p = \frac{1}{2} \frac{V_N^2}{\Delta f} \frac{1}{(2\pi\, R\, B\rho)^2} \tag{4.27}$$

where $R$ is the accelerator radius and $B\rho$ the magnetic rigidity.

### Approximations

In the following some approximations are used to obtain numbers for the frequency spectrum of the noise, the voltage and the resulting power.

The frequency bandwidth of the ”waiting” beam can be calculated from the momentum or energy spread. Assuming a momentum spread of $\Delta p/p \approx 0.4\%$ yields bandwidths in the revolution frequencies $\Delta f_{\text{"waiting"beam}}$ between 4 and 6 kHz depending on the particle and design energy. The bandwidth of the noise has to be larger than those numbers and also cover the initial distance to the resonance and some margins. Assuming that the bandwidth is centered around the ”waiting” beam, it has to cover a region in momentum space of about $\Delta p/p_{signal} \approx 0.9\%$. This results in signal bandwidths $\Delta f$ of about 10 kHz (see table 4.14).

| **Protons** | | **Carbon ions** | |
|---|---|---|---|
| Energy [MeV] | $\Delta f$ [kHz] | Energy [MeV/u] | $\Delta f$ [kHz] |
| 60 | 10.527 | 120 | 12.715 |
| 800 | 8.595 | 400 | 12.239 |

Table 4.14: Necessary bandwidths of the RF-noise for proton and carbon ion beams with an momentum spread $\Delta p/p \approx 0.4\%$ at different design energies

In the PIMMS study [4] it is demonstrated that an RMS voltage in the RF cavity in the order of 500 V is necessary to achieve spill times of 1 s for top energy carbon ions. To obtain spill times of 0.1 s at MedAustron the diffusion constant of the process has to be increased via a larger voltage. Because of the quadratic behavior approximately a three times higher RMS voltage of about 1500 V has to be delivered. Assuming a resistance of $Z = 50\,\Omega$, the total power of the noise signal calculates to $W = 45$ kW.

### Tracking

To simulate the noise, random numbers between -1 and 1 are used as weights for a maximum voltage. This is not accounting for the frequency bandwidth but all particles will see the same longitudinal kicks. For all other aspects the tracking jobs are like the standard betatron core driven extraction job, meaning ramp of the resonant sextupole, fake chromaticity rotations, etc., of course the betatron core is not active.

Already the first simulations, in which 400 protons (60 MeV) have been tracked, showed fine results, almost identical to the betatron core extraction in terms of the extracted distribution in $x$-$x'$-phase space (see figures 4.28(a) & 4.28(b)). In this simulation an RF cavity voltage of 1500 V has been used. Figure 4.29(a) shows that this rather high voltage for the case of low energy protons results in the extraction of the beam in two slices separated in time. As illustrated in figure 4.29(b), by decreasing the voltage (e.g. 1200 V) the beam is extracted in a more continuous way with a total spill time of about 0.1 s. However, these slices are probably only simulation artefacts, as in this simulation the effect of different revolution frequencies in the "waiting" beam in combination with a colored noise is not accounted for. This should produce smother spills, as different particles will be subject to different kicks and thus will become unstable at different times. In general, RF-noise seems to be a promising candidate as an alternative extraction method at MedAustron.

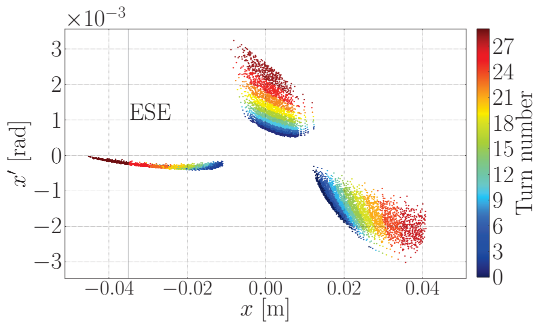


(a) $x$-$x'$-last 30 turns

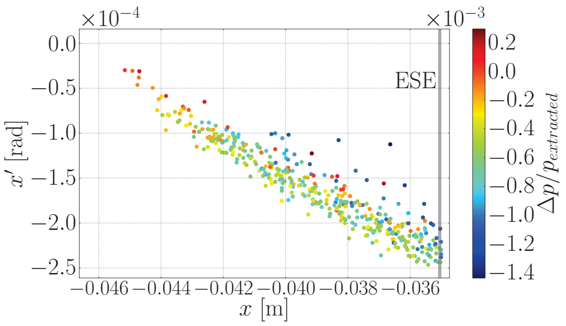


(b) $x$-$x'$-$\Delta p/p_{extr}$

Figure 4.28: Subfigures (a) and (b) show phase space maps at the electrostatic extraction septum for a low energy proton beam excited with longitudinal RF-noise

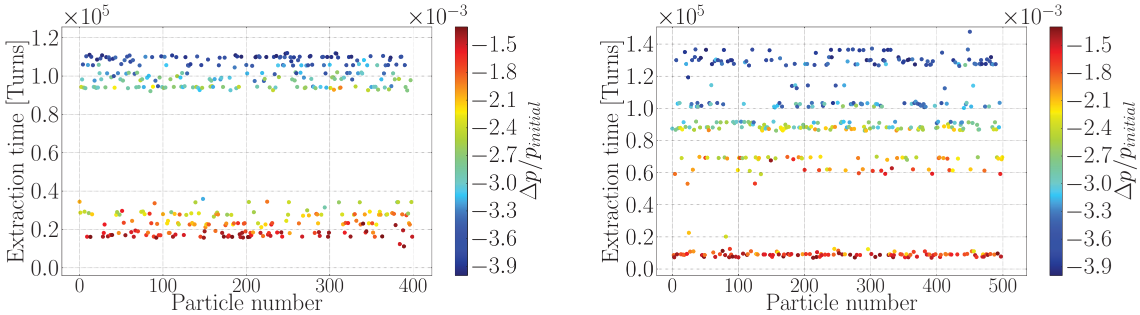


(a) Particle-$t_{extr}$-$\Delta p/p_{init}$

(b) Particle-$t_{extr}$-$\Delta p/p_{init}$

Figure 4.29: Subfigures (a) and (b) show the time structure of the extracted beam for a low energy proton beam excited with longitudinal RF-noise. The initial momentum distribution is given as color code.

### 4.4.2 Moving the resonance using quadrupoles

#### Overview

In the extraction methods described so far, beam properties like the momenta or the amplitudes are adjusted to move the beam towards the resonance. However, the opposite is also possible, keeping the beam properties constant but moving the resonance towards the beam by adjusting lattice properties. This is commonly done by changing the quadrupole settings or employing a dedicated quadrupole to alter the lattice tune. Figures 4.30(a) to 4.30(c) show the extraction method in Steinbach diagrams.

The momentum of a particle stays constant during extraction and the momenta in the "waiting" beam are handed over to the extracted beam. Thus, to obtain extracted particles at design energy (on-momentum) and with a momentum spread comparable to the betatron core extraction, the beam has to be accelerated up to the design energy during the RF acceleration. Moreover, the momentum spread has to be limited or reduced to values about $\Delta p/p \approx 1.2 \cdot 10^{-3}$. During the preparation for the extraction the lattice tune can not be moved as close to the resonance as in the betatron core case, because the on-momentum particles would get unstable as soon as the resonant sextupole is ramped. Hence, the lattice tune has to be kept at least at a minimum distance to the resonance. This distance has to be chosen according to the amplitudes in the "waiting" beam and the slope of the unstable region as it is displayed in the Steinbach diagram 4.30(b). Using the nominal parameters from the betatron core extraction for chromaticity, sextupole strength and beam emittance the necessary minimum initial tune distance is calculated to $\Delta Q_{x,init} = 5.3 \cdot 10^{-3}$. Therefore, the horizontal lattice tune has to be set above $Q_x \geq 1.6719$ to keep the beam stable before extraction.

The advantage of this method is clearly simplicity compared to other methods. No addi-

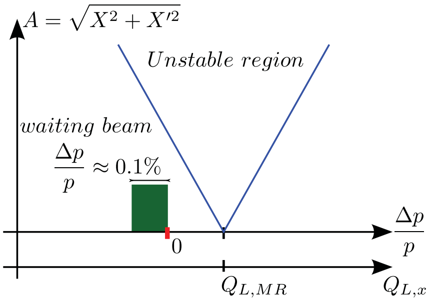


(a) "Waiting" beam at flat top, resonant sextupole has already been ramped

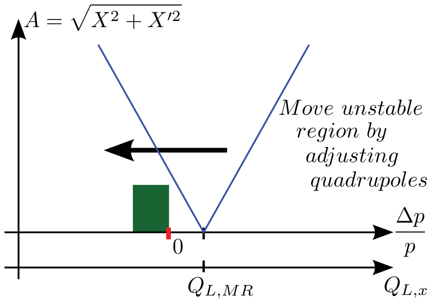


(b) Quadrupole settings are adjusted to move resonance towards beam

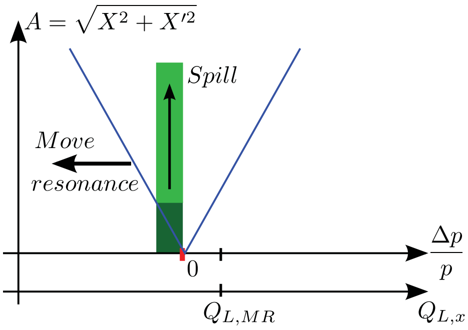


(c) Extraction of spill

Figure 4.30: Subfigures (a), (b) and (c) display the 'Moving the resonance' extraction method in a schematic way, the $x$-axes are the momentum deviation $\Delta p/p$ and the horizontal lattice tune $Q_{L,x}$, on the $y$-axes the normalized particle amplitude is given

tional equipment is necessary, as only the quadrupole strengths have to be adjusted via the power supply.

The major disadvantage of this method is that the quadrupole magnets are not maintained at a constant level during extraction. Consequently, the lattice functions like the Twiss and dispersion functions are also subject to changes. For example, as a result dispersion leaks into nominally dispersion-free regions such as the position of the resonant sextupole. As a further example, changes in the lattice functions also affect the closed orbit. Furthermore, altering the quadrupole magnets settings also makes the extraction process more sensitive towards current ripple. Moreover, the extraction energy is not constant but is decreasing as the resonance is swept over the "waiting" beam assuming a finite chromaticity. Further problems or challenges with this extraction method will be discussed in the next section on the basis of a tracking study.

### Tracking results

For a comparison with the nominal betatron core method a tracking job with the same values for almost all parameters as in the standard betatron core job has been done. Only the lattice tune has been altered to keep the "waiting" beam stable as described in the previous section and the "waiting" beam has been placed in momentum space between $\Delta p/p_{min,init} = -4 \cdot 10^{-3}$ and $\Delta p/p_{max,init} = 0$. For this job 1000 particles have been tracked over $10^5$ turns. After the resonant sextupole has been ramped, the tune is adjusted to move the resonance towards and across the "waiting" beam. The tune shift per turn was chosen to be $\Delta Q/Turn = -3 \cdot 10^{-7}$ in order to obtain extraction times of up to $10^5$ turns.

Figures 4.30(a) to 4.30(c) display the particle distribution at the entry to the electrostatic extraction septum in horizontal phase space. The extracted relative momentum deviation is used as color code in the first plot 4.31(a) and the normalized amplitude in the second one 4.31(b). These pictures have not been taken at one time, but display the accumulations of all extracted particles over the whole extraction time.

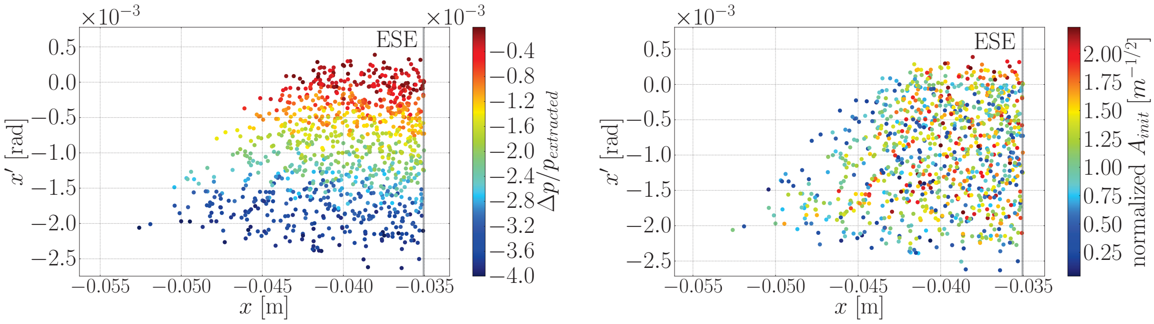


(a) $x$-$x'$-$\Delta p/p_{extracted}$

(b) $x$-$x'$-$A_{init}$

Figure 4.31: Subfigures (a) and (b) show phase space maps at the electrostatic extraction septum for low energy protons

Two main features of the distributions in the figures 4.4.2 are discussed in the following:

- Some of the off momentum particles exhibit large spiral steps of up to 17 mm. This might be surprising considering the results from betatron core extraction, where on-momentum particles are subject to the largest spiral steps. However, the circumstances are different here, because, as the resonance is swept across the beam, low amplitude particles are extracted with all the different momenta in the "waiting" beam and not only on-momentum as in the betatron core case. Figure 4.31(b) shows that low amplitude particles exhibit larger spiral steps than particles with a large amplitude due to the larger tune distance. The spiral step of the off-momentum particles is increasing because of the dispersion. The dispersion shifts the off-momentum (below design momentum) particles away from the septum. Hence, the particles stay longer on the separatrix on their way to the septum, which results in a larger final spiral step. Therefore, to obtain maximum spiral steps of about 10 mm, shorter "waiting" beams in momentum space have to be created with momentum spread of $\Delta p/p_{wait} \approx 1.2 \cdot 10^{-3}$.

- The extent in $x'$ is about a factor of 10 larger than in the betatron core extraction. The change in the quadrupole settings also affects the chromaticity. Thus, the Hardt condition is not fulfilled. The chromaticity sextupoles could be used to keep the chromaticity constant. However, as explained in the previous bullet point, low amplitude particles become unstable with different momenta. Hence, they follow separatrices which are shifted according to the dispersion and result in a larger spread in $x'$. This is the major reason for the large spread. A shorter "waiting" beams in momentum space would also help with this problem, but can not solve it. As a solution adjustments of the dispersion could be done, however, this is not a realistic approach, because the dispersion is rather fixed by other constraints imposed by the lattice design and extraction process.

# 5 Long term power converter stability

This chapter discusses the requirements on the long term stability of the electrostatic and magnetic fields of different beam line elements in the synchrotron and the High Energy Beam Transfer Line (HEBT). In this context “long term“ means times longer than one cycle (maximum cycle duration = 120 s, typical cycle duration is a few seconds). The beam spill is very sensitive to all ripple and transient effects, but these aspects will not be dealt with in this thesis. However, a discussion of the short time precision requirements for MedAustron can be found in [35].

## 5.1 Reference case

The beam line elements of interest are the dipoles, quadrupoles, sextupoles and extraction septa. Due to the small deflection angle of the orbit correctors, a relative error in these correctors is assumed to be negligible .

A real system will always be subject to some errors due to the drift over time and the temperature behavior of the components. As a starting point one can assume a system[1] [36] with a temperature dependence of the power converter of 2 ppm/ 1 °C and additionally about 10 ppm/ 1 °C from the beam line elements themselves (e.g. thermal expansion). In the specification for the Environmental Impact Assessment [37] the aim for the global temperature variations in the whole accelerator area including the power converter hall is $|\Delta T| < 2\,°\mathrm{C}$, which would correspond to deviations of ±24 ppm with this system. However, larger, local temperature fluctuations can not be excluded. Furthermore, there will also be errors from drifts of e.g. the DCCTs (DC current transformers), ADCs (Analog to Digital converter) or the internal references, which are used for measurements of the delivered current. The cumulated drifts can yield additional errors up to ±35 ppm In total the introduced systems is subject of errors of about ±60 ppm This system will be referred to as reference system in this chapter.

**In the whole chapter field errors are given as ppm of the maximum magnetic field $B_{max}$ of the magnets. An analog convention is used for electrostatic fields.**

$$'given - error' = \frac{\Delta B}{B_{max}} = \frac{\Delta B}{B_{set}} \cdot \frac{B_{set}}{B_{max}} \tag{5.1}$$

[1] The system is based on the ’HITEC TOPACC’ DCCT and the ’Texas Instruments ADS1281’ ADC.

To obtain the 'actual-error' $\Delta B/B_{set}$ for a specific field setting, the 'given-error' and the quotient of the maximum $B_{max}$ and the actual field $B_{set}$ have to be taken into account. The necessary fields to bend a particle's trajectory to be subject to a certain radius, can be calculated via formula (5.2). The maximum fields are required for top energy carbon ions with 400 MeV/u. In the other cases, medical and experimental, lower fields are necessary. For instance, protons with 60 MeV need fields about $B_{max}/B_{p,60\,MeV} = 5.58$ times smaller than the maximum fields. Thus, a given-error of 60 ppm has to be multiplied by this factor to get the actual error of 334.8 ppm for low energy protons.

## 5.2 Requirements

On the one hand the constraints are derived from the requirement to achieve the requested irradiation dose homogeneity. Hence, the following high stability is required from the particle energy and the beam size of the extracted beam.

- Energy: variations less than 0.1 MeV[2] [38]
- Beam size: changes less than 0.1 mm

On the other hand, losses at the extraction and the need for correction by the scanning system of the final beam position at the end of the beam lines have to be minimized. Thus, high stability is also requested from the beam position at the magnetic extraction septa and at the ends of the beam lines. At the end of the lines corrections with the scanning system can be envisioned. Thus, there the constraints are less tight than at the magnetic septa.

- Horizontal beam position at thin magnetic extraction septum: changes less than 0.1 mm

Furthermore, the number of necessary recalibration actions should be limited, depending on the time and man-power effort required for it: recalibration for temperature drifts on a daily basis, other recalibration less often e.g. every few months.

The quoted energy precision is the one required for protons with 60 MeV (lowest extraction energy) as this represents the tightest requirement on the energy stability. For 250 MeV (top energy protons in medical application) and carbon ions in the range from 120 MeV/u to 400 MeV/u the limits are at least larger by a factor of two. The energy precision requirement for carbon ions is not yet completely established, but it is reasonable to assume that it is also less tight. For more detailed information see [38] (section 2.5).

[2]This is actually the requirement of energy stability within the irradiation of one field in order to avoid "cold" spots. If all layers are offset, the precision requirement is less tight as margins are taken into account during treatment planning. Thus this number is a conservative approximation.

These requirements can be mapped to stability requirements on the variations in the electric and magnetic fields of different beam line elements. These are subject to variations arising from e.g. temperature variations and the precision of the power converter. These dependencies will be examined in the following sections.

## 5.3 Dipoles in the synchrotron

A variation in the dipole field leads via the radial loop of the RF (The radius of the orbit of the reference particle is constant) to a beam energy at flat top, different to the requested one (see equation (5.9)). This relationship can be derived from a variation of the formula (5.2) that links the magnets' magnetic rigidity $B\rho$ to the particle momentum $p$ and particle charge $q$ (see section 3.1.1).

$$B\rho = \frac{p}{q} \tag{5.2}$$

Variation of the parameters in equation (5.2) (The radius of curvature $\rho$ is supposed to be constant):

$$B_{actual} = B_{set} + \Delta B = B_{set}\left(1 + \frac{\Delta B}{B_{set}}\right) \tag{5.3}$$

$$p_{actual} = p_{set} + \Delta p = p_{set}\left(1 + \frac{\Delta p}{p_{set}}\right) \tag{5.4}$$

The momentum is related to the kinetic energy via the total energy and the rest energy:

$$E = E_0 + E_{kin} = \sqrt{(pc)^2 + E_0^2} \tag{5.5}$$

where $E_0 = mc^2$ is the rest energy and $c$ is the speed of light. A change in momentum is linked to one in kinetic energy via:

$$\frac{\Delta p}{p} = \frac{\gamma_{rel}}{1+\gamma_{rel}}\frac{\Delta E_{kin}}{E_{kin}} = \frac{1}{1+\sqrt{1-\beta_{rel}^2}}\frac{\Delta E_{kin}}{E_{kin}} \tag{5.6}$$

where $\beta$ and $\gamma$ are the relativistic parameters. Inserting equations (5.3) & (5.4) into formula (5.2):

$$B_{set}\left(1+\frac{\Delta B}{B_{set}}\right)\rho = \frac{p_{set}}{q}\left(1+\frac{\Delta p}{p_{set}}\right) = B_{set}\,\rho\left(1+\frac{\Delta p}{p_{set}}\right) \tag{5.7}$$

Canceling yields:

$$\frac{\Delta B}{B_{set}} = \frac{\Delta p}{p_{set}} \tag{5.8}$$

Using formula (5.6), equation (5.8) can be written in terms of energy:

$$\frac{\Delta B}{B_{set}} = \frac{1}{1+\sqrt{1-\beta^2}} \frac{\Delta E_{kin}}{E_{kin,set}} \tag{5.9}$$

As the precision is quoted as ppm of $I_{max}$[3], it is useful to rewrite this:

$$\frac{\Delta B}{B_{max}} = \frac{B_{set}}{B_{max}} \frac{1}{1+\sqrt{1-\beta^2}} \frac{\Delta E_{kin}}{E_{kin}} \tag{5.10}$$

Evaluating formula 5.10, one finds the most sensitive case to be the one of protons with 60 MeV. In this case an error of about $\pm 60$ ppm results in a kinetic energy deviation of $\Delta E_{kin} \approx \pm 39$ keV,which is well below the acceptable limit of $\pm 0.1$ MeV. In the case of 250 MeV protons the energy deviation increases to $\Delta E_{kin} \approx \pm 69.6$ keV for a $\pm 60$ ppm error. However, the requirements on the energy stability of these high energy protons are about a factor two less tight than for the 60 MeV protons. For completeness also the other extreme medical case of the top energy carbon ions with 400 MeV/u has been checked. An error of $\pm 60$ ppm here leads to an energy shift of $\Delta E_{kin} \approx \pm 40.8$ keV. This shift is less critical than the one for 60 MeV protons as the tolerances for carbon ions are also about a factor two less tight. In the physics mode where protons up to 800 MeV will be used, the requirements are actually less crucial than in the medical mode. In this mode a $\pm 60$ ppm error results in an energy shift of $\Delta E_{kin} \approx \pm 96$ keV. The values for all discussed cases are summarized in table 5.1.

| Particle | Energy [MeV/u] | Error [ppm] | Energy shift [keV] |
|---|---|---|---|
| Proton | 60 | ±60 | ±39 |
| Proton | 250 | ±60 | ±69.6 |
| Proton | 800 | ±60 | ±96 |
| Carbon | 400 | ±60 | ±40.8 |

Table 5.1: Energy deviations due to error in the dipole fields for different particles and energies

So far we have considered the beam energy reached at the end of the acceleration. However, the extracted energy depends on the chosen extraction mechanism.

In case of the acceleration driven extraction an energy error will be compensated for. In this scheme before the extraction the beam energy is intentionally set to an energy level below the desired one. This beam has got a relative momentum spread of $\Delta p/p \approx 4 \cdot 10^{-3}$. To extract the particles the beam is inductively accelerated by the betatron core towards the targeted extraction energy. The resonance condition (fractional part of horizontal tune $Q_x = 2/3$) determines

[3] An error in the current from the power converter due to long term instabilities is directly mapped to one in the magnetic field of the magnets.

the extraction energy. Thus, as long as the position of the resonance in momentum space is fixed (which is done by setting the quadrupole strengths such that the tune of a fictitious on-axis particle with the desired extraction energy is $Q_x = 2/3$), also the extracted energy is fixed. A visualization of the extraction is given in figures 4.6(a) to 4.6(d) in the form of Steinbach diagrams. The impact of a change of the dipole fields during the extraction process is not covered in this thesis, as this is a ”short term” effect.

→ It can therefore be concluded that a dipole field error does not lead to an energy error in the extracted beam.

A constraint for the betatron core is that it has to be able to accelerate the whole ”waiting” beam by the sum of its initial distance to the resonance, its energy spread and a possible energy shift from a dipole error into the resonance. This has to be considered in the design of the betatron core, as the possible flux change has to be high enough to achieve the acceleration (see section 4.2.3). The betatron core has to be able to move the beam up to almost 1 MeV in the case of high energy carbon, hence an additional shift of 0.04 MeV seems feasible.

The situation is different for an extraction mechanism that increases the amplitude of the particles to drive them into resonance, like RF-knockout. Here an energy change in the ”waiting” beam is directly passed on to the extracted beam. However, the energy deviations given above are always below the $\pm 0.1$ MeV tolerances.

An error in the dipole fields also has an impact on the normalized quadrupole gradients, which will be discussed in the next section.

## 5.4 Quadrupoles in the synchrotron

Variations in the normalized quadrupole gradients $k$ (see equation (5.11)) change the tune and hence the spiral step at the extraction. The spiral step finally determines the beam size and position of the extracted beam. The main influences on the normalized quadrupole gradient can be investigated by the variation of formula (5.11), as done below. It shows that a variation $\delta$ in the quadrupole gradient (not normalized) and a variation of the beam energy $\Delta p/e = \Delta(B\rho)$ (due to e.g. an error in the dipole field during acceleration) result in a change $\Delta k/k$ of the normalized quadrupole gradient.

$$k = \frac{1}{B\rho}\,\frac{dB}{dx} \tag{5.11}$$

Variation of the parameters in formula (5.11):

$$k_{actual} = k_{set}\left(1 + \frac{\Delta k}{k_{set}}\right) \tag{5.12}$$

$$\left(\frac{dB}{dx}\right)_{actual} = \left(\frac{dB}{dx}\right)_{set} (1+\delta) \tag{5.13}$$

$$(B\rho)_{actual} = (B\rho)_{set}\ (1+\Delta(B\rho)) \tag{5.14}$$

Inserting equations (5.14) & (5.13) into formula (5.11), followed by a Taylor expansion of the denominator:

$$k_{actual} = \frac{\left(\frac{dB}{dx}\right)_{set} (1+\delta)}{(B\rho)_{set}\ (1+\Delta(B\rho))} = k_{set}\ \frac{1+\delta}{1+\Delta(B\rho)} = k_{set}\ (1+\delta)\ (1-\Delta(B\rho)+O(2)) \tag{5.15}$$

Inserting equation (5.12) on left side of equation (5.15), multiplying the brackets on the right and neglecting terms of order $\geq 2$:

$$k_{set}\ \left(1+\frac{\Delta k}{k_{set}}\right) \approx k_{set}\ (1+\delta-\Delta(B\rho)) \tag{5.16}$$

Canceling yields:

$$\frac{\Delta k}{k_{set}} \approx \delta - \Delta(B\rho) \tag{5.17}$$

As stated in section 5.2, the spiral step of on-resonance particles should not deviate more than 0.1 mm from the nominal value of about 10 mm. Using the function 'transverse maps' in WinAgile to perform tracking studies, it was found that this constraint allows a $\Delta k/k$ of about $\pm 60$ ppm assuming a worst case scenario. Figure 5.1 compares the following two scenarios:

- Reference case: All quadrupole families are subject to the same variation $\Delta k/k_{set}$ in equation (5.11).
- Worst case scenario: The quadrupole families are subject to variations of identical absolute value but of different signs. The signs are chosen such to produce the largest possible tune shift (e.g. focusing quadrupoles become stronger whereas defocussing ones weaker)

The effects of different $\Delta k/k$ on the tunes $Q_x$, $Q_y$ and consequently spiral step / kick are displayed in the Figure 5.2 for the previously described reference case. In the following, it is assumed that the error in the normalized quadrupole gradient can be attributed 50/50 to the two error sources, the quadrupole itself and the dipole (see equation (5.17)). Considering once again a worst case scenario where both errors add up, the variations of each source separately should be less than $\pm 30$ ppm This condition is not fulfilled by the reference system described in the section 5.1. Thus, from this point improvements are necessary.

As the three quadrupole families will be powered from power converters of the same type, one can assume, that they will exhibit similar temperature behavior. Furthermore, the converters will be placed close to each other in the power converter hall and hence will be exposed to

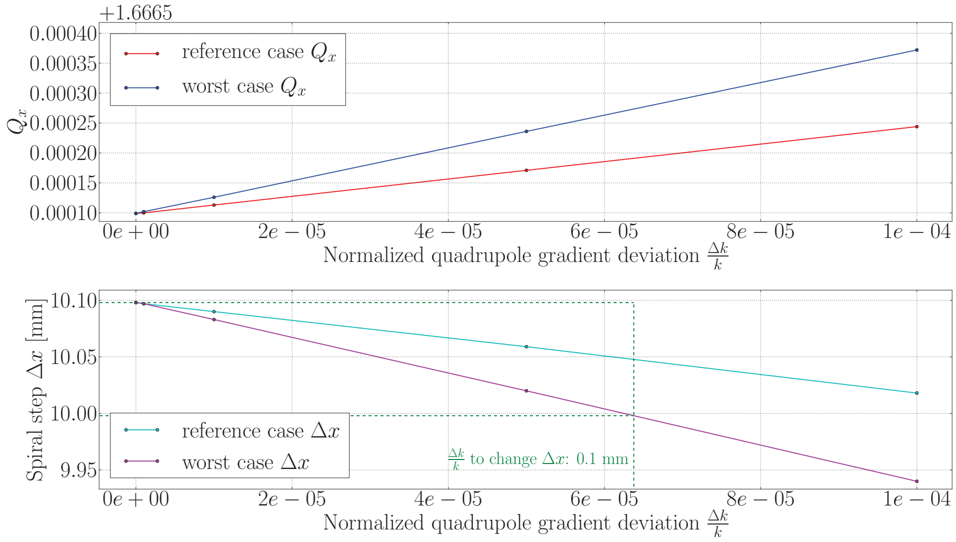


Figure 5.1: Dependence of the tune $Q_x$ and the spiral step on variations $\Delta k/k$ in the normalized quadrupole gradient for reference and worst case scenario

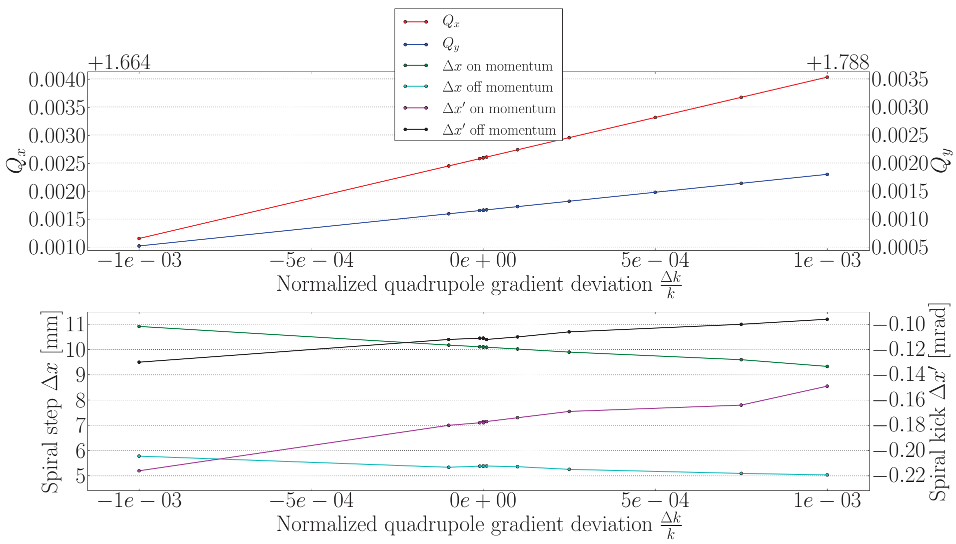


Figure 5.2: Dependence of the tunes $Q_x$, $Q_y$ and the spiral step / kick on variations $\Delta k/k$ in the normalized quadrupole gradient

the same temperature variations. Therefore, the reference case is more likely to describe the real-life situation than the worst case one. In figure 5.1 it can be seen that the tolerable error in the reference scenario is about a factor two higher than in the worst case one. This sheds a better light on the reference system. However, for safety reasons and to have some margins, improvements are still necessary.

In addition to the effects mentioned above, variations in the normalized quadrupole gradients can also have an influence on the energy of the extracted particles. Whether this is the case, depends on the chosen extraction mechanism. For extraction, the particles are driven into resonance by adjusting the single-particle-tune.

In acceleration driven extraction the particles energy is increased until the tune reaches the resonance condition via the chromaticity (see figures 4.6(a) to4.6(d)). Any change in the lattice tune corresponds to a horizontal shift of the unstable zone in the Steinbach diagram, which is shown in figure 5.3. The dependence of the lattice tune on the quadrupole settings is shown in figure 5.2 & 5.1.

A particle with a momentum deviation, that compensates via the chromaticity for the normalized quadrupole gradient induced changes in the tune, fulfills the resonance condition. Thus, it becomes unstable. To achieve the compensation, the chromatic tune shift has to be inverse to the lattice tune shift. A momentum deviation is equivalent to an energy deviation (see formula (5.6)). Hence, a change in the lattice tune results in a change of energy of the extracted particles. In contrast to the dipole induced energy changes the acceleration process, which steers the extraction, is not able to compensate for ones due to normalized quadrupole gradient errors. This acceleration process only drives the beam into resonance but does not determine the place of the resonance in momentum space and therefore not the extracted energy.

To examine the consequences of this effect an error in the normalized quadrupole gradient of $\Delta k/k = 60$ ppm has been assumed. Figure 5.1 directly shows the resulting horizontal lattice tune shift $\Delta Q_x \approx 1.6 \cdot 10^{-4}$ (The worst case scenario is used). An increase in the normalized quadrupole gradient corresponds to a larger tune. Via formula (3.25) the necessary momentum deviation to fulfill the resonance condition is calculated to $\Delta p/p \approx 3.96 \cdot 10^{-5}$.[4] The corresponding error in energy is obtained via formula (5.6). Within the medical applications top energy carbon particles with 400 MeV/u get the largest energy shift in extracted energy of $\Delta E_{kin} \approx 26.9$ keV.

The energy spread of the extracted beam[5] due to the extraction mechanism is $\Delta E_{kin} \approx 0.2$ MeV. Therefore, the calculated kinetic energy shift of $\Delta E_{kin} \approx 27$ keV is about a fac-

[4] It has to be considered that also the chromaticity C depends on the normalized quadrupole gradient. In the studied case the chromaticity becomes $C_{x,actual} \approx -4.039$ instead of the nominal value of $C_{x,set} = -4.041$. (These numbers were calculated by WinAgile via an extrapolation formula from the central orbit tune values, after inserting the changes in the quadrupoles. Hence, these figures are only approximations.)

[5] The energy spread in the extracted beam is determined by the slope of the unstable zone and the emittance

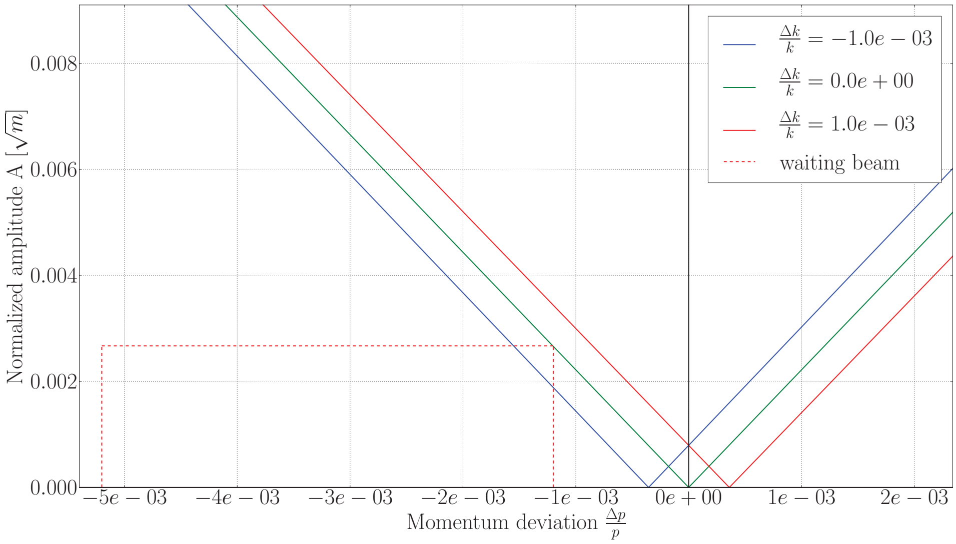


Figure 5.3: Dependence of the unstable zone in the Steinbach diagram on variations $\Delta k/k$ in the normalized quadrupole gradient (high $\Delta k/k$ values chosen for a better visualization of the effect, actually expected values about 20 times smaller)

tor of 7 smaller than the allowed energy shift for top energy carbon of $\Delta E_{kin} \approx \pm 0.2$ MeV. In physics mode for the top energy protons with 800 MeV the extracted energy is shifted by $\Delta E_{kin} \approx 49$ keV, but also this is safely away from the limits on energy stability.

For extraction schemes, where the particle momentum is not changed, the effect described above has no impact on the extracted energy. However, the error from the dipoles, which is in the same order as the normalized quadrupole gradient one, is not compensated for. Hence, in all extraction mechanism a similar error in the extracted energy due to long term instabilities can be expected.

## 5.5 Other magnets in the synchrotron

Beside the magnets described so far, there are additional magnets in the synchrotron like sextupoles and correctors. Yet their effects are negligible compared to those above. For the resonant sextupole a variation of its normalized gradient in the order of 1% (equal to 10,000 ppm ) would be necessary to result in a change of the spiral step of 1%. Also the 11 correctors only

of the ”waiting” beam (see figure 4.6(d)). The dependence in terms of relative momentum spread is given by equation (4.10). As the slope depends on the chromaticity, also the extracted energy spread is subject to variations due to errors in the normalized quadrupole gradients. However, for the studied errors the change in relative extracted momentum spread is in the order of $10^{-7}$. Thus, this effect is completely negligible.

have a negligible impact. Additionally, due to the high number of individually powered correctors errors should statistically level each other out.

## 5.6 Magnets in the HEBT

Errors in the normalized gradient of the quadrupoles in the HEBT are negligible compared to the ones in the synchrotron. However, the dipole fields (bending dipoles and extraction septa) have a major effect on the final beam position. Although, beam position errors due to long term instabilities can probably be compensated for by the scanning system, the errors should as small as possible.

The momentum of the particles in the HEBT is constant. Hence, an error in the dipole field leads via a deviation in the deflection angle of the dipoles to an error in the beam position. This can be derived from a variation of the magnetic rigidity (similar to section 5.3):

$$B\rho = \frac{p}{q} \tag{5.18}$$

Variation of the parameters in equation (5.18):

$$B_{actual} = B_{set}\left(1 + \frac{\Delta B}{B_{set}}\right) \tag{5.19}$$

$$\rho_{actual} = \rho_{set}\left(1 + \frac{\Delta\rho}{\rho_{set}}\right) \tag{5.20}$$

Inserting equations (5.19) & (5.20) into formula (5.18):

$$B_{set}\left(1 + \frac{\Delta B}{B_{set}}\right)\rho_{set}\left(1 + \frac{\Delta\rho}{\rho_{set}}\right) = \frac{p_{set}}{q} = B_{set}\,\rho_{set} \tag{5.21}$$

Canceling and multiplying the brackets yield:

$$1 + \frac{\Delta B}{B_{set}} + \frac{\Delta\rho}{\rho_{set}} + \frac{\Delta B}{B_{set}}\frac{\Delta\rho}{\rho_{set}} = 1 \tag{5.22}$$

Neglecting terms of order $\geq 2$ and rearranging:

$$\frac{\Delta B}{B_{set}} \approx -\frac{\Delta\rho}{\rho_{set}} \tag{5.23}$$

The radius of curvature $\rho$ is linked to the bending angle $\alpha$ via the arc length $l$:

$$\alpha = \frac{l}{\rho} \tag{5.24}$$

Variation of α and ρ:

$$\alpha_{set}\left(1+\frac{\Delta\alpha}{\alpha_{set}}\right)=\frac{l}{\rho_{set}\left(1+\frac{\Delta\rho}{\rho_{set}}\right)}=\alpha_{set}\,\frac{1}{\left(1+\frac{\Delta\rho}{\rho_{set}}\right)} \tag{5.25}$$

Canceling and Taylor expansion of the denominator on the right side gives:

$$1+\frac{\Delta\alpha}{\alpha_{set}}=1-\frac{\Delta\rho}{\rho_{set}}+O(2) \tag{5.26}$$

Neglecting terms of order $\geq 2$ and canceling result:

$$\frac{\Delta\alpha}{\alpha_{set}}\approx-\frac{\Delta\rho}{\rho_{set}} \tag{5.27}$$

Inserting equation (5.23) yields:

$$\frac{\Delta\alpha}{\alpha_{set}}\approx\frac{\Delta B}{B_{set}} \tag{5.28}$$

Rearranging the equation and considering that the precision is quoted as ppm of $I_{max}$, the deviation in the deflection angle can be expressed by:

$$\Delta\alpha\approx\frac{\Delta B}{B_{max}}\,\frac{B_{max}}{B_{set}}\,\alpha_{set}=\frac{\Delta B}{B_{max}}\,\frac{B_{max}}{B_{set}}\,\frac{l}{\rho_{set}} \tag{5.29}$$

For the 22.5° dipoles with a length of $l=2$ m and a field error of $\pm 50$ ppm the deviation in deflection angle is calculated to about $\Delta\alpha\approx\pm 1.1\cdot 10^{-4}$ rad for 60 MeV protons and $\Delta\alpha\approx\pm 2\cdot 10^{-5}$ rad for 400 MeV/u carbon ions. In a thin lens model the variation in the deflection angle can be approximated by a kick $\Delta x'$ of the same amplitude. To obtain the effect on the beam position, an additional kick has to be tracked to the end of the beam line of interest by applying the transfer matrix $T$. In a transfer line the particles are passing the elements only once. Hence, for a horizontal bend the only matrix element of interest from the transfer matrix (3.19) is the $T(0,1)$ that gives the effect of a kick $\Delta x'$ on the space coordinate $x$.

$$\Delta x=T(0,1)\,\Delta x' \tag{5.30}$$

The matrix element $T(0,1)$ between two lattice elements can be written with the horizontal Twiss beta functions at the two lattice elements and the horizontal phase advance $\Delta\mu$ between the two elements:

$$T(0,1)=\sqrt{\beta_{x,1}\,\beta_{x,2}}\,\sin(\Delta\mu_x) \tag{5.31}$$

For vertical bends the same holds true only all $x$ have to be replaced by $y$ and the matrix element of interest is the $T(2,3)$.

For quick estimations the sinus can be approximated as 1 and thus the knowledge of the beta function is enough to calculate the shift of the beam position. However, in the following the shifts have been obtained by applying the full matrix element. The accelerator and transfer line lattices are approximated to be linear systems. Thus, the kick of each dipole can be separately tracked till the end of the line and there the contributions from the different dipoles can be summed up.

For the EX[6]-T1 line (see figure 2.1), which delivers the particles to the experimental area, four dipoles and four magnetic septa have to be taken into account. The first septum has a length of $l = 0.594$ m and a bending angle of $\alpha = 3.11°$. The following three septa are identically with a length of $l = 0.84$ m and bending angles of $\alpha = 5.65°$. The four septa are powered in series. All the dipoles have bending angles of $\alpha = 22.5°$ and a lengths of $l = 2$ m. The two dispersion suppressor dipoles in the extraction line are powered in series, as well as the two switching dipoles from the extraction line to the T1 line. Dipoles that are powered in series will be referred to as one dipole family. It is assumed that the dipoles of one family are subject to the same errors. Because of the phase advance between the dipoles of one family, errors partly compensate each other. Furthermore, it is supposed that the three families also suffer from equal errors as this represents the worst case.

The horizontal shift of the beam position at the end of the T1 line for different field errors is shown in the plot 5.4. For an error of $\pm 50$ ppm for all dipoles and septa the horizontal shift is calculated to be $\Delta x_C \approx \pm 0.39$ mm for 400 MeV/u carbon ions and $\Delta x_p \approx \pm 2.17$ mm for 60 MeV protons. As one can see, the low energy protons are the more sensitive case. Although the septa are shorter and have smaller bending angles than the dipoles, the septa's contribution to the beam position shift is about three times larger than the one from the dipoles (see figure 5.4). The reason is that the septa are placed close to each other at positions with a high beta function of $\beta_x \approx 25$ m. The high beta values directly influence the shift via the transfer matrix. Moreover, because of the high beta function the phase advance between the septa is small. Hence, the septa do not compensate for each other, because the transfer matrices to the end of the line all have the same sign and thus they shift the beam in the same direction.

In the EX-T2-V2 line (see figure 2.3) there are horizontal and vertical bends, thus field errors yield shifts in the $x$ and in the $y$ coordinate. For this line in total 9 dipoles and the four magnetic septa have to be considered. First there are the four septa and the two dispersion suppressors at the beginning of the extraction line analog to the T1 case above. Next there are the two switching dipoles to the T2 line. These are the horizontal bends in this line and hence they are capable of causing horizontal shifts. For the powering the same holds true as in the T1 line. At first it is supposed they are subject to equal errors. However, the matrix elements are different compared to the T1 case. In the V2 line the worst case is no longer represented be assuming equal errors. To obtain a worst case scenario the errors of the switching dipoles and

[6] Here only the part of the extraction (EX) line from the magnetic extraction septa to the switching dipoles to the T1 line is meant

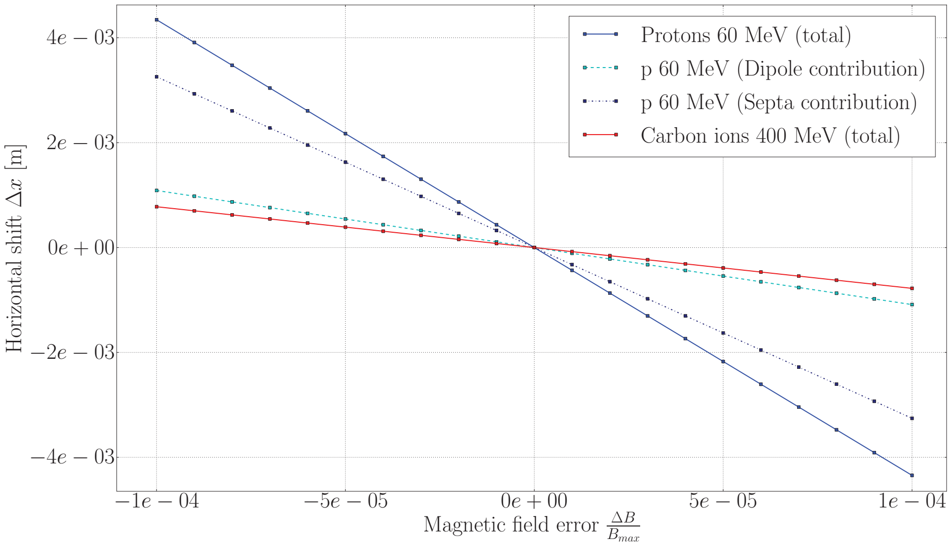


Figure 5.4: Dependence of the horizontal beam position at the end of the T1 line on variations in the magnetic field $\Delta B/B_{max}$ of the dipoles and the magnetic extraction in the HEBT

of the four septa have to be set with the opposite signs as for the other families. Next there are four vertical bends which are powered in series and thus form a dipole family, which suffers from equal errors. The first of these four is the switching dipole to the V2 line. Also these four vertical bends are 22.5° ones. Finally, there is a special vertical bend with a bending angle of $\alpha = 90°$ and a length of $l = 5.733$ m. For this dipole the kick due to field errors is recalculated according to the different angle, length and strength. For the vertical shift it is the worst case if the vertical dipole family and the 90° dipole are subject to equal errors.

The shift of the beam position at the end of the V2 line assuming equal errors for all magnets can be seen in the plot 5.5. For an error of ±50 ppm for all dipoles and septa the horizontal shift is calculated to be $\Delta x_C \approx \pm 0.066$ mm for 400 MeV/u carbon ions and $\Delta x_p \approx \pm 0.37$ mm for 60 MeV protons. In the vertical plane the results are $\Delta y_C \approx \pm 0.34$ mm for 400 MeV/u carbon ions and $\Delta y_p \approx \pm 1.89$ mm for 60 MeV protons. These values are calculated with the nominal TWISS beta functions of e.g. $\beta_y = 3$ m at the end of the V2 line. However, in the V2 line the beta functions will be used to adjust the beam size and can get as high as $\beta_y = 27$ m at the end of the line. A change in the beta function directly influences the shifts due to dipole field errors. For example an increase in $\beta_y$ from 3 to 27 m results in three times higher shifts. The special worst case scenario in the horizontal plane with different errors for the magnet families is shown in the figure 5.6. In this plot also the "normal" case assuming equal errors is shown. For an absolute error value of ±50 ppm for all dipoles and septa the horizontal shift is calculated to be $\Delta x_C \approx \pm 0.28$ mm for 400 MeV/u carbon ions and $\Delta x_p \approx \pm 1.57$ mm for 60 MeV protons.

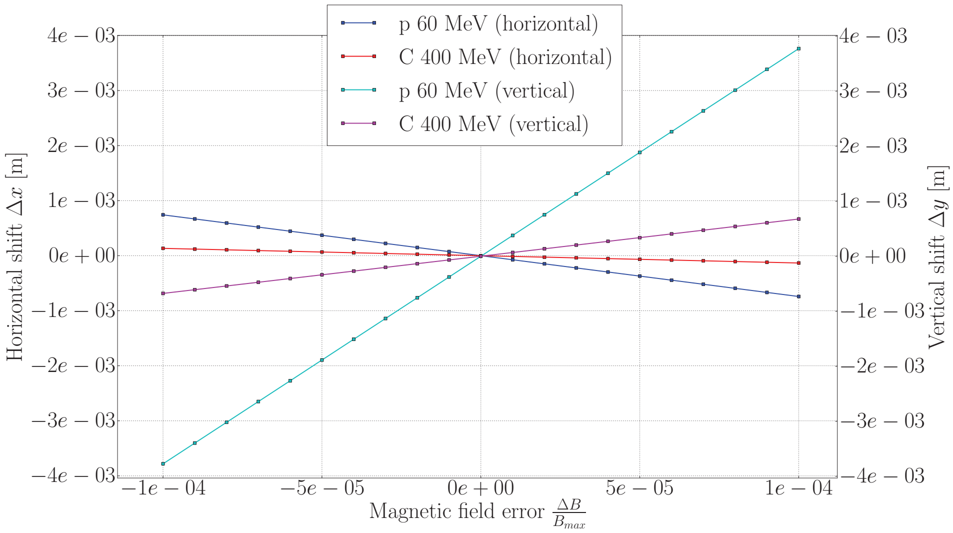


Figure 5.5: Dependence of the horizontal and vertical beam position at the end of the V2 line on equal variations in the magnetic field $\Delta B/B_{max}$ of the dipoles and the magnetic extraction septa in the HEBT

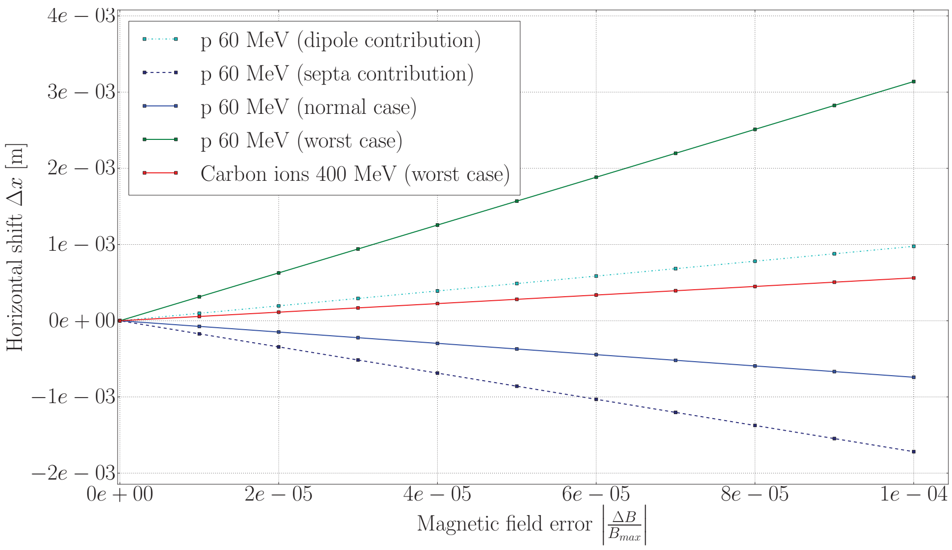


Figure 5.6: Dependence of the horizontal beam position at the end of the V2 line on variations in the magnetic field $\Delta B/B_{max}$ of the dipoles and the magnetic extraction septa in the HEBT assuming a worst case scenario

## 5.7 The electrostatic extraction septum

The task of the electrostatic extraction septum (ESE) is to apply a kick to particles just before they are extracted. This kick has the nominal strength of $\Delta x' = 2.5$ mrad. Till the thin magnetic extraction septum (MST) the kick is partly transformed into a gap in the space coordinate between the still circulating beam and the particles to be extracted. The MST has to fit into this gap. Therefore, if the kick is too small because of errors e.g. in the ESE power converter, the gap will not be wide enough and particles will hit the septum wall. Thus, the particle losses will increase.

To evaluate the effects of errors at the ESE the same procedure as for the magnets in the HEBT can be used (see section 5.6), except that the ESE is a electrostatic device instead of a magnet. Thus, instead of a variation of the magnetic rigidity (see equation (5.18)), the electric rigidity is used (see formula (5.32) or section 3.1.1). $E$ gives the electric field, $T$ the kinetic energy and $\gamma_{rel}$ the relativistic $\gamma$ factor. $T$ and $\gamma$ a are both assumed to be constant during a particle moves from the ESE to the MST.

$$|E_0\,\rho_0| = \frac{T}{q}\,\frac{\gamma+1}{\gamma} \tag{5.32}$$

Applying the same procedure as in the HEBT dipole case yields an analog result:

$$\frac{\Delta\alpha}{\alpha_{set}} \approx \frac{\Delta E}{E_{set}} = \frac{\Delta E}{E_{max}}\,\frac{E_{max}}{E_{set}} \tag{5.33}$$

An error in the electric field is directly converted into a deviation of the kick angle. To approximate the errors in the beam position at the MST and the end of the beam lines due to electric field errors at the ESE, a thin lens model is used. The errors are tracked from the ESE towards the other points of interest by applying the transfer matrix as done in the HEBT magnets section. This procedure yields the following plots 5.7 and 5.8, showing the dependence of the beam position on ESE field errors.

As it can be seen in the figure 5.7 the error in the ESE field should stay below $\pm 800$ ppm to limit the shifts in beam position to less than $\Delta x = \pm 0.1$ mm at the MST. The consequences at the end of the V2 line are even smaller and an error of $\pm 1000$ ppm in the ESE field, leads to a shift of about $\Delta x = \pm 0.08$ mm. However, if the ESE is not used at the nominal voltage of 150 kV, but instead at 70 kV, a factor of about 2 has to taken into account and would tighten the constraints.

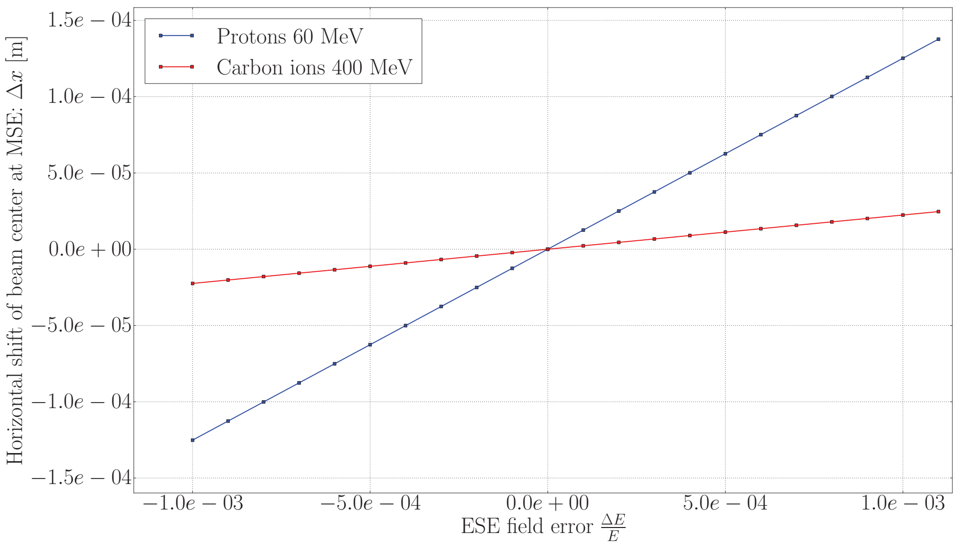


Figure 5.7: Dependence of the horizontal beam position at the MST on variations in the electric field $\Delta E/E_{max}$ of the electrostatic extraction septum

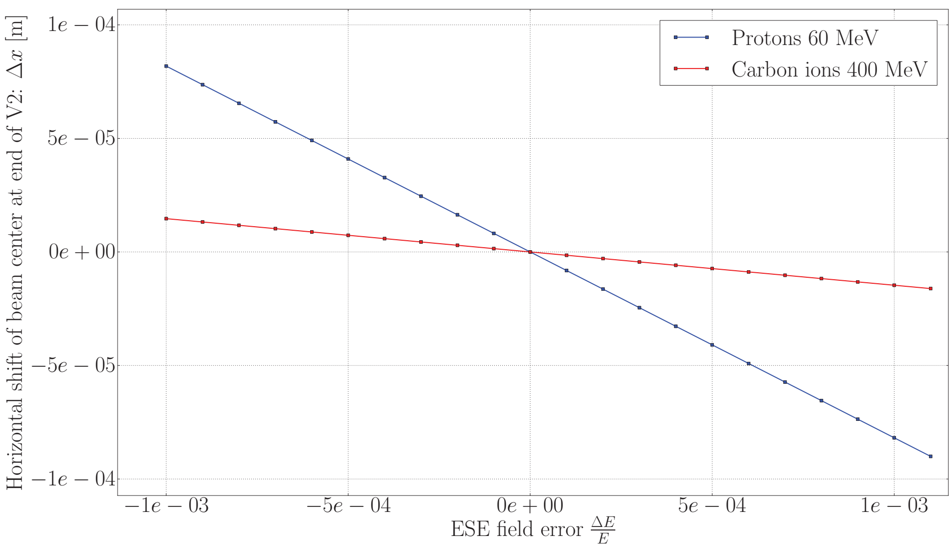


Figure 5.8: Dependence of the horizontal beam position at the end of the V2 line on variations in the electric field $\Delta E/E_{max}$ of the electrostatic extraction septum

## 5.8 Conclusions from the stability investigations

As it is derived above the main constraint in the synchrotron is imposed by the normalized quadrupole gradients, because they have a major influence on the tune and spiral step. To guarantee the necessary long term stability a system is needed which has variations of maximum $\pm 30$ ppm from $I_{max}$ for quadrupoles and dipoles, to be on the safe side even in worst case scenarios. This is a very conservative limit, which is imposed by the low energy protons, because then the machine runs only at a fraction of its capacity. As expected, the carbon ions, which are used in a higher energy range then the medical protons, show a higher stability. The other magnets in the synchrotron only have negligible effects or it can be compensated for errors.

Consequently, the reference system assumed in the introduction exhibits too large errors (about a factor 2). However, this system is based on components which have not been completely optimized yet. It seems to be possible to reduce the errors for example by using temperature controlled electronic systems. To achieve further error minimizations also a reasonable higher recalibration rate can be envisioned, e.g. calibration of the internal references during each of the monthly foreseen technical stops of the accelerator complex. After taking these possible improvements into account, it seems to be feasible to stay within the requirements.

The electrostatic extraction septum influences the beam position at the magnetic extraction septa and also at the end of the beam lines. Especially, the position at the magnetic septa is important, as errors increase particles losses during extraction. Thus, the electrostatic septum field should not deviate more than $\pm 400$ ppm from its nominal maximum value, assuming worst case scenarios.

In the HEBT the dipoles and the magnetic extraction septa have strong influences on the final beam position. As already small errors lead to serious shifts (errors of about 50 ppm can cause shifts in the mm range), the scanning system has to be designed in a way to be able to compensate for such errors.

# 6 Summary & Conclusion

The extraction from the synchrotron is a crucial process to deliver a high quality beam for cancer therapy in a treatment facility like MedAustron. Therefore, the employed third-order resonance extraction was studied analytically and in simulation in the framework of this thesis. Furthermore, long term stability requirements on the power converter have been set up to ensure the energy, position and shape of the extracted beam.

During the work on this thesis the tracking code TrackIt! was further enhanced to be able to simulate different extraction methods. The code was tested in numerous tracking studies of different extraction schemes and typical problems using the code were documented and explained.

First the baseline extraction method for MedAustron — the betatron core driven extraction scheme — was studied in detail. The obtained parameters of the extracted beam like the spiral step are in good accordance with the PIMMS study. In general the results are as expected, however, two results have to be pointed out, as they may suggest adaptions of the current design or acceleration program:

- The betatron core is at its limit in terms of necessary flux change for extracting top energy carbon beams. Hence, to leave some margins and to allow for errors, a larger possible flux change compared to the CNAO betatron core design should be envisaged. The flux change should be increased by more than 10%.
- The momentum distribution of the ”waiting” beam should be Gaussian instead of homogeneous to minimize the number of particles in the parts at the beginning and end of each spill that can not be used in medical application due to unfavorable beam quality.

To increase the versatility of MedAustron alternative extraction schemes were investigated, as e.g. the betatron core method is not able to provide spill lengths below one second, which is required for non-clinical research.

The first studied alternative extraction method was RF-knockout as this scheme is used at most synchrotron based cancer treatment facilities. Because of favorable beta functions at the horizontal Schottky monitor, the latter is the element of choice to drive RF-knockout at MedAustron. From tracking studies it was found that kicks in the order of a few μrad per turn are necessary to deliver spill lengths of 0.1 s. The current design of the Schottky monitor is capable of producing the necessary electric field to cause such kicks. Furthermore, the preparation of the machine and the beam for RF-knockout was elaborated and the process was simulated in tracking studies. The most important findings for RF-knockout are:

- An about a factor two stronger resonant sextupole seems to be favorable to obtain acceptable spiral steps. However, a stronger sextupole may also pose new problems, as the stable islands would move inwards towards the axis. Hence, this should be subject of further investigations.
- The chromaticity has to be set close to zero to prevent aperture problems with off-momentum particles.
- A short beam in momentum space, placed at the design energy before the extraction, is necessary to obtain similar results as in the betatron core driven method. To maintain the stability of the "waiting" beam the tune has to be kept away from the third-order resonance.

Although the method seems to be feasible, it still faces several problems like a) the smaller spiral steps as compared to the betatron core driven scheme and b) that with the current lattice design the Hardt condition is not fulfilled due to the changed chromaticity.

Additionally, two further methods were studied. The rather simple method to employ the quadrupoles to alter the tune to make particles unstable is not suitable for medical applications because it is too sensitive to magnetic field ripple. Still it can be used for non-medical applications. On the other side the stochastic RF-noise method seems to be more promising. From tracking very similar results as compared to betatron core extraction, especially spiral step and Hardt condition, were found and spill lengths of 0.1 s were achieved. The obtain more realistic results an improved noise function and beam model has to be implemented. Furthermore, the RF-noise voltage and bandwidth have to optimized.

RF-knockout and RF-noise extraction both seem to be feasible, however, further investigations are still necessary.

To find requirements for the long term stability of the power converters, effects of power converter errors on beam energy and positions were investigated. It was found that in the synchrotron the normalized quadrupole gradients are crucial and variations of the fields of dipoles and quadrupoles should be less than $\pm 30$ ppm This requirement is imposed by the low energy protons, whereas, as expected, carbon ions are more stable. The current power converter design has to be slightly improved to reach this goal, e.g. as a consequence temperature controlled racks will be used. In case the goal can not be reached with state-of-the-art power converters, recalibration will be necessary more often. The electrostatic extraction septum field should not deviate more than $\pm 400$ ppm from its nominal maximum value. In the HEBT even small errors cause large effects on the beam position at the ISO-center. Hence, the scanning system has to be able to compensate for these errors.

# 7 Acknowledgments

First of all I want to thank my parents who have supported and encouraged me during my whole life. Moreover, I would like to thank my girlfriend Ramona for enduring our spatial separation due to my work in Geneva and for still supporting me during this time. Next I want to thank my supervisor Michael Benedikt for enabling me to do this thesis, to work at CERN and for all his help and support. Special thanks also go to Phil J. Bryant for answering all my e-mails and questions and for helping me many times with my work and thesis. Additionally, I really appreciate the help I have received from all the people at CERN and EBG MedAustron I have worked with, especially from my two office mates Fabian Moser and Marcus Palm. Furthermore, I want to thank all the people who have helped me with this diploma thesis, especially John Baillie, Daniel Lemon, Tom Levens, Nick Shipman and Adam Thornton. Last but definitely not least, sincere thanks go to Ulrich Dorda for assigning me interesting tasks and for his endless help, support, guidance and time he spent on discussing problems with me.

# A Appendix

## A.1 Constants

### A.1.1 Natural Constants

| Parameter | Value | Unit |
|---|---|---|
| elementary charge | 1.602E-19 | C |
| speed of light | 2.998E+08 | m/s |

### A.1.2 $H_1^{1+}$

| Parameter | Value | Unit |
|---|---|---|
| charge | 1 | e |
| mass number A | 1 | nucleons |
| rest energy | 9.383E+08 | $eV/u$ |
| $B\rho$ 60 MeV | 1.137 | |
| $\beta$ 60 MeV | 0.342 | |
| $\gamma$ 60 MeV | 1.064 | |
| $B\rho$ 250 MeV | 2.432 | |
| $\beta$ 250 MeV | 0.614 | |
| $\gamma$ 250 MeV | 1.266 | |
| $B\rho$ 800 MeV | 4.881 | |
| $\beta$ 800 MeV | 0.842 | |
| $\gamma$ 800 MeV | 1.853 | |

### A.1.3 $C_{12}^{6+}$

| Parameter | Value | Unit |
|---|---|---|
| charge | 6 | e |
| mass number A | 1.200E+01 | nucleons |
| rest energy | 9.315E+08 | $eV/u$ |
| $B\rho$ 120 MeV | 3.254 | |
| $\beta$ 120 MeV | 0.464 | |
| $\gamma$ 120 MeV | 1.129 | |
| $B\rho$ 400 MeV | 6.347 | |
| $\beta$ 400 MeV | 0.715 | |
| $\gamma$ 400 MeV | 1.430 | |

## A.2 Synchrotron

### A.2.1 General

| Parameter | Value | Unit |
|---|---|---|
| Particle types | P, $C_{12}^{6+}$ | |
| Circumference | 77.6500 | m |
| Operation mode | cyclic | |
| Cycling frequency | $<0.8$ | Hz |
| Max dipole ramp rate | 3.000 | T/s |

### A.2.2 Lattice

| Parameter | Value | Unit |
|---|---|---|
| Lattice type | Split FODO | |
| Super periodicity | 2 | |
| Nr of long straight sections | 2 | |
| Length of long straight sections | 7.6250 | m |
| Nr of dipoles | 16 | |
| Dipole bending radius | 4.231 | m |
| Dipole $\alpha_{bend}$ | 22.5 | degree |
| Dipole $B_{max}$ | 1.25 | T |
| Nr of quadrupole families | 3 | |
| Nr of quadrupoles per family | 8 | |
| Quadrupole $\frac{dB}{dx}_{max}$ | 4.138 | T/m |
| Nr of sextupole families | 2 + resonant sextupole | |
| $\gamma_{transition}$ | 1.9700 | |
| $\beta_{x,max}$ | 16.90 | m |
| $\beta_{y,max}$ | 16.60 | m |
| $D_{x,max}$ | -8.66 | m |

### A.2.3 Circulating beam

| Parameter | Value | Unit |
|---|---|---|
| Transverse beam profile | Bi-gaussian truncated at $\sqrt{5}\sigma$ | |
| Normalized emittance p ($1\sigma$) | 0.52 | $\pi$ mm mrad |
| Max geometric emittance p ($\sqrt{(}5)\sigma$) | 21.20 | $\pi$ mm mrad |
| Min geometric emittance p ($\sqrt{(}5)\sigma$) | 1.66 | $\pi$ mm mrad |
| Normalized emittance C ($1\sigma$) | 0.75 | $\pi$ mm mrad |
| Max geometric emittance C ($\sqrt{(}5)\sigma$) | 30.40 | $\pi$ mm mrad |
| Min geometric emittance C ($\sqrt{(}5)\sigma$) | 3.66 | $\pi$ mm mrad |
| Max p intensity | 2.30E+10 | |
| Min p intensity | 1.15E+09 | |
| Max number of stored C | 1.15E+09 | |
| Min number of stored C | 4.60E+08 | |
| Synchroton frequency | 0.5 - 2.1 | kHz |
| Min revolution time (p800) | 0.3000 | $\mu$s |
| Max revolution time | 2.1300 | $\mu$s |

### A.2.4 Extraction

| Parameter | Value | Unit |
|---|---|---|
| Extraction mechanism | Betatron core driven third order resonant extraction with RF-channeling | |
| Tunes extraction [H / V] | 1.666 / 1.789 | |
| Spill length | 0.1 - 10 | s |
| Extraction energy range | P: 60-800, C: 120-400 | MeV/u |
| Extraction efficiency | 0.87 | |
| Chromaticity | -4.041 / -0.195 | |
| Spiral step | 10 | mm |
| dp/p (intentional blow up) | 0.4 | % |

## A.3 High energy beam transfer line (HEBT)

### A.3.1 Beam

| Parameter | Value | Unit |
|---|---|---|
| Energy range EX, T1 | p: 60 - 800, $C_{12}^{6+}$: 120 - 400 | MeV/u |
| Energy range T2, T3, V2 | p: 60 - 250, $C_{12}^{6+}$: 120 - 400 | MeV/u |
| Energy range T4 | p: 60 - 250 | MeV/u |
| Hor. Profile | bar of charge | |
| Fitted hor. emittance | 5.00 | π mm mrad |
| Ver. Profile | Gaussian | |
| Vert. normalized emittance P (1σ) | 0.52 | π mm mrad |
| Vert. normalized emittance C (1σ) | 0.750 | π mm mrad |
| Max geometric emittance P ($\sqrt(5)\sigma$) | 7.14 | π mm mrad |
| Min geometric emittance P ($\sqrt(5)\sigma$) | 1.66 | π mm mrad |
| Max geometric emittance C ($\sqrt(5)\sigma$) | 7.14 | π mm mrad |
| Min geometric emittance C ($\sqrt(5)\sigma$) | 3.66 | π mm mrad |
| Max nr of particles per spill in irradiation room | p: 2E10; $C_{12}^{6+}$: 1E9 | |
| range of possible intensity variations | >1:100 | |

### A.3.2 Lattice

| Parameter | Value | Unit |
|---|---|---|
| $D_{x,max}$ (EX) | -6.200 | m |
| $D_{y,max}$ V2 | -2.600 | m |
| Beam size at iso center [σ, FWHM] | 4 to 10 | mm |
| Beam size variation principle | Phase-stepper in EX | |

# Bibliography


[1] M. Benedikt, J. Gutleber, M. Palm, W. Pirkl, U. Dorda, and A. Fabich. Overview of the MedAustron design and technology choices. In *1st. International Particle Accelerator Conference IPAC10*, pages 109–111, Kyoto, Japan, 2010.

[2] M. Benedikt, H. Leeb, and T. Schreiner. *Physics opportunities at MedAustron*. Vienna University of Technology, Vienna, Austria, 2009.

[3] MedAustron Research. http://www.medaustron-research.at/.

[4] P.J. Bryant, M. Benedikt, L. Badano, M. Crescenti, P. Holy, A.T. Maier, M. Pullia, S. Rossi, and P. Knaus. Proton-Ion Medical Machine Study (PIMMS), 1. (CERN-PS-99-010-DI), 1999.

[5] CERN. http://www.cern.ch/.

[6] M. Pullia. Status Report on the Centro Nazionale di Adroterapia Oncologica (CNAO). In *11th. European Particle Accelerator Conference EPAC08*, pages 982–4, Genoa, Italy, 2008.

[7] PSI. www.psi.ch/.

[8] E. Dallago, G. Venchi, S. Rossi, M. Pullia, T. Fowler, and U. Nielsen. The power supply for a medical synchrotron Beam Chopper System. In *Industrial Electronics, 2008. IECON 2008. 34th Annual Conference of IEEE*, pages 1016–1020, Orlando, Florida, USA, 2008.

[9] P.J. Bryant, M. Benedikt, L. Badano, M. Crescenti, P. Holy, A.T. Maier, M. Pullia, S. Reimoser, S. Rossi, G. Borri, P. Knaus, F. Gramatica, M. Pavlovic, and L. Weisser. Proton-Ion Medical Machine Study (PIMMS), 2. (CERN-PS-2000-007-DR), 2000.

[10] E. Sargsyan. MedAustron Injector design report. Technical Report FS-100705-a-ESA-V1.0, EBG MedAustron, Wiener Neustadt, Austria, 2010.

[11] U. Dorda. DRAFT: MedAustron Accelerator Complex design report. Technical report.

[12] B. Goddard. Injection and Extraction. In *CAS - CERN Accelerator School: Introduction to Accelerator Physics*, Varna, Bulgaria, 2010. CERN.

[13] U. Dorda. DRAFT: MedAustron Accelerator Paramter List. Technical report.

[14] S.Y. Lee. *Accelerator Physics (Second Edition)*. World Scientific, Singapore, 2007.

[15] E.D. Courant and H.S. Snyder. Theory of the alternating-gradient synchrotron. *Ann. Phys.*, 3:1–48, 1958.

[16] P.J. Bryant and K. Johnsen. *The Principles of Circular Accelerators and Storage Rings*. Cambridge Univ. Press, Cambridge, United Kingdom, 1993.

[17] A.W. Chao and M. Tigner. *Handbook of Accelerator Physics and Engineering (Second Printing)*. World Scientific, Singapore, 2002.

[18] Y. Kobayashi and H. Takahashi. Improvement of the emittance in the resonant ejection. In *Proc. 6th Int. Conf. on High Energy Accelerators*, pages 347–351, Cambridge, Massachusetts, USA, 1967.

[19] K.N. Henrichsen and M.J. De Jonge. Acceleration by phase displacement in the ISR. (CERN-ISR-RF-MA-74-21.):4 p, 1974.

[20] G. Guignard. A general treatment of resonances in accelerators. Geneva, Switzerland, 1978. CERN.

[21] W. Hardt. Ultraslow extraction out of LEAR. Technical Report CERN-PS-DL-LEAR-Note-81-6, CERN, Geneva, Switzerland, 1981.

[22] P.J. Bryant. AGILE - a tool for interactive lattice design. Technical Report CERN-PS-2000-036-DR, CERN, Geneva, Switzerland, 2000.

[23] U. Dorda. private communication.

[24] Python Programming Language. http://www.python.org/.

[25] H. Grote and F. Schmidt. MAD-X: An Upgrade from MAD8. (CERN-AB-2003-024-ABP):4 p, 2003.

[26] L. Badano and S. Rossi. Characteristics of a betatron core for extraction in a proton-ion medical synchrotron. Technical Report CERN-PS-97-019-DI, CERN, Geneva, Switzerland, 1997.

[27] M. Crescenti. Rf empty bucket channelling combined with a betatron core to improve slow extraction in medical synchrotrons. Technical Report CERN-PS-97-068-DI, CERN, Geneva, Switzerland, 1998.

[28] S. Rossi. Specification of the betatron core and power supply. Technical Report CNA-SPDP-007WXX-00221, CNAO, Pavia, Italy, 2003.

[29] M. Tomizawa, M. Yoshizawa, K. Chida, J. Yoshizawa, Y. Arakaki, R. Nagai, A. Mizobuchi, A. Noda, K. Noda, M. Kanazawa, A. Ando, H. Muto, and T. Hattori. Slow beam extraction at TARN II. *Nuclear Instruments and Methods in Physics Research Section A: Accelerators, Spectrometers, Detectors and Associated Equipment*, 326(3):399–406, 1993.

[30] T. Furukawa, T. Uesugi, T. Fujimoto, M. Kanazawa, K. Noda, S. Shibuya, E. Takada, S. Yamada, and T. Naruse. Recent Improvement of Slow-extraction at HIMAC Synchrotron. In *9th. European Particle Accelerator Conference EPAC04*, pages 267–9, Lucerne, Switzerland, 2004.

[31] HIT. http://www.hit-centrum.de/.

[32] N. Carmignani, C. Biscari, M. Serio, G. Balbinot, E. Bressi, M. Caldara, M. Pullia, J. Bosser, and G. Venchi. RF-knockout Extraction System for the CNAO Synchrotron. In *1st. International Particle Accelerator Conference IPAC10*, pages 3891–3, Kyoto, Japan, 2010.

[33] S. Van der Meer. Stochastic extraction, a low-ripple version of resonant extraction. Technical Report CERN-PS-AA-78-6, CERN, Geneva, Switzerland, 1978.

[34] D. Boussard, M. Gyr, K.H. Kissler, and T. Linnecar. Slow extraction at 400 GeV/c with stochastic RF noise. Technical Report CERN-SPS-AOP-MG-jf. CERN-SPS-Improvement-Report-179, CERN, Geneva, Switzerland, 1980.

[35] M. Palm. DRAFT: Synchrotron third integer resonance extraction spill generator. Technical Report TN-101125-a-MPA, EBG MedAustron, Wiener Neustadt, Austria, 2010.

[36] P. Fraboulet. private communication, MedAustron PIMS: PP-101110-a-PFR.

[37] Vasko + Partner Ziviltechniker GmbH. EIA documents: Haustechnik - HKLS. Technical Report PM-090918-a-EBG-V2.0, EBG MedAustron, Wiener Neustadt, Austria, 2010.

[38] F. Moser. Analysis of Energy Verification. Technical Report TN-091120-a-FMO, EBG MedAustron, Wiener Neustadt, Austria, 2010.